

รอยร้าวเส้นตรงภายใต้แรงกระทำรูปแบบที่ 1 และอิทธิพลของหน่วยแรงที่ผิว



นายเหิงวียน งอก เซอน

จุฬาลงกรณ์มหาวิทยาลัย

CHULALONGKORN UNIVERSITY

บทคัดย่อและแฟ้มข้อมูลฉบับเต็มของวิทยานิพนธ์ตั้งแต่ปีการศึกษา 2554 ที่ให้บริการในคลังปัญญาจุฬาฯ (CUIR)

เป็นแฟ้มข้อมูลของนิสิตเจ้าของวิทยานิพนธ์ ที่ส่งผ่านทางบัณฑิตวิทยาลัย

The abstract and full text of theses from the academic year 2011 in Chulalongkorn University Intellectual Repository (CUIR) are the thesis authors' files submitted through the University Graduate School.

วิทยานิพนธ์นี้เป็นส่วนหนึ่งของการศึกษาตามหลักสูตรปริญญาวิศวกรรมศาสตรมหาบัณฑิต

สาขาวิชาวิศวกรรมโยธา ภาควิชาวิศวกรรมโยธา

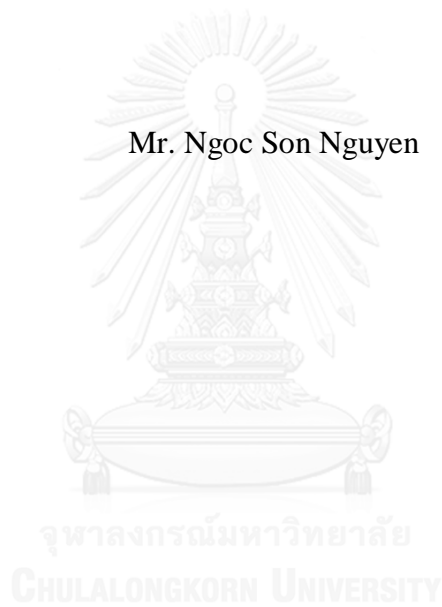
คณะวิศวกรรมศาสตร์ จุฬาลงกรณ์มหาวิทยาลัย

ปีการศึกษา 2557

ลิขสิทธิ์ของจุฬาลงกรณ์มหาวิทยาลัย

INFLUENCE OF RESIDUAL SURFACE TENSION ON STRAIGHT CRACK
UNDER MODE-I LOADING

Mr. Ngoc Son Nguyen



A Thesis Submitted in Partial Fulfillment of the Requirements
for the Degree of Master of Engineering Program in Civil Engineering

Department of Civil Engineering

Faculty of Engineering

Chulalongkorn University

Academic Year 2014

Copyright of Chulalongkorn University

เหิงเวียน งอก เซอน : รอยร้าวเส้นตรงภายใต้แรงกระทำรูปแบบที่ 1 และอิทธิพลของหน่วยแรงที่ผิว (INFLUENCE OF RESIDUAL SURFACE TENSION ON STRAIGHT CRACK UNDER MODE-I LOADING) อ.ที่ปรึกษาวิทยานิพนธ์
 หลัก: รศ. ดร. จุณญ รุ่งอมรรตน์, อ.ที่ปรึกษาวิทยานิพนธ์ร่วม: ศ. ดร. ชีรพงศ์ เสนจันทร์
 ฒิไชย, 76 หน้า.

วิทยานิพนธ์ฉบับนี้นำเสนอผลการศึกษาอิทธิพลของแรงดึงผิวคงค้างที่มีต่อสนามยืดหยุ่นใกล้จุดปลายรอยร้าวแบบเส้นตรงภายใต้แรงกระทำรูปแบบที่หนึ่ง แบบจำลองผิวหืดหยุ่นของเกอร์ติน-เมอร์คอคแบบไร้โมดูลัสในระนาบถูกนำมาใช้ร่วมกับทฤษฎีความยืดหยุ่นเชิงเส้นเพื่อจำลองอิทธิพลในระดับนาโนและการขึ้นอยู่กับขนาดของสนามยืดหยุ่น สมการกำกับในเทอมของการเคลื่อนเปิดของรอยร้าวถูกสร้างขึ้นในรูปแบบของสมการร่วมปริพันธ์-อนุพันธ์ซึ่งเกี่ยวข้องกับเคอร์เนลเอกฐานสูง จากนั้นได้ประยุกต์ใช้ระเบียบวิธีน้ำหนักคงค้างและการหาปริพันธ์แยกส่วนเพื่อพัฒนาสมการรูปแบบอ่อนสมมาตรซึ่งเกี่ยวข้องกับเฉพาะเคอร์เนลเอกฐานต่ำ ต่อมาระเบียบวิธีพื้นฐานของกาเลอร์คินได้ถูกนำมาใช้ในการหาคำตอบเชิงตัวเลขของสมการดังกล่าว ในขั้นตอนการประมาณ ฟังก์ชันพื้นฐานสร้างจากโครงตาข่ายของชิ้นส่วนแบบเชิงเส้น กำลังสอง กำลังสาม และชิ้นส่วนแบบเฮอร์มิตได้ถูกนำมาใช้ จากการศึกษาอัตราการลู่เข้าของผลเฉลยเชิงตัวเลขพบว่าการประมาณโดยใช้ฟังก์ชันรูปร่างแบบกำลังสอง กำลังสาม และแบบเฮอร์มิต ให้อัตราการลู่เข้าเท่ากันและสูงกว่าในกรณีฟังก์ชันรูปร่างแบบเชิงเส้น และความชันของการเคลื่อนเปิดของรอยร้าวที่จุดปลายรอยร้าวมีค่าจำกัดในกรณีที่แรงดึงผิวคงค้างไม่เท่ากับศูนย์ นอกจากนี้ผลจากการศึกษาพารามิเตอร์ต่างๆระบุว่า แรงดึงผิวคงค้างไม่เพียงส่งผลให้ค่าการเคลื่อนเปิดรอยร้าวและหน่วยแรงที่ใกล้ปลายรอยร้าวลดลงอย่างมีนัยสำคัญ แต่ยังลดความเป็นเอกฐานของหน่วยแรงที่ปลายของรอยร้าวและส่งผลให้คำตอบที่ทำนายได้ขึ้นอยู่กับขนาดอีกด้วย.

ภาควิชา วิศวกรรมโยธา

สาขาวิชา วิศวกรรมโยธา

ปีการศึกษา 2557

ลายมือชื่อนิสิค _____

ลายมือชื่อ อ.ที่ปรึกษาหลัก _____

ลายมือชื่อ อ.ที่ปรึกษาร่วม _____

5670513021 : MAJOR CIVIL ENGINEERING

KEYWORDS: CRACK-OPENING DISPLACEMENT, NEAR-TIP STRESS, GURTIN-MURDOCH, NANO-SIZED CRACKS, RESIDUAL SURFACE TENSION.

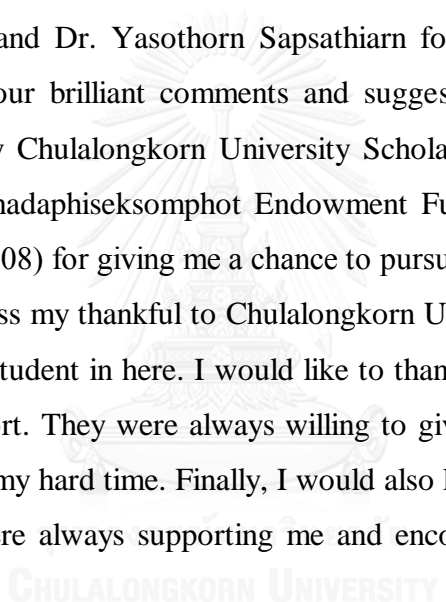
NGOC SON NGUYEN: INFLUENCE OF RESIDUAL SURFACE TENSION ON STRAIGHT CRACK UNDER MODE-I LOADING.
 ADVISOR: ASSOC. PROF. JAROON RUNGAMORN RAT, Ph.D., CO-ADVISOR: PROF. TEERAPONG SENJUNTICHAI, Ph.D., 76 pp.

In this thesis, the influence of residual surface tension on the near-tip elastic field of a straight crack under mode-I loading condition is fully investigated. The surface effect via the Gurtin-Murdoch surface elasticity model without the in-plane modulus is integrated into the classical theory of linear elasticity to capture the nano-scale influence and the size-dependent behavior of the elastic field. The governing equation is formulated in terms of the crack-opening displacement and finally expressed in a form of an integro-differential equation involving a strongly singular kernel. A weighted residual technique together with the integration by parts is utilized to derive the symmetric weak-form equation involving only a weakly singular kernel. Standard Galerkin method is then adopted to construct numerical solutions of the weak-form equation. In the approximation, basis functions constructed locally on linear, quadratic, cubic, and Hermite finite element mesh have been employed. The rate of convergence of numerical solutions is fully explored and it is found that approximations using quadratic, cubic and Hermite shape functions yield the same rate of convergence that is higher than that of the linear case and the gradient of the crack-opening displacement becomes finite at the crack-tip for non-zero residual surface tension. Based on an extensive parametric study, it is indicated that the residual surface tension not only significantly reduces the overall crack-opening displacement and the near-tip stresses but also weakens the crack-tip stress singularity and renders the predicted solutions strongly size-dependent.

Department:	Civil Engineering	Student's Signature
Field of Study:	Civil Engineering	Advisor's Signature
Academic Year:	2014	Co-Advisor's Signature

ACKNOWLEDGEMENTS

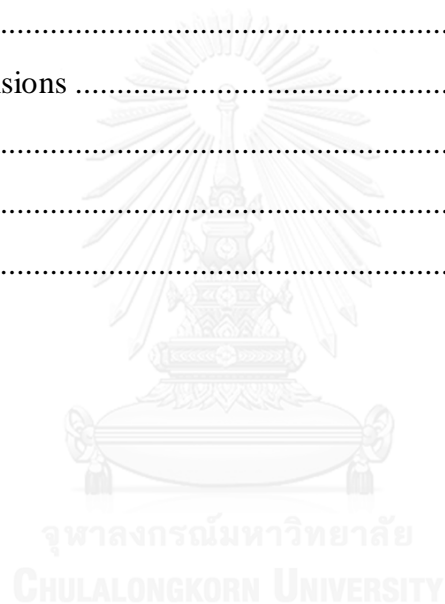
I would like to express my sincerest gratitude to my advisor, Associate Professor Dr. Jaroon Rungamornrat and co-advisor, Professor Dr. Teerapong Senjuntichai, who have supported me throughout my thesis. I would like to thank you for encouraging my study and for providing me with an excellent atmosphere for doing research. This thesis would not have been able to finish without your guidance, patience and knowledge. I would also like to thank my committee members, Assistant Professor Dr. Watanachai Smittakorn, Associate Professor Dr. Akhrawat Lenwari and Dr. Yasothorn Sapsathiarn for serving as my committee members and for your brilliant comments and suggestions. I am grateful to the support provided by Chulalongkorn University Scholarship Program for ASEAN Countries and Ratchadaphiseksomphot Endowment Fund 2013 of Chulalongkorn University (CU-56-908) for giving me a chance to pursue a Master's Degree in Civil Engineering. I express my thankful to Chulalongkorn University for letting me fulfil my dream of being student in here. I would like to thank all of my good friends for their help and support. They were always willing to give their best suggestion and stood by me during my hard time. Finally, I would also like to thank my parents and my sisters. They were always supporting me and encouraging me with their best wishes.



CONTENTS

	Page
THAI ABSTRACT.....	iv
ENGLISH ABSTRACT	v
ACKNOWLEDGEMENTS	vi
CONTENTS.....	vii
LIST OF TABLES	ix
LIST OF FIGURES	x
CHAPTER I	1
INTRODUCTION.....	1
1.1 General.....	1
1.2 Background and Review	4
1.2.1 Experimental investigations	4
1.2.2 Mathematical modeling.....	5
1.3 Research Objectives	9
1.4 Scope of Work.....	9
1.5 Research Methodology	9
1.6 Research Significance.....	10
CHAPTER II.....	11
PROBLEM FORMULATION.....	11
2.1 Problem Description	11
2.2 Domain Decomposition	12
2.3 Basic Field Equations	13
2.4 Formulation of Governing Equations for Cracked Medium.....	15
CHAPTER III.....	18
SOLUTION PROCEDURE.....	18
3.1 Discretization	18
3.2 Shape Functions	19
3.3 Evaluation of involved integrals	22
CHAPTER IV	23

	Page
NUMERICAL RESULTS	23
4.1 Crack under Uniform Normal Traction	23
4.1.1 Verification.....	23
4.1.2 Parametric study	32
4.2 Crack under Linear Normal Traction	40
4.2 Crack under Quadratic Normal Traction	47
CHAPTER V.....	54
CONCLUSIONS	54
5.1 Summary	54
5.2 Potential Extensions	55
REFERENCES.....	56
APPENDIX.....	63
VITA.....	76



LIST OF TABLES

Table 4.1. Values of $d\bar{u}/d\bar{x}$ at the crack tip for $\bar{\tau}^s / \bar{a} = 0.133$ and $\bar{t}_o = 0.00266$	27
Table 4.2. Values of $d\bar{u}/d\bar{x}$ at the crack tip for $\bar{\tau}^s / \bar{a} = 0.133$ and $\bar{t}_o = 0.00532$	27
Table 4.3. Values of $d\bar{u}/d\bar{x}$ at the crack tip for $\bar{\tau}^s / \bar{a} = 0.133$ and $\bar{t}_o = 0.01064$	28
Table 4.4. L ₂ -norm error $\ e\ _2$ for $\bar{\tau}^s / \bar{a} = 1$ and $\bar{t}_o = 1$	31
Table 4.5. Rate of convergence p for $\bar{\tau}^s / \bar{a} = 1$ and $\bar{t}_o = 1$	31



LIST OF FIGURES

Figure 2.1: Schematic of a finite straight crack embedded in a two-dimensional, infinite medium and subjected to arbitrarily normal traction.	12
Figure 2.2: Schematic of (a) bulk cracked medium, (b) zero-thickness material layer S_c^+ , and (c) zero-thickness material layer S_c^-	13
Figure 3.1. Schematic indicating the global basis functions and element shape functions for 4 types of elements.	20
Figure 4.1. Schematic of straight crack of length $2a$ under self-equilibrated uniformly distributed normal traction.....	24
Figure 4.2. Profile of crack opening displacement gradient for straight crack under uniformly distributed normal traction for $\bar{t}_o = 0.00266, 0.00532, 0.01064$ and $\bar{\tau}^s / \bar{a} = 0.133$	29
Figure 4.3. Profile of crack opening displacement gradient for straight crack under uniformly distributed normal traction for $\bar{\tau}^s / \bar{a} = 0.133, 0.266, 0.532$ and $\bar{t}_o = 0.00532$	29
Figure 4.4. Log-log plots of L ₂ -norm error $\ e\ _2$ versus the element size h_e for $\bar{\tau}^s / \bar{a} = 1$ and $\bar{t}_o = 1$	32
Figure 4.5. (a) Normalized crack opening displacement and (b) normalized normal stress components along the x_1 -axis for crack under uniformly distributed normal traction without the residual surface tension and for $E = 89.5 \text{ GPa}$, $\nu = 0.3$	33
Figure 4.6. (a) Normalized crack opening displacement and (b) normalized normal stress components along the x_1 -axis of straight crack under uniformly distributed normal traction for five different values of $\bar{\tau}^s$ ranging from 0.005 to 2 and for $E = 89.5 \text{ GPa}$ and $\nu = 0.3$	35
Figures 4.7. Normalized crack opening displacement $\Delta\bar{u} / \bar{t}_o$ for $\bar{x} = 0, 0.5, 0.75$ versus normalized residual surface tension $\bar{\tau}^s$ of straight crack under uniformly distributed normal traction for $E = 89.5 \text{ GPa}$, $\nu = 0.3$ and $\bar{a} = 10$	36
Figures 4.8. Normalized normal stress components $\bar{\sigma}_{11} / \bar{t}_o = \bar{\sigma}_{22} / \bar{t}_o$ for $\bar{x} = 1.001, 1.01, 1.1$ versus normalized residual surface tension $\bar{\tau}^s$ of straight crack under uniformly distributed normal traction for $E = 89.5 \text{ GPa}$, $\nu = 0.3$ and $\bar{a} = 10$	36

- Figure 4.9.** (a) Normalized crack opening displacement and (b) normalized normal stress components along the x_1 -axis for straight crack under uniformly distributed normal for five different values of $\bar{a} = a/\Lambda = 10, 50, 250, 500, 2500$ and for $E = 89.5 \text{ GPa}$ and $\nu = 0.3$ 37
- Figures 4.10.** Normalized crack opening displacement $\Delta\bar{u}/\bar{t}_o$ for $\bar{x} = 0, 0.5, 0.75$ versus normalized crack length \bar{a} of straight crack under uniformly distributed normal traction for $E = 89.5 \text{ GPa}$, $\nu = 0.3$ and $\bar{\tau}^s = 0.7$ 38
- Figures 4.11.** Normalized normal stress components $\bar{\sigma}_{11}/\bar{t}_o = \bar{\sigma}_{22}/\bar{t}_o$ for $\bar{x} = 1.001, 1.01, 1.1$ versus normalized crack length \bar{a} of straight crack under uniformly distributed normal traction for $E = 89.5 \text{ GPa}$, $\nu = 0.3$ and $\bar{\tau}^s = 0.7$. 38
- Figure 4.12.** Schematic of straight crack of length $2a$ under self-equilibrated linearly distributed normal traction.41
- Figure 4.13.** (a) Normalized crack opening displacement and (b) normalized normal stress components along the x_1 -axis of straight crack under linearly distributed normal traction for five different values of $\bar{\tau}^s$ ranging from 0.005 to 2 and for $E = 89.5 \text{ GPa}$ and $\nu = 0.3$ 43
- Figures 4.14.** Normalized crack opening displacement $\Delta\bar{u}/\bar{t}_o$ for $\bar{x} = 0, 0.5, 0.75$ versus normalized residual surface tension $\bar{\tau}^s$ of straight crack under linearly distributed normal traction for $E = 89.5 \text{ GPa}$, $\nu = 0.3$ and $\bar{a} = 10$ 44
- Figures 4.15.** Normalized normal stress components $\bar{\sigma}_{11}/\bar{t}_o = \bar{\sigma}_{22}/\bar{t}_o$ for $\bar{x} = 1.001, 1.01, 1.1$ versus normalized residual surface tension $\bar{\tau}^s$ of straight crack under linearly distributed normal traction for $E = 89.5 \text{ GPa}$, $\nu = 0.3$ and $\bar{a} = 10$ 44
- Figure 4.16.** (a) Normalized crack opening displacement and (b) normalized normal stress components along the x_1 -axis of straight crack under linearly distributed normal traction for five different values of $\bar{a} = a/\Lambda = 10, 50, 250, 500, 2500$ and for $E = 89.5 \text{ GPa}$ and $\nu = 0.3$ 45
- Figures 4.17.** Normalized crack opening displacement $\Delta\bar{u}/\bar{t}_o$ for $\bar{x} = 0, 0.5, 0.75$ versus normalized crack length \bar{a} of straight crack under linearly distributed normal traction for $E = 89.5 \text{ GPa}$, $\nu = 0.3$ and $\bar{\tau}^s = 0.7$ 46
- Figures 4.18.** Normalized normal stress components $\bar{\sigma}_{11}/\bar{t}_o = \bar{\sigma}_{22}/\bar{t}_o$ for $\bar{x} = 1.001, 1.01, 1.1$ versus normalized crack length \bar{a} of straight crack under linearly distributed normal traction for $E = 89.5 \text{ GPa}$, $\nu = 0.3$ and $\bar{\tau}^s = 0.7$ 46

- Figure 4.19.** Schematic of straight crack of length $2a$ under self-equilibrated, quadratic normal traction.47
- Figure 4.20.** (a) Normalized crack opening displacement and (b) normalized normal stress components along the x_1 -axis of straight crack under quadratic normal traction for five different values of $\bar{\tau}^s$ ranging from 0.005 to 2 and for $E = 89.5 \text{ GPa}$ and $\nu = 0.3$ 50
- Figures 4.21.** Normalized crack opening displacement $\Delta\bar{u} / \bar{t}_o$ for $\bar{x} = 0, 0.5, 0.75$ versus normalized residual surface tension $\bar{\tau}^s$ of straight crack under quadratic normal traction for $E = 89.5 \text{ GPa}$, $\nu = 0.3$ and $\bar{a} = 10$ 51
- Figures 4.22.** Normalized normal stress components $\bar{\sigma}_{11} / \bar{t}_o = \bar{\sigma}_{22} / \bar{t}_o$ for $\bar{x} = 1.001, 1.01, 1.1$ versus normalized residual surface tension $\bar{\tau}^s$ of straight crack under quadratic normal traction for $E = 89.5 \text{ GPa}$, $\nu = 0.3$ and $\bar{a} = 10$ 51
- Figure 4.23.** (a) Normalized crack opening displacement and (b) normalized normal stress components along the x_1 -axis of straight crack under quadratic normal traction for five different values of $\bar{a} = a / \Lambda = 10, 50, 250, 500, 2500$ and for $E = 89.5 \text{ GPa}$ and $\nu = 0.3$ 52
- Figures 4.24.** Normalized crack opening displacement $\Delta\bar{u} / \bar{t}_o$ for $\bar{x} = 0, 0.5, 0.75$ versus normalized crack length \bar{a} of straight crack under quadratic normal traction for $E = 89.5 \text{ GPa}$, $\nu = 0.3$ and $\bar{\tau}^s = 0.7$ 53
- Figures 4.25.** Normalized normal stress components $\bar{\sigma}_{11} / \bar{t}_o = \bar{\sigma}_{22} / \bar{t}_o$ for $\bar{x} = 1.001, 1.01, 1.1$ versus normalized crack length \bar{a} of straight crack under quadratic normal traction for $E = 89.5 \text{ GPa}$, $\nu = 0.3$ and $\bar{\tau}^s = 0.7$ 53

CHAPTER I

INTRODUCTION

This chapter begins with the motivation and significance of the present research. Then, the research objectives, scope of work, and the methodology and procedure are clearly addressed. Finally, findings and contribution of the current investigation are summarized.

1.1 General

Nowadays, nanotechnology has become an interesting discipline and remarkably influenced the lifestyle of people around the world. A significant amount of resources has been invested in this century to carry out extensive researches and develop various technologies and devices by taking advantages of desirable features found in such a tiny scale. It has been recognized that, for materials with their characteristic size less than 100 nanometers, the common rules of chemistry and physics no longer apply, and they begin, most of the time, to exhibit unique and remarkable properties. They may become much stronger, more conductive, and more reactive in comparison with their macroscopic form. For instance, solid materials such as gold can turn into a liquid state at the room temperature; inert materials such as gold and platinum can be used as catalysts; and a stable material such as aluminum can be converted to that combustible. Manipulating the properties of constituting materials, atom-by-atom, can offer a potential means to enhance the performance of various devices, tools, objects and related items encountered in people daily life: from cosmetics to food/medicine, from communication/information to entertainments, from transportations on earth to aerospace, and from future and clean energy concept to environments/securities.

Nano-materials can lead to radical, new approaches for manufacturing advanced materials into better products and devices such as faster computers, more advanced pharmaceuticals for drug delivery, better skin-care protection, better tissue and nerve repairing, more effective catalyst, smaller but enhanced sensors, more effective communication systems. Titanium oxide at the nano-scale can be used to reduce organic pollutants. Moreover, silver nano-particles have the ability to reduce biological

pollutants such as bacteria. Other applications can be found in nano-filtration membranes for removal of heavy metals and pesticides from drinking water, removal of pollutants from industrial effluents and in particular water softening. Another impressive application of nano-technology is plastic nano-composites that are used for “step assists” in the aeronautic and automobile industries. Their desirable properties such as scratch-resistance, light-weight, and rush-proof can lead to the strength improvement, reductions in weight, fuel saving and increased longevity. In addition, metal nano-crystals can be integrated to build car bumpers, to make it stronger or to aluminums to make them more long-lasting. For usages in the area of electronics and information technology, faster, more powerful, increasingly energy-efficient nano-scale transistors are currently under development and, soon, the entire memory of computers may be stored on a single tiny chip. Moreover, organic LED’s, displays, sensors, electronics can be made of organic materials with high thermal stability, low power consumption. In the field of medicine and healthcare, gold nano-particles could be used to detect early-stage Alzheimer’s disease. By operating at very small scale, like the virus in a bloodstream, nano-particles can be targeted at specific organs of the body. Here, their photo-thermal properties can be used to heat up and destroy cancerous tissues. In material science and technology, the development of nano-scale and nano-structured materials such as carbon nano-tubes, nano-wires, nano-rods, nano-composites, nano electromechanical systems (NEMS), nano-scale thin films and coatings have appeared continuously and remarkably. For instance, nano-structures such as carbon nano-tubes, possessing very high strength and stiffness, were first discovered in 1991 by Iijima (Iijima, 1991; Iijima and Ichihashi, 1993). The single-walled carbon nano-tubes have strength of up to 100 GPa, Young’s modulus values of ~ 1 TPa and failure strains about 15–30% (Peng *et al.*, 2008). Nano-material science and technology can lead to the breakthrough in many disciplines in the near future, and solutions for urgent problems in our society. It will become the next industrial revolution.

The rapid development of nano-materials requires the fundamental understanding of key governing physics, underlying structures, and processes at the nano-scales. Advances in the knowledge of the connections between their basic properties and structures have led to the remarkable progress in design, fabrication, and

characterization of novel materials at the nanometer length scale. Vast applications of such materials to assemble small scale devices, tools, products, and components have been evident in various fields as previously mentioned (e.g., NEMS). Design of those tiny-scale objects to ensure the integrity and safety throughout their lifespan essentially requires the basic knowledge of failure mechanism of constituting materials. It has been well recognized that presence of defects/flaws within materials can generate high stress localization and accumulation of damages, and may finally lead to fatigue growth and their global failure. Investigation of fundamental fracture behavior of materials containing very small-scale defects/flaws is essential, and results and findings can be potentially useful in the failure/damage assessment.

Mathematical modeling has been found a common, useful, and alternative means to investigate physical phenomena in the nano-scale level. Due to the capability and versatility of available theoretical simulation schemes, various aspects of new developed nano-materials such as responses to excitations, size-dependent characteristics, mechanical and related properties, and failure mechanism can be extensively explored with acceptable predicted results and reasonable use of resources. A continuum-based theory of linear elasticity has been well established and used extensively in the modeling of macroscopic fracture problems and predicted solutions have been found in good agreement with experimental evidences. However, this classical theory, when applied directly to nano-size crack problems, has failed to capture the actual physical phenomena due to the incapability of the underlying governing physics to mimic various inherent features such as size-dependency, surface effects, non-locality, etc. To maintain their positive features such as the mathematical simplicity of governing physics and low requirement of computational resources in comparison with available discrete-based schemes (e.g., atomistic and molecular dynamics simulations), continuum-based theories and techniques with the integration of intrinsic nano-scale influences such as surface effects to enhance the underlying governing physics have been continuously proposed.

While modified continuum-based theories have been utilized by various investigators to study nano-size crack problems (e.g., Wu, 1999; Wu and Wang, 2000, 2001; Oh *et al.*, 2006; Wang *et al.*, 2008; Fang *et al.*, 2009; Fu *et al.*, 2008, 2010; Wang and Li, 2013; Sendova and Walton, 2010; Kim *et al.*, 2010, 2011a, 2011b, 2013; Nan

and Wang, 2012, 2013; Walton, 2014), certain crucial aspects such as the local near-tip field and the existence of stress singularity along the crack front are still not well understood and, most of the time, it is predetermined without the formal mathematical proof. Lack of information about the near-tip field, analogous to William's asymptotic expansion for macroscopic cracks, can either limit the capability or deteriorate the accuracy of various approximate methods requiring the knowledge of a solution form a priori. Inaccurate solutions of the local dominant field near the crack-tip can further mislead the prediction of related fracture process such as crack advances. This existing gap of knowledge is found significant and attracts the present study.

1.2 Background and Review

In the past three decades, studies focusing on nano-size crack problems have received enormous attention from various researchers. Several techniques including experimental investigations and mathematical modeling using various forms of governing physics have been continuously proposed. Results from comprehensive review of existing literatures concerning nano-size cracks and related problems are organized into two different groups depending on the key approach employed.

1.2.1 Experimental investigations

A selected set of relevant experiment-based investigations can be briefly summarized as follows. Karimi *et al.* (2002) applied both nano-scratch procedure and depth sensing nano-indentation technique to measure the fracture toughness of thin films to offer better insight in the crack formation and fracture characteristics of TiAlN(Si, C, ...) hard thin films. Guin *et al.* (2005) conducted a series of experiments to examine the crack tip using atomic force microscopy (AFM). In their study, the extent of the dissolution of crack faces was measured when the crack in the soda-lime glass was arrested and aged in the proximity of the propagation threshold. Chen *et al.* (2008) utilized the digital image correlation (DIC) along with the atomic force microscopy to investigate the local mechanical and fracture behavior on the epoxy-silica composites. Fracture strength of multi-wall carbon nano-tubes (MWNTs) of greater than 100 GPa has been currently measured by employing the technique of in-situ transmission electron microscopy (TEM) and it was found agree with theoretically predicted solutions of non-defective MWNTs (e.g., Peng *et al.* 2008). According to the work of

Zhao and Xing (2008), (2010), micro-cracks in single-crystal silicon were observed by the transmission electron microscopy with high resolution. The local near-front deformation field of single-crystal silicon containing a loaded quasi-cleavage crack running in the alignment was also examined using the technique of nano-moiré.

Later, Yan *et al.* (2011) performed a series of stable tearing tests on four-point bending specimens of millimeter-size and nano-cantilevers to simulate crack formation and delamination processes along the interface of Cu/Si in the nano-scale. Liu *et al.* (2013) experimentally investigated a micro-crack and studied the local deformation field in the neighborhood of the crack front in single-crystal silicon by employing various techniques such as the numerical moiré (NM) method, the geometric phase analysis (GPA), and the high-resolution transmission electron microscopy (HRTEM). Most recently, Kawai *et al.* (2014) conducted extensive tests of four different, nano-scale cantilever specimens with embedded singular stress field at the interface between copper and silicon nitride to study the formation of cracks from the interfacial edge of a nano-scale component.

1.2.2 Mathematical modeling

Mathematical modeling of nano-sized crack problems using discretize-based theories such as atomistic and molecular dynamic simulations has been well recognized in the literature. For example, Buehler *et al.*, 2003, Zhang *et al.* (2005), Rafii-Tabar *et al.* (2006), Buehler and Gao (2006), Pugno *et al.* (2008), Masuda-Jindo *et al.* (2009), Huang *et al.* (2009), Adnan and Sun (2010), and Nazmus Sakib and Adnan (2012) studies problems of nano-size cracks via the theoretical atomistic and molecular dynamics calculations. Most recently, Yang *et al.* (2014) applied the MD simulations to investigate the crack advances at the interface of Cu/SiC under the action of both the tensile load and the combined tensile and shear loads. Also, Yamakov *et al.* (2014) investigated the full dislocation emission and deformation twinning at a crack tip in single crystalline aluminum by using both multi-scale MD-continuum simulations and the continuum-based theory. Although the discrete atomic-scale models have been provided precise response prediction due to the physically suitable governing physics, the simulation requires significant amount of computational resources.

Consequently, approaches based on continuum-based theories are considered attractive since the underlying governing physics are less complicated and the corresponding solution procedure is computationally more efficient. A continuum-based model commonly employed in the investigation of fundamental problems in solid mechanics is the one integrating the influence of surface effects via the surface elasticity model (e.g., Gurtin and Ian Murdoch, 1975; Gurtin and Ian Murdoch, 1978; Gurtin *et al.*, 1998). In this theory, an elastic surface is mathematically modeled as a zero-thickness layer bonded to the bulk material and possessing different material properties. Over past decades, several researchers have been interested in the role of surface stresses on the properties and behavior of nano-scale materials and nano-components, and Gurtin and Murdoch surface elasticity concept has been one of the most mathematical models used in the simulations. For instance, Gurtin-Murdoch model was extensively applied to predict both static and dynamic mechanical behaviors of nano-wires and nano-plates (Wang and Feng, 2007,(2009); Wang and Yang, 2011; Wang and Wang, 2012); Sharma *et al.* (2003) utilized the theory of surface elasticity to examine the size-dependent elastic field of nano-inhomogeneities; Dingreville *et al.* (2005) investigated the role of surface stresses on the elastic properties of wires, extra-thin films and nano-scale particles; Cammarata (1997), Sharma and Ganti (2004), Cuenot *et al.* (2004), Shenoy (2005), Duan *et al.* (2005a), (2005b), Wang and Wang (2006), Jing *et al.* (2006), Tian and Rajapakse (2006), (2007), Ou *et al.* (2008), Zhao and Rajapakse (2009) applied the model of Gurtin-Murdoch to examine elastic mechanical properties of both homogeneous and heterogeneous nano-structured materials.

Nevertheless, applications of Gurtin-Murdoch surface elasticity theory to model nano-size fracture problems have still been limited. Wu (1999) and Wu and Wang (2000), (2001) addressed the effect of residual surface tension on the elastic deformation of two-dimensional crack problems using the surface elasticity model along with the analysis procedure for an elliptical void, and they concluded in this study that the residual surface tension generally introduces a pair of concentrated loads at the crack tip to maintain equilibrium. As a result, the near-tip elastic stress field is $1/r$ singular instead of $1/\sqrt{r}$ as in the classical case without the residual surface tension. Wang *et al.* (2008) employed a crack model with the finite root radius along with Gurtin-Murdoch model to investigate the role of the surface stresses on the near-tip

field of cracks under both mode-I and mode-III loading conditions. They pointed out in their study that the surface stresses play a significant role on both displacement and stress fields near the blunt crack tip and such influence becomes more prominent when the radius of the crack-tip root reduces to a nano-scale. Later, Fang *et al.* (2009) explored the surface stress effect on the dislocation emission from a crack subjected to both mode-I and mode-II conditions and the crack-tip geometry was assumed elliptically blunt. It was found in their study that the critical value of the stress intensity factors to induce the dislocation emission was significantly influenced by the surface stresses when the crack size becomes tiny, generally in the range of a nano-scale. It should be remarked, however, that the prediction of stresses by Wang *et al.* (2008) and Fang *et al.* (2009) is applicable only in the local region near the blunt crack-tip. Fu *et al.* (2008), (2010) employed the finite element method, via ANSYS® and ABAQUS®, to study the role of the surface energy on the near-tip field of blunt cracks under mode-I/mode-II conditions. Recently, Wang and Li (2013) investigated the near-tip elastic field of mode-I cracks with the consideration of the residual surface tension, and they concluded that integration of the surface elasticity in the modeling can considerably alter the characteristics of near-tip stress state when the crack-tip radius reduces to a nano-meter scale.

Modeling of nano-sized cracks using a sharp crack-tip model has also been well recognized in the literature. For instances, Oh *et al.* (2006) applied a generalized continuum-based model incorporating the nano-scale influence to investigate the Griffith crack problem under pure mode-I loading. In their study, the shape of the opened crack surfaces and the stress profile within the body, particularly in the interfacial region, was predicted by the long-range inter-molecular force obtained from atomistic simulations. They also deduced that the crack-tip geometry should be modeled by a sharp-tip model rather than a blunt-tip model, and the slope of the crack-face displacement and the stress at the crack tip are finite. Kim *et al.* (2010), (2011a), (2011b) applied the Gurtin-Murdoch model along with the complex variable technique to solve mode-I, mode-II and mode-III nano-crack problems. In their solution procedure, the stress at the crack-tip was assumed finite a priori and this stems directly from the physical argument without the mathematical proof. Sendova and Walton (2010) explored cracks in two-dimensional, elastic, infinite medium with the influence

of both constant and curvature-dependent residual surface tension. It was concluded in this study that the stress field at the crack tip becomes logarithmically singular and finite for the case of constant and curvature-dependent residual surface tension, respectively. The near-tip field with the logarithmic singularity was also addressed in the work of Kim *et al.* (2013) when Gurtin-Murdoch model was utilized to treat the surface stress effects. Nan and Wang (2012) also applied Gurtin-Murdoch model with the influence of the residual surface tension to obtain the elastic near-tip field and the corresponding essential fracture data such as stress intensity factors and crack-face displacements. Results from their study revealed that the role of the surface stresses on the near-tip field becomes prominent at a nanometer scale. In addition, the residual surface tension was found to considerably affect both the crack-face displacement profile and stress intensity factors. The extension of the work by Nan and Wang (2012) to treat nano-scale cracks in piezoelectric materials was carried out later by Nan and Wang (2013). It was found that the surface stresses significantly affect both the electric intensity factors along the crack front and the electro-mechanical elastic responses, and such influence depends mainly on the electrical boundary conditions. Most recently, Walton (2014) demonstrated that a simple modification of the non-uniform residual surface tension model with the dependence on curvature can lead to the bounded strain and stress at the tip of cracks subjected combined mode-I/mode-II loads.

Results from an extensive literature survey clearly indicate that the role of the surface energy or surface stresses on the near-tip field of nano-size cracks is not well established and still requires further investigations. Most of existing researches modeled cracks within the context of two-dimensional settings and solutions of the resulting mathematical models were mostly determined by analytical approaches such as series-solution schemes, integral-transform-based methods, and complex-variable-representation techniques. However, the treatment of general loading conditions, boundary conditions, and fracture configurations are still restricted in most of existing studies. For instance, Sendova and Walton (2010) focused on the analysis of two-dimensional nano-sized cracks under mode-I loading conditions and no extensive parametric study of involved parameters is considered. Although, for the case of the constant residual surface tension, Gurtin-Murdoch model was employed to model the role of the residual surface tension, it was still limited to a particular crack size, certain

material properties, and specific loading conditions. As a result, a straight, sharp crack under pure mode-I loading condition integrating the influence of the residual surface tension should be fully re-investigated. Gurtin–Murdoch surface elasticity model without the in-plane stiffness is adopted in the formulation to describe the role of the residual surface tension. A numerical scheme based on Galerkin approximation method is adopted to efficiently determine the solution of an integro-differential equation governing the unknown crack-face data. Results and findings from the present work should directly offer the fundamental insight of the near-tip elastic field when the influence of the surface stressed is integrated.

1.3 Research Objectives

The key objectives of the present investigation are (i) to develop a solution technique for modeling cracks with consideration of the residual surface tension and (ii) to investigate the role of the residual surface tension and size-dependent behavior of predicted solutions.

1.4 Scope of Work

The proposed work is carried out within the context of two-dimensional fracture analysis. The body is modeled as a two-dimensional infinite medium and the geometry of the crack is assumed straight. The bulk material is assumed homogeneous, isotropic, and linear elastic whereas the thin layer on the crack surface assumes zero in-plane elasticity but possesses a non-zero residual surface tension. Only cracks under mode-I loading condition are investigated and the contribution of the initial residual stress and the body force within the bulk material is fully neglected.

1.5 Research Methodology

Fundamental theories and assumptions, key methodology, and research procedures employed to develop a mathematical model and the corresponding solution technique capable of modeling cracks with the consideration of the residual surface tension can be summarized below.

- (i) A domain decomposition scheme is employed to separate the cracked body into a bulk material and zero-thickness layers.

- (ii) A classical theory of linear elasticity is utilized to obtain basic field equations of the bulk material. The key governing equation for the crack within the bulk material is obtained in a form of Cauchy singular integral equation by using the concept of the continuous distribution of dislocations.
- (iii) Gurtin-Murdoch surface elasticity model with only non-zero residual surface tension (ignoring the surface elastic constants) is adopted to derive the differential equation governing behavior of surface layers.
- (iv) Continuity of tractions and displacements across the interface between the surface layers and the bulk material is fully enforced to derive the integro-differential equation governing the whole cracked body.
- (v) A standard weighted residual technique together with the integration by parts and a special representation of the strongly singular kernels is adopted to derive the weakly singular weak-form equation.
- (vi) A numerical technique based on standard Galerkin approximation is established to construct numerical solutions of the integro-differential equation.

1.6 Research Significance

Unlike macroscopic or classical crack problems, the asymptotic behavior of the near-tip field such as stresses and displacements of relatively small-sized cracks is quite complex due to the dominated small-scale effects and still unclear from various existing literatures. Lack of this essential near-tip information, as a result, poses a major problem in the development of numerical techniques where the form of the solution must be pre-assumed (e.g., standard finite element methods and boundary integral equation techniques). This present research should partially fulfill this gap of knowledge by offering the fundamental understanding of the complete elastic field in the vicinity of the crack-tip accounting the small-scale effect. Although the current investigation focuses mainly on a two-dimensional problem with a simple crack geometry and a simplified model for treating small-scale influence, all involved methodology and useful findings can be carried to more general problems.

CHAPTER II

PROBLEM FORMULATION

This chapter presents the clear description and statement of the research problem, the domain decomposition technique used to decompose a cracked body into the bulk and surface parts, and the derivation of the key governing equations for the surface layers, the bulk material, and the whole cracked body.

2.1 Problem Description

Let us focus attention to a two-dimensional infinite body Ω containing a straight crack of a finite length $2a$ as illustrated in Figure 2.1. The crack geometry, in its undeformed state, is fully described by two geometrically coincident, straight lines S_c^+ and S_c^- with corresponding outward unit normal vectors \mathbf{n}^+ and \mathbf{n}^- , respectively. The entire cracked medium is made of a homogeneous, isotropic, linear elastic material with prescribed Poisson ratio ν and elastic shear modulus μ . Two material layers of zero thickness, one attached to the top crack line S_c^+ and the other adhered to the bottom crack line S_c^- , possess zero surface elastic constants and a constant residual surface tension τ^s . The body is loaded by arbitrarily distributed normal tractions t_0^+ on the top crack line S_c^+ and t_0^- on the bottom crack line S_c^- whereas both the body force and remote loading are absent. In the present study, only self-equilibrated applied tractions are considered, i.e., $t_0^+ = -t_0^-$.

For a purpose of representing all involved quantities and equations in the development to follow, a two-dimensional, reference Cartesian coordinate system $\{\mathbf{0}; x_1, x_2\}$ with the origin $\mathbf{0}$ at the center of the crack, the x_1 -axis directing along the crack-line, and the x_2 -axis directing normal to the crack-line (i.e., parallel to the normal vector \mathbf{n}^-) as indicated in Figure 2.1 is introduced. Standard indicial notations within the context of two-dimensional settings are also applied and, in particular, Greek

symbols are used throughout as indices unless stated otherwise and they take the value 1 and 2.

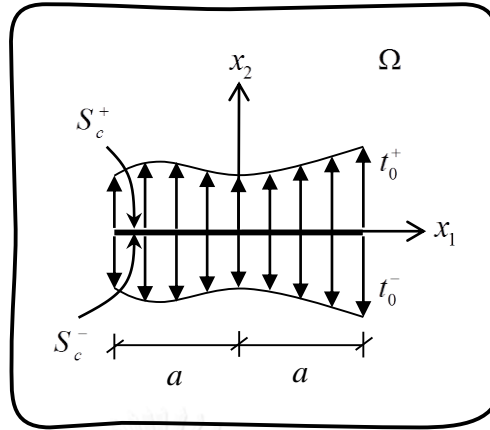


Figure 2.1: Schematic of a finite straight crack embedded in a two-dimensional, infinite medium and subjected to arbitrarily normal traction.

2.2 Domain Decomposition

To formulate the corresponding boundary value problem, the cracked medium is first divided into three portions: (i) a zero-thickness material layer on the top crack line S_c^+ (see Figure 2.2(b)), (ii) a zero-thickness material layer on the bottom crack line S_c^- (see Figure 2.2(c)), and (iii) the remaining bulk medium $\bar{\Omega}$ (see Figure 2.2(a)). According to this decomposition, the bulk medium is clearly homogeneous and, in addition, its geometry is identical to that of the original cracked body since the two material layers possess a zero thickness. The material layer S_c^+ is viewed as a line with two sides subjected to the known traction t_0^+ at the bottom and the unknown normal traction t_2^{+s} exerted by the bulk material at the top. Also, the material layer S_c^- is considered as a line with two sides subjected to the known traction t_0^- at the top and the unknown normal traction t_2^{-s} exerted by the bulk material at the bottom. The bulk cracked medium is subjected to the unknown normal tractions t_2^{+b} and t_2^{-b} exerted by the material layers on the crack lines S_c^+ and S_c^- . Since both material layers are adhered perfectly to the bulk medium, the tractions and displacements are continuous on the material interface, i.e.

$$u_{\alpha}^{+b}(x_1, x_2 = 0) = u_{\alpha}^{+s}(x_1), \quad x_1 \in [-a, a] \quad (2.1)$$

$$u_{\alpha}^{-b}(x_1, x_2 = 0) = u_{\alpha}^{-s}(x_1), \quad x_1 \in [-a, a] \quad (2.2)$$

$$t_2^{+b}(x_1) + t_2^{+s}(x_1) = 0, \quad x_1 \in [-a, a] \quad (2.3)$$

$$t_2^{-b}(x_1) + t_2^{-s}(x_1) = 0, \quad x_1 \in [-a, a] \quad (2.4)$$

where u_{α}^{+b} and u_{α}^{-b} denote components of the displacement at the crack lines S_c^+ and S_c^- of the bulk medium, respectively, and u_{α}^{+s} and u_{α}^{-s} denote components of the displacement at the material layers S_c^+ and S_c^- , respectively. It can be further invoked from symmetry that the normal tractions exerted to the bulk and material layers are self-equilibrated, i.e., $t_2^{+b} + t_2^{-b} = 0$ and $t_2^{+s} + t_2^{-s} = 0$.

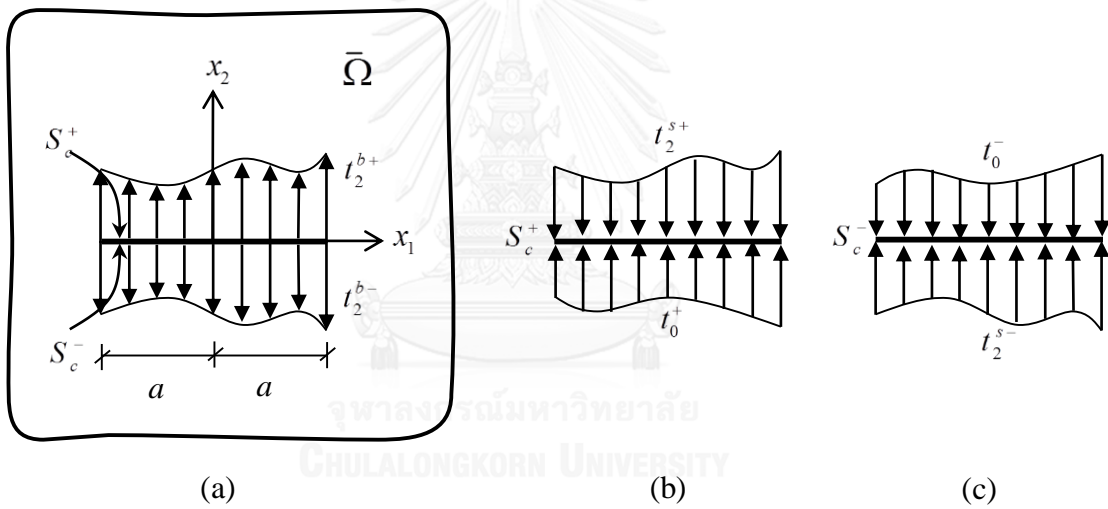


Figure 2.2: Schematic of (a) bulk cracked medium, (b) zero-thickness material layer S_c^+ , and (c) zero-thickness material layer S_c^- .

2.3 Basic Field Equations

A conventional linear theory of elasticity is adopted to derive the key equation governing the bulk cracked medium. For a two-dimensional, homogeneous, isotropic body with zero body force, basic field equations (e.g., in-plane strain-displacement relations, in-plane constitutive relations, and in-plane equilibrium equations) are given by

$$\sigma_{\beta\alpha,\beta}^b = 0 \quad (2.5)$$

$$\sigma_{11}^b = \mu \frac{\kappa+1}{\kappa-1} \varepsilon_{11}^b + \mu \frac{3-\kappa}{\kappa-1} \varepsilon_{22}^b \quad (2.6a)$$

$$\sigma_{22}^b = \mu \frac{3-\kappa}{\kappa-1} \varepsilon_{11}^b + \mu \frac{\kappa+1}{\kappa-1} \varepsilon_{22}^b \quad (2.6b)$$

$$\sigma_{12}^b = 2\mu \varepsilon_{12}^b \quad (2.6c)$$

$$\varepsilon_{\alpha\beta}^b = \frac{1}{2} (u_{\alpha,\beta}^b + u_{\beta,\alpha}^b) \quad (2.7)$$

where the subscript “*b*” is utilized to indicate quantities associated with the bulk medium; $\sigma_{\alpha\beta}$, $\varepsilon_{\alpha\beta}$, and u_α denote the in-plane components of stress and strain tensors and displacement vector, respectively; $\kappa = 3 - 4\nu$ for plane strain problems and $\kappa = (3 - \nu) / (1 + \nu)$ for plane stress problems; and $f_{,\alpha}$ denotes the partial derivative of a function f with respect to the coordinate x_α . The field equations (2.5)-(2.7) are essential for the development of fundamental results (e.g., dislocation solutions) useful for formulating the governing equations of the bulk cracked medium.

To describe the behavior of a zero-thickness material layer adhered perfectly to the bulk, Gurtin-Murdoch surface elasticity theory is utilized (e.g., Gurtin and Murdoch, 1975; Gurtin and Murdoch, 1978; Gurtin et al., 1998). For a material layer occupying a straight line in the x_1 -coordinate direction and possessing no in-plane stiffness, the basic field equations simply reduce to

$$\frac{d\sigma^s}{dx_1} + t_2^s + t_2^o = 0 \quad (2.8)$$

$$\sigma^s = \tau^s \frac{du_2^s}{dx_1} \quad (2.9)$$

where σ^s denotes the apparent out-of-plane stress component resulting from the presence of the residual surface tension; t_2^s denotes the normal traction exerted by the bulk material; and t_2^o denotes the prescribed normal traction on the layer. By combining (2.8) and (2.9), it leads to

$$\tau^s \frac{d^2 u_2^s}{dx_1^2} + t_2^s + t_2^o = 0 \quad (2.10)$$

2.4 Formulation of Governing Equations for Cracked Medium

By employing results of a semi-infinite straight dislocation in a two-dimensional, infinite medium (e.g., Barber, 1992) and the representation of a crack in terms of a continuous distribution of dislocations (e.g., Hirth and Lothe, 1982), the crack opening displacement of the bulk, defined by $\Delta u_2^b = u_2^{+b} - u_2^{-b}$, can be related to the applied normal traction on both crack lines by

$$t_2^{+b}(x_1) = -t_2^{-b}(x_1) = \frac{2\mu}{\pi(\kappa+1)} \int_{-a}^a \frac{1}{x_1 - \xi} \frac{d\Delta u_2^b}{d\xi} d\xi \quad (2.11)$$

It is worth noting that the integral appearing in (2.11) is strongly singular due to the involved kernel $1/(x_1 - \xi)$ and its value must be interpreted properly in the Cauchy principal sense.

By applying the ordinary differential equations (2.10) to the zero-thickness material layers S_c^+ and S_c^- , it results in

$$\tau^s \frac{d^2 u_2^{+s}}{dx_1^2} + t_2^{+s} + t_0^+ = 0 \quad (2.12)$$

$$\tau^s \frac{d^2 u_2^{-s}}{dx_1^2} + t_2^{-s} + t_0^- = 0 \quad (2.13)$$

Combing (2.12) and (2.13) and using the fact that $t_0^+ = -t_0^-$ and $t_2^{+s} = -t_2^{-s}$ yield

$$\tau^s \frac{d^2 \Delta u_2^s}{dx_1^2} + 2t_2^{+s} + 2t_0^+ = 0 \quad (2.14)$$

where $\Delta u_2^s = u_2^{+s} - u_2^{-s}$.

By enforcing the continuity conditions across the interfaces (2.1)-(2.4), the governing equation for the bulk medium (2.11) and that for the two material layers (2.14) can be combined to obtain the integro-differential equation governing the original cracked medium

$$\frac{1}{2} \tau^s \frac{d^2 \Delta u_2^b}{dx_1^2} + t_0^+ = \frac{2\mu}{\pi(\kappa+1)} \int_{-a}^a \frac{1}{x_1 - \xi} \frac{d\Delta u_2^b}{d\xi} d\xi \quad (2.15)$$

By further introducing following non-dimensional parameters $\Lambda = \tau^{so} / \mu$, $\bar{a} = a / \Lambda$, $\bar{\tau}^s = \tau^s / \tau^{so}$, $\bar{x} = x_1 / a$, $\bar{\xi} = \xi / a$, $\bar{t}_0 = t_0^+ / \mu$, $\Delta\bar{u} = \Delta u_2^b / a$ and $\bar{\kappa} = 4 / \pi(\kappa + 1)$ where τ^{so} is the reference residual surface tension, the above equation (2.15) can be expressed as

$$\frac{\bar{\tau}^s}{\bar{a}} \frac{d^2 \Delta\bar{u}}{d\bar{x}^2} + 2\bar{t}_0 = -\bar{\kappa} \int_{-1}^1 \frac{1}{\bar{\xi} - \bar{x}} \frac{d\Delta\bar{u}}{d\bar{\xi}} d\bar{\xi} \quad (2.16)$$

The integro-differential equation (2.16) is employed as the key governing equation of the given problem and its solution will be compared with Sendova and Walton (2010) discussed in chapter IV.

To construct an equivalent weak-form of (2.16), a standard weighted residual technique is adopted as indicated below. By multiplying (2.16) by a sufficiently well-behaved test function $\tilde{v} = \tilde{v}(\bar{x})$ and then integrating the result over the entire crack line, it yields

$$\frac{\bar{\tau}^s}{\bar{a}} \int_{-1}^1 \tilde{v} \frac{d^2 \Delta\bar{u}}{d\bar{x}^2} d\bar{x} + \int_{-1}^1 2\tilde{v}\bar{t}_0 d\bar{x} = -\bar{\kappa} \int_{-1}^1 \tilde{v} \int_{-1}^1 \frac{1}{\bar{\xi} - \bar{x}} \frac{d\Delta\bar{u}}{d\bar{\xi}} d\bar{\xi} d\bar{x} \quad (2.17)$$

By integrating the first term on the left hand side of (2.17) by parts and choosing the test function to satisfy the homogeneous conditions $\tilde{v}(-1) = \tilde{v}(1) = 0$ at the crack-tip, equation (2.17) now becomes

$$-\frac{\bar{\tau}^s}{\bar{a}} \int_{-1}^1 \frac{d\tilde{v}}{d\bar{x}} \frac{d\Delta\bar{u}}{d\bar{x}} d\bar{x} + \int_{-1}^1 2\tilde{v}\bar{t}_0 d\bar{x} = -\bar{\kappa} \int_{-1}^1 \tilde{v} \int_{-1}^1 \frac{1}{\bar{\xi} - \bar{x}} \frac{d\Delta\bar{u}}{d\bar{\xi}} d\bar{\xi} d\bar{x} \quad (2.18)$$

By utilizing the representation of the involved strongly singular kernel

$$\frac{1}{\bar{\xi} - \bar{x}} = -\frac{\partial}{\partial \bar{x}} \ln |\bar{\xi} - \bar{x}| \quad (2.19)$$

the integral equation (2.18) now takes the form

$$-\frac{\bar{\tau}^s}{\bar{a}} \int_{-1}^1 \frac{d\tilde{v}}{d\bar{x}} \frac{d\Delta\bar{u}}{d\bar{x}} d\bar{x} + \int_{-1}^1 2\tilde{v}\bar{t}_0 d\bar{x} = \bar{\kappa} \int_{-1}^1 \tilde{v} \frac{d}{d\bar{x}} \int_{-1}^1 \ln |\bar{\xi} - \bar{x}| \frac{d\Delta\bar{u}}{d\bar{\xi}} d\bar{\xi} d\bar{x} \quad (2.20)$$

By performing the integration by parts of the last term and then enforcing the homogeneous conditions of the test function, it finally leads to

$$-\frac{\bar{\tau}^s}{\bar{a}} \int_{-1}^1 \frac{d\bar{v}}{d\bar{x}} \frac{d\Delta\bar{u}}{d\bar{x}} d\bar{x} + \int_{-1}^1 2\bar{v}\bar{t}_0 d\bar{x} = -\bar{\kappa} \int_{-1}^1 \frac{d\bar{v}}{d\bar{x}} \int_{-1}^1 \ln|\bar{\xi} - \bar{x}| \frac{d\Delta\bar{u}}{d\bar{\xi}} d\bar{\xi} d\bar{x} \quad (2.21)$$

It is apparent that the resulting weak-form equation (2.21) contains a weakly singular kernel $\ln|\bar{\xi} - \bar{x}|$ and values of the singular integral can be interpreted in the sense of Riemann. The weak-form equation (2.21) forms the sufficient basis for the implementation of a solution procedure by Galerkin approximation.



CHAPTER III

SOLUTION PROCEDURE

In this chapter, a solution procedure based on Galerkin method is established to construct numerical solutions of the governing weak-form equation (2.21). Standard finite element procedures (e.g., Becker *et al.*, 1981; Bathe, 2006; Reddy, 1993) are also adopted in the discretization of the geometry of a crack, crack-face displacement and the test function.

3.1 Discretization

To construct numerical solutions of the weak-form equation (2.21), Galerkin approximation procedure is employed. Both the trial function $\Delta\bar{u} = \Delta\bar{u}(\bar{x})$ and the test function $\bar{v} = \bar{v}(\bar{x})$ are discretized by

$$\Delta\bar{u}(\bar{x}) = \sum_{i=1}^N \alpha_i \varphi_i(\bar{x}) \quad (3.1)$$

$$\bar{v}(\bar{x}) = \sum_{i=1}^N \beta_i \varphi_i(\bar{x}) \quad (3.2)$$

where $\varphi_i(\bar{x})$ are selected basis functions satisfying the conditions $\varphi_i(-1) = \varphi_i(1) = 0$; α_i are unknown constants; β_i are arbitrary constants; and N is the number of degrees of freedom. By substituting (3.1) and (3.2) into the weak-form equation (2.21) and then employing the arbitrariness of β_i , it yields a system of linear algebraic equations

$$\sum_{i=1}^N \Gamma_{ji} \alpha_i = P_j \quad j = 1, 2, 3, \dots, N \quad (3.3)$$

where

$$\Gamma_{ji} = \frac{\bar{\tau}^s}{\bar{a}} \int_{-1}^1 \frac{d\varphi_j}{d\bar{x}} \frac{d\varphi_i}{d\bar{x}} d\bar{x} - \bar{\kappa} \int_{-1}^1 \frac{d\varphi_j}{d\bar{x}} \int_{-1}^1 \ln|\bar{\xi} - \bar{x}| \frac{d\varphi_i}{d\bar{\xi}} d\bar{\xi} d\bar{x} \quad (3.4)$$

$$P_j = \int_{-1}^1 2\varphi_j(\bar{x}) \bar{t}_0(\bar{x}) d\bar{x} \quad (3.5)$$

It is evident from (3.4) that the coefficient matrix Γ is symmetric. Evaluation of Γ_{ji} and P_j can be achieved via a proper numerical quadrature; in particular, all regular single and double line integrals are integrated using standard Gaussian quadrature whereas the nearly singular and weakly singular double line integrals are evaluated using standard Gaussian quadrature along with a family of variable transformations. It is also important to remark that Γ_{ji} and P_j can also be obtained analytically for the case of piecewise polynomial basis functions.

Once the system of linear algebraic equations (3.3) is solved for all unknown constants α_i , the approximate crack-opening displacement can be obtained from (3.1) and other related quantities can then be post-processed as follows. For instance, the non-zero stress components within the bulk medium at any point $(x_1, 0)$, $|x_1| > a$ can readily be obtained from

$$\sigma_{\alpha\beta}(x_1, 0) = \int_{-a}^a \Sigma_{\alpha\beta}^2(x_1 - \xi, 0) \frac{d(\Delta u_2)}{d\xi} d\xi \quad (3.6)$$

where

$$\Sigma_{\alpha\beta}^2(x_1 - \xi, 0) = -\frac{2\mu}{\pi(\kappa + 1)} \frac{1}{x_1 - \xi} \quad (3.7)$$

By introducing the following non-dimensional parameters $\bar{x} = x_1/a$, $\bar{\xi} = \xi/a$, $\bar{\sigma}_{\alpha\beta} = \sigma_{\alpha\beta}/\mu$, $\Delta\bar{u} = \Delta u_2/a$, and $\bar{\kappa} = 4/\pi(\kappa + 1)$, equation (3.6) becomes

$$\bar{\sigma}_{11}^b(x_1, 0) = \bar{\sigma}_{22}^b(x_1, 0) = \frac{\bar{\kappa}}{2} \int_{-1}^1 \frac{1}{\bar{\xi} - \bar{x}} \frac{d\Delta\bar{u}}{d\bar{\xi}} d\bar{\xi} \quad (3.8)$$

3.2 Shape Functions

In the current investigation, the global basis functions $\varphi_i(\bar{x})$ are constructed locally using the finite element procedure. In particular, four types of elements including type-1 for C^0 -linear elements, type-2 for C^0 -quadratic elements, type-3 for C^0 -cubic elements and type-4 for C^1 -Hermite elements, as indicated in Figure 3.1, are employed to form the basis functions. These standard elements can be found in Becker et al. (1981), Bathe

(2006) and Reddy (1993). The element shape functions, for all four types of elements, are also summarized below.

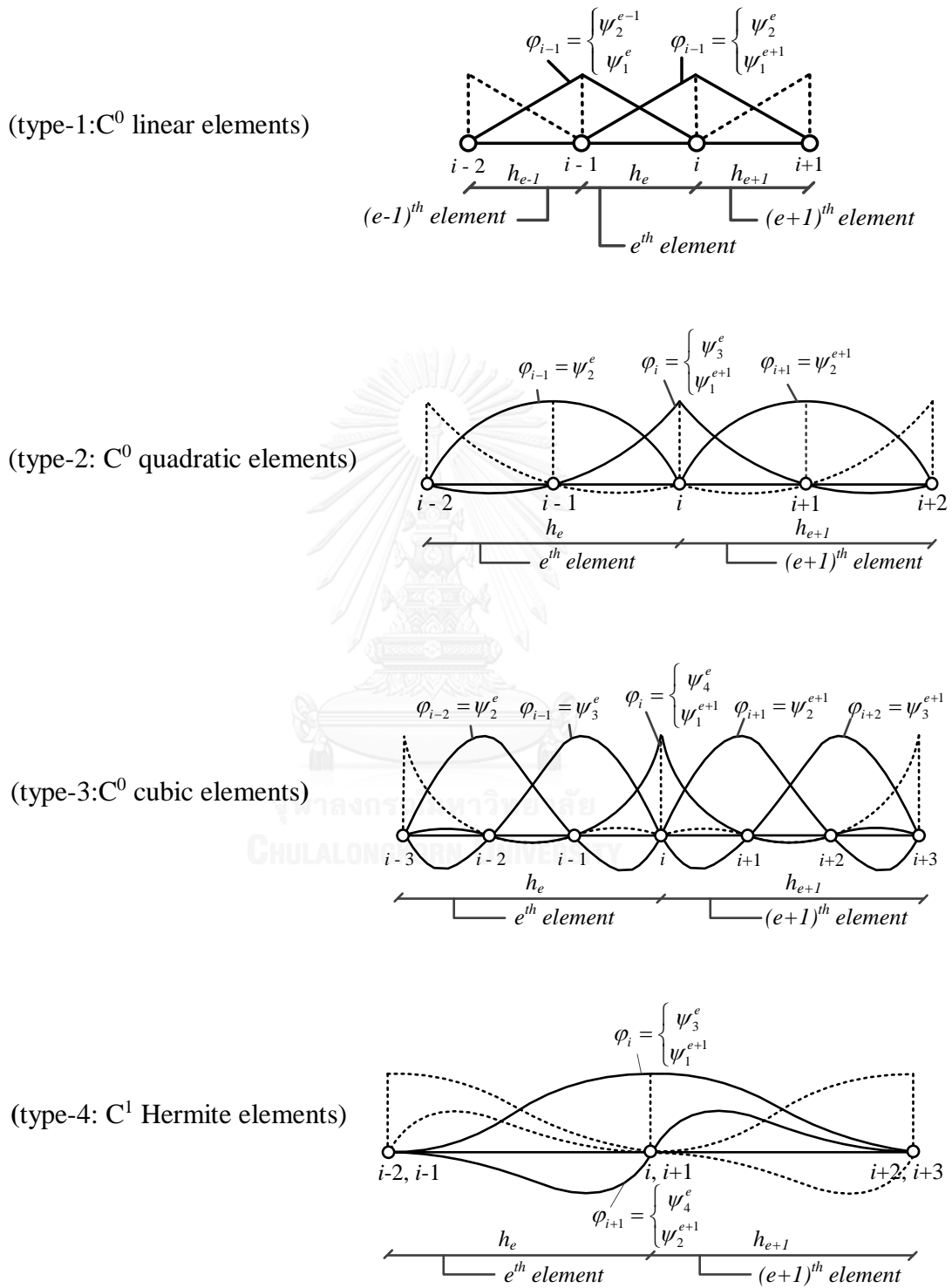


Figure 3.1. Schematic indicating the global basis functions and element shape functions for 4 types of elements.

- Type-1: Linear shape functions

$$\begin{aligned}\psi_1^e(s) &= 1 - s \\ \psi_2^e(s) &= s\end{aligned}\tag{3.9}$$

- Type-2: Quadratic shape functions

$$\begin{aligned}\psi_1^e(s) &= (1 - s)(1 - 2s) \\ \psi_2^e(s) &= 4s(1 - s) \\ \psi_3^e(s) &= -s(1 - 2s)\end{aligned}\tag{3.10}$$

- Type-3: Cubic shape functions

$$\begin{aligned}\psi_1^e(s) &= \frac{1}{2}(1 - s)(2 - 3s)(1 - 3s) \\ \psi_2^e(s) &= \frac{9}{2}s(1 - s)(2 - 3s) \\ \psi_3^e(s) &= \frac{9}{2}s(1 - s)(3s - 1) \\ \psi_4^e(s) &= \frac{1}{2}s(2 - 3s)(1 - 3s)\end{aligned}\tag{3.11}$$

- Type-4: Hermite shape functions

$$\begin{aligned}\psi_1^e(s) &= 1 - 3s^2 + 2s^3 \\ \psi_2^e(s) &= h_e s (s - 1)^2 \\ \psi_3^e(s) &= 2s^2 (3 - 2s) \\ \psi_4^e(s) &= h_e s^2 (s - 1)\end{aligned}\tag{3.12}$$

where $h_e = x_{i+1} - x_i$ is the length of a generic element $\Omega^e = (\bar{x}_i, \bar{x}_{i+1})$ and s is a local coordinate defined such that

$$s = \frac{\bar{x} - \bar{x}_i}{\bar{x}_{i+1} - \bar{x}_i} = \frac{\bar{x} - \bar{x}_i}{h_e}\tag{3.13}$$

To evaluate Γ_{ji} and P_j in an efficient manner, the computation is performed in an element level and their contribution to the global matrix and vector is achieved via standard direct assembly procedure.

3.3 Evaluation of involved integrals

From the discretization, entries of the coefficient matrix Γ and the vector \mathbf{P} can be obtained from the contribution of all elements as follows

$$\Gamma_{ji} = \sum_{e=1}^m \Gamma_{ji}^e + \sum_{p=1}^m \sum_{q=1}^m \Gamma_{ji}^{pq} \quad (3.14)$$

$$P_j = \sum_{e=1}^m P_j^e \quad (3.15)$$

where m is the number of elements and

$$\Gamma_{ji}^e = \frac{\bar{\tau}^s}{\bar{a}} \int_{\Omega_e} \frac{d\varphi_j}{d\bar{x}} \frac{d\varphi_i}{d\bar{x}} d\bar{x} \quad (3.16)$$

$$\Gamma_{ji}^{pq} = -\bar{k} \int_{\Omega_p} \frac{d\varphi_j}{d\bar{x}} \int_{\Omega_q} \ln |\bar{\xi} - \bar{x}| \frac{d\varphi_i}{d\bar{\xi}} d\bar{\xi} d\bar{x} \quad (3.17)$$

$$P_j^e = \int_{\Omega_e} 2\varphi_j(\bar{x}) \bar{t}_0(\bar{x}) d\bar{x} \quad (3.18)$$

It should be evident from (3.16) and (3.18) that the single line integrals Γ_{ji}^e and P_j^e over an element Ω^e contain the regular integrand and, as a result, they can readily be computed either by using standard Gaussian quadrature or by performing the direct integration for all four types of elements considered (see Appendix).

A double line integral Γ_{ji}^{pq} over a pair of elements (Ω^p, Ω^q) can be divided into two different cases depending mainly on such pair of elements obtained from the approximation of the crack line. The first type of integrals is associated with a pair of the same elements and the involved integrand, for this particular case, is clearly weakly singular. The other case corresponds to a pair of different elements and, in particular case, the integrand is either nearly singular or regular. To evaluate the double line integral Γ_{ji}^{pq} for both cases, an efficient numerical quadrature based on standard Gaussian quadrature and a family of transformation to remove the weak singularity and alleviate the near singularity can be employed. Alternatively, for all four types of elements considered in the current study, the direct integration of Γ_{ji}^{pq} can also be performed to obtain the closed-form expression (see Appendix).

CHAPTER IV

NUMERICAL RESULTS

To verify the formulation and solution procedure of the proposed method, a straight nano-sized crack under a self-equilibrated, uniformly distributed normal traction for the plain strain case is considered first. Results of the crack-face displacement gradient at the crack-tip are compared with existing benchmark solution proposed by Sendova and Walton (2010). Once the technique is fully tested, it is utilized as a computational tool in the investigation of the influence of residual surface tension and the size-dependent behaviors of predicted solutions. In addition, cracks under linearly distributed normal traction and quadratic normal traction are investigated.

In the analysis, four types of elements (i.e., type-1, type-2, type-3, and type-4) are employed. For each type of elements, several levels of the meshes are employed to fully explore the convergence behavior of numerical solutions. Poisson's ratio and Young's modulus for the bulk material and the residual surface tension are taken as $\nu = 0.3$, $E = 89.5 \text{ GPa}$ and $\tau^s = 0.9108 \text{ N/m}$, respectively. These material parameters are estimated properties of Al [1 1 1] obtained from the work of Miller and Shenoy (2000). It is convenient to introduce all quantities involved in the key governing integro-differential equation in a non-dimensional fashion. For instance, the crack length a is normalized by a special length scale $\Lambda = \tau^{so} / \mu = 0.03864 \text{ nm}$ (i.e., $\bar{a} = a / \Lambda$) where the reference residual surface tension is chosen identical to that utilized by Sharma and Ganti (2004) as $\tau^{so} = 1.3 \text{ N/m}$.

4.1 Crack under Uniform Normal Traction

As a demonstrative example, consider a crack subjected to a self-equilibrated, uniformly distributed normal traction t_0 as shown schematically in Figure 4.1.

4.1.1 Verification

A straight crack of a finite length in a two-dimensional, linearly elastic body under uniform far-field tensile load was previously studied by Sendova and Walton (2010).

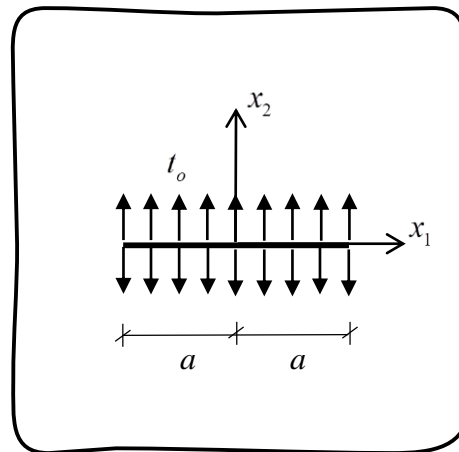


Figure 4.1. Schematic of straight crack of length $2a$ under self-equilibrated uniformly distributed normal traction.

It should be evident from the principle of superposition and the zero in-plane stiffness of the surface layer that the crack-face displacement of the crack under uniformly distributed normal traction is identical to that of the crack under the uniform remote tension of the same magnitude. This is due to the fact that there is no crack opening displacement introduced for the un-cracked case under the uniform far field and the stress field of the un-cracked medium containing the straight surface layers is trivially uniform. As a consequence, results presented in the work of Sendova and Walton (2010) are employed as the benchmark solution to verify the proposed numerical technique

Sendova and Walton (2010) formulated the governing integro-differential equation for a crack under the uniform remote tension and the influence of constant residual surface tension in a form

$$-\sigma - \gamma u_{2,11}^0(x,0) = \frac{E}{2(1-\nu^2)\pi} \int_{-1}^1 \frac{u_{2,1}^0(r,0)}{r-x} dr \quad (4.1)$$

where ν denotes the Poisson's ratio and E denotes the Young's modulus, x and r are non-dimensional length normalized by a half-crack length, u_2^0 is the displacement of the upper crack surface in the direction normal to the crack normalized by a half-crack length, and σ is the uniform remote tension. With the introduction of non-

dimensional parameters $\phi(x) = u_{2,1}^0(x)$, $\tilde{\sigma} = \sigma / E$, $\tilde{\gamma} = \gamma / E$ and $\zeta = 1/2(1 - \nu^2)$, the above equation becomes

$$\tilde{\gamma}\phi'(x) + \frac{\zeta}{\pi} \int_{-1}^1 \frac{\phi(r)}{r-x} dr = -\tilde{\sigma}, \quad x \in [-1, 1] \quad (4.2)$$

The resulting equation (4.2) is known as a Cauchy singular, linear integro-differential equation and its solution has been studied by various investigators. For instance, Frankel (1995) derived the solution in terms of a series of Chebyshev polynomials whereas Abdou (2003) and Badr (2001) proposed the solution in terms of a series of Legendre polynomials. Moreover, numerical solutions for integro-differential equations of a similar type were also reported in Atkinson (1997) and Saranen and Vainikko (2013). Most of them assumed the unknown solution $\phi(x)$ in a form of an finite series of polynomial-based basis functions

$$\phi(x) = \sum_{n=0}^{\infty} C_n P_n(x) \quad (4.3)$$

where the unknown coefficients C_n are determined based on a collocation technique or Galerkin-based methods and $P_n(x)$ are polynomial-base basis functions such as the Legendre polynomials and Chebyshev polynomials which satisfy the orthogonal condition. The assumed infinite series solution (4.3) results in an infinite system of linear equations and the convergence of approximate solution depends primarily on the truncation of terms in the series. Unlike those existing studies, in the present investigation, the unknown solution is discretized using the finite element approximation along with the classical Galerkin method.

It is worth noting that the key governing equation (2.16) can also be rewritten in terms of $\phi(x)$ as

$$\frac{\bar{\tau}^s}{\bar{a}} \phi'(x) + \bar{\kappa} \int_{-1}^1 \frac{\phi(\bar{\xi})}{\bar{\xi} - \bar{x}} d\bar{\xi} = -\bar{t}_0 \quad (4.4)$$

Since the two governing equations (4.2) and (4.4) are essentially identical, the following relations of all involved parameters are obtained:

$$\mu\bar{k} = \frac{E\zeta}{\pi} \Rightarrow \bar{k} = \frac{E\zeta}{\mu\pi} = \frac{2\zeta(1+\nu)}{\pi} = \frac{1}{\pi(1-\nu)} \quad (4.5)$$

$$\mu\bar{k} = \frac{E\zeta}{\pi} \Rightarrow \bar{k} = \frac{E\zeta}{\mu\pi} = \frac{2\zeta(1+\nu)}{\pi} = \frac{1}{\pi(1-\nu)} \quad (4.6)$$

$$\mu\bar{t}_o = E\tilde{\sigma} \Rightarrow \bar{t}_o = \frac{E\tilde{\sigma}}{\mu} = 2\tilde{\sigma}(1+\nu) \quad (4.7)$$

The relations (4.5)-(4.7) are utilized to choose the parameters in the simulations to allow the comparison with results by Sendova and Walton (2010).

In the verification, numerical results for the crack-face displacement gradient $d\bar{u}/d\bar{x}$ at the crack-tip are obtained for four type of elements. To examine the convergence behavior of computed numerical solutions, various levels of mesh refinement for each type of elements starting from that containing 2 identical elements to that containing 2048 identical elements are adopted. Results are compared with Sendova and Walton (2010) for three values of the non-dimensional remote loading parameter $\tilde{\sigma} = 0.001, 0.002, 0.004$ and the normalized residual surface tension $\tilde{\gamma} = 0.05$ as reported in Tables 4.1, 4.2 and 4.3, respectively. Using the values of $\tilde{\sigma}$ and $\tilde{\gamma}$ indicated above together with the relations (4.5)-(4.7) yields the following parameters employed in the present simulations: $\bar{\tau}^s / \bar{a} = 2\tilde{\gamma}(1+\nu) = 0.133$, $\bar{k} = 1/[\pi(1-\nu)] = 0.475$, $\bar{t}_o = 2\tilde{\sigma}(1+\nu) = 0.00266, 0.00532, 0.01064$. It is evident from the obtained results that the crack-face displacement gradient at the crack-tip agrees very well with the available existing solution when the mesh is sufficiently refined. This partially serves as the verification of the proposed technique.

The crack-face displacement gradient profile for different values of residual surface tensions and applied normal traction are also reported in Figure 4.2 and Figure 4.3 along with the benchmark solution generated by Sendova and Walton (2010). One can observe that the difference between results is nearly indistinguishable. From the numerical experiments, it is seen that the derivative of the crack-face displacement increases when the magnitude of the applied traction increases but decreases when the magnitude of the residual surface tension increases. In addition, Sendova and Walton

(2010) concluded that the opening angle at the crack tip becomes finite and the stress along the crack front has a logarithmic singularity.

Table 4.1. Values of $d\bar{u}/d\bar{x}$ at the crack tip for $\bar{\tau}^s / \bar{a} = 0.133$ and $\bar{t}_o = 0.00266$.

$\tilde{\gamma};$ $\bar{\tau}^s / \bar{a}$	$\tilde{\sigma};$ \bar{t}_o	Number of elements	Type-1 $\frac{d\bar{u}}{d\bar{x}}(1,0)$	Type-2 $\frac{d\bar{u}}{d\bar{x}}(1,0)$	Type-3 $\frac{d\bar{u}}{d\bar{x}}(1,0)$	Type-4 $\frac{d\bar{u}}{d\bar{x}}(1,0)$	Sendova &Walton $u_{2,1}(1,0)$ (400 terms)
0.05; 0.133	0.001; 0.00266	2	-0.00168	-0.00358	-0.00463	-0.00442	-0.0069
		4	-0.00257	-0.00449	-0.00549	-0.00541	
		8	-0.00353	-0.00535	-0.00613	-0.00608	
		16	-0.00443	-0.00600	-0.00652	-0.00649	
		32	-0.00521	-0.00643	-0.00673	-0.00672	
		64	-0.00581	-0.00667	-0.00684	-0.00683	
		128	-0.00624	-0.00681	-0.00687	-0.00687	
		256	-0.00652	-0.00687	-0.00689	-0.00689	
		512	-0.00669	-0.00689	-0.00692	-0.00692	
		1024	-0.00680	-0.00691	-0.00693	-0.00693	
		2048	-0.00690	-0.00693	-0.00694	-0.00694	

Table 4.2. Values of $d\bar{u}/d\bar{x}$ at the crack tip for $\bar{\tau}^s / \bar{a} = 0.133$ and $\bar{t}_o = 0.00532$.

$\tilde{\gamma};$ $\bar{\tau}^s / \bar{a}$	$\tilde{\sigma};$ \bar{t}_o	Number of elements	Type-1 $\frac{d\bar{u}}{d\bar{x}}(1,0)$	Type-2 $\frac{d\bar{u}}{d\bar{x}}(1,0)$	Type-3 $\frac{d\bar{u}}{d\bar{x}}(1,0)$	Type-4 $\frac{d\bar{u}}{d\bar{x}}(1,0)$	Sendova& Walton $u_{2,1}(1,0)$ (400 terms)
0.05; 0.133	0.002; 0.00532	2	-0.00338	-0.00719	-0.00931	-0.00885	-0.0139
		4	-0.00514	-0.00904	-0.01104	-0.01088	
		8	-0.00710	-0.01076	-0.01231	-0.01222	
		16	-0.00891	-0.01206	-0.01309	-0.01304	
		32	-0.01044	-0.01291	-0.01351	-0.01345	
		64	-0.01164	-0.01339	-0.01373	-0.01371	
		128	-0.01252	-0.01366	-0.01383	-0.01382	
		256	-0.01309	-0.01375	-0.01385	-0.01385	
		512	-0.01344	-0.01385	-0.01390	-0.01390	
		1024	-0.01365	-0.01390	-0.01392	-0.01392	
		2048	-0.01390	-0.01391	-0.01392	-0.01392	

Table 4.3. Values of $d\bar{u}/d\bar{x}$ at the crack tip for $\bar{\tau}^s / \bar{a} = 0.133$ and $\bar{t}_o = 0.01064$.

$\tilde{\gamma};$ $\bar{\tau}^s / \bar{a}$	$\tilde{\sigma};$ \bar{t}_o	Number of elements	Type-1 $\frac{d\bar{u}}{d\bar{x}}(1,0)$	Type-2 $\frac{d\bar{u}}{d\bar{x}}(1,0)$	Type-3 $\frac{d\bar{u}}{d\bar{x}}(1,0)$	Type-4 $\frac{d\bar{u}}{d\bar{x}}(1,0)$	Sendova& Walton $u_{2,1}(1,0)$ (400 terms)
0.05; 0.133	0.004; 0.01064	2	-0.00672	-0.01430	-0.01850	-0.01770	-0.0278
		4	-0.01027	-0.01797	-0.02197	-0.02164	
		8	-0.01411	-0.02142	-0.02451	-0.02432	
		16	-0.01773	-0.02402	-0.02608	-0.02597	
		32	-0.02083	-0.02571	-0.02692	-0.02687	
		64	-0.02324	-0.02670	-0.02735	-0.02732	
		128	-0.02494	-0.02723	-0.02765	-0.02765	
		256	-0.02607	-0.02754	-0.02774	-0.02775	
		512	-0.02685	-0.02773	-0.02775	-0.02780	
		1024	-0.02725	-0.02775	-0.02781	-0.02782	
2048	-0.02780	-0.02780	-0.02782	-0.02782			

In the theory of finite element approximation, the finite element solution $\Delta\bar{u}_h$ is said to converge to the true solution $\Delta\bar{u}$ with respect to the L_2 -norm if (Becker et al., 1981)

$$\|e\|_2 = \left\{ \int_{-1}^1 [e^2 + (e')^2] dx \right\}^{1/2} \leq Ch_e^p \quad (4.8)$$

where C is a constant independent of $\Delta\bar{u}$ and $\Delta\bar{u}_h$, h_e is the characteristic length of an element, the constant p denotes the rate of convergence, and the function $e = \Delta\bar{u}_h - \Delta\bar{u}$ is the error from the finite element approximation which is defined as the difference between the approximate and exact solutions. If p is positive then the error $\|e\|_2$ clearly approaches zero when h tends to zero. It can be said that the approximation converges to the exact solution with respect to the L_2 -norm when $\|e\|_2$ approaches zero.

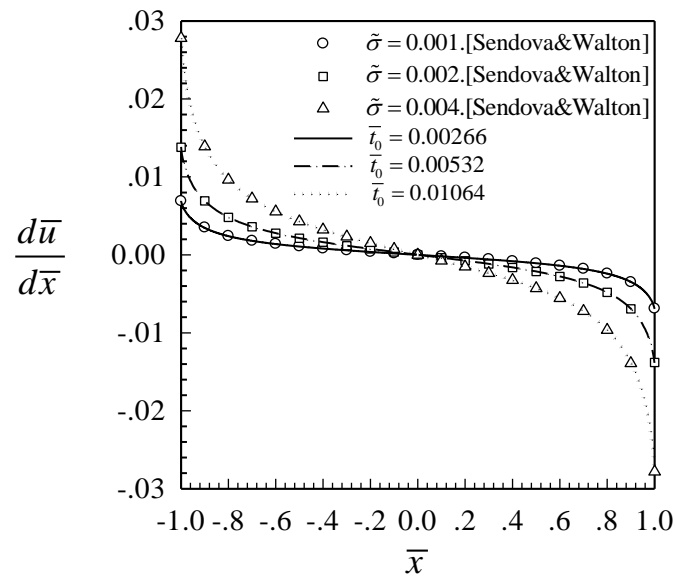


Figure 4.2. Profile of crack opening displacement gradient for straight crack under uniformly distributed normal traction for $\bar{\tau}_o = 0.00266, 0.00532, 0.01064$ and $\bar{\tau}^s / \bar{a} = 0.133$.

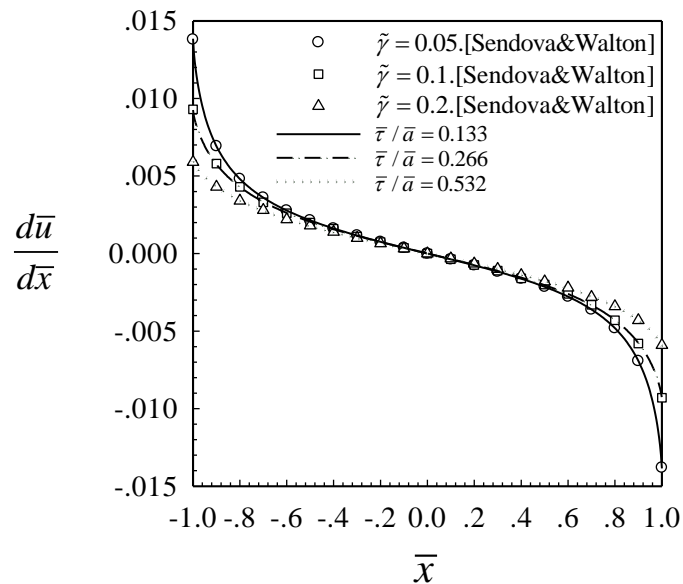


Figure 4.3. Profile of crack opening displacement gradient for straight crack under uniformly distributed normal traction for $\bar{\tau}^s / \bar{a} = 0.133, 0.266, 0.532$ and $\bar{\tau}_o = 0.00532$.

In equation (4.8), it is evident that the actual error can never be calculated unless the exact solution is known a priori; however, when $\Delta\bar{u}$ is unknown, it is possible to construct the estimate of the errors if it decreases as h_e decreases and the number of elements is sufficiently large. Based on extensive numerical experiments, using elements of type-2, type-3 and type-4 in the analysis yields better solutions in comparison with those of type-1 for the same level of mesh refinement. As a result, results obtained from elements of type-4 are employed as a reference solution in the error estimation.

To estimate the rate of convergence, the L_2 -norm error $\|e\|_2$ is plotted with the size of the element h_e in the log-log scale and the slope of a straight portion for sufficiently small h_e is taken as the value of p . Alternatively, the value of p can be also estimated from the following relation

$$\frac{\|e_{h_e}\|_2}{\|e_{h_e/2}\|_2} = \frac{Ch_e^p}{C(h_e/2)^p} = 2^p \quad (4.9)$$

where $\|e_{h_e}\|_2$ and $\|e_{h_e/2}\|_2$ are L_2 -norm errors associated with the uniform mesh containing elements of size h_e and $h_e/2$, respectively. The value of p obtained from (4.9) generally converges to a constant number when the size of the element h decreases to zero. The L_2 -norm error $\|e\|_2$ for all four types of elements with different sizes of elements is reported in Table 4.4 for $\bar{\tau}^s / \bar{a} = 1$ and $\bar{t}_o = 1$. These results indicate that elements of type-3 and type-4 yield almost the same errors for the same level of mesh refinement and better than those generated by elements of type-1 and type-2. The estimated rate of convergence for all four types of elements is also reported in Table 4.5. It can be concluded from this set of results that the rate of convergence for elements of type-2, type-3 and type-4 are approximately the same ($p \approx 1.5$) and is greater than that of elements of type-1 ($p \approx 1$). This implies that the solution has limited degree of smoothness since increasing the degree of polynomials in the approximation does not alter the rate of convergence. The log-log plot of the L_2 -norm error $\|e\|_2$ versus the size of the elements is also reported in Figure 4.4 for all types of elements. It can be seen

that the portion of each line becomes straight when the size of elements is sufficiently small. Results from the convergence study indicate that the proposed method yields the converged numerical solutions and elements of type-4 generally generate the best solutions. It is also found that the mesh containing 512 elements of type-4 is sufficient for obtaining accurate results and then it is utilized to generate results in the parametric study.

Table 4.4. L_2 -norm error $\|e\|_2$ for $\bar{\tau}^s / \bar{a} = 1$ and $\bar{t}_o = 1$.

Number of elements	h	$\ e\ _E$			
		Type-1	Type-2	Type-3	Type-4
2	1	4.1425×10^{-1}	9.5756×10^{-2}	4.0075×10^{-2}	4.5800×10^{-2}
4	1/2	2.3362×10^{-1}	4.5618×10^{-2}	1.5170×10^{-2}	1.6677×10^{-2}
8	1/4	1.2846×10^{-1}	1.9045×10^{-2}	5.4275×10^{-3}	5.9815×10^{-3}
16	1/8	6.8290×10^{-2}	7.3367×10^{-3}	1.8826×10^{-3}	2.0832×10^{-3}
32	1/16	3.5404×10^{-2}	2.6924×10^{-3}	6.4845×10^{-4}	7.1843×10^{-4}
64	1/32	1.8068×10^{-2}	9.6192×10^{-4}	2.2427×10^{-4}	2.4838×10^{-4}
128	1/64	9.1365×10^{-3}	3.3921×10^{-4}	7.8080×10^{-5}	8.6405×10^{-5}
256	1/128	4.5965×10^{-3}	1.1902×10^{-4}	2.7335×10^{-5}	3.0228×10^{-5}
512	1/256	2.3060×10^{-3}	4.1725×10^{-5}	9.5990×10^{-6}	1.0611×10^{-5}
1024	1/512	1.1551×10^{-3}	1.4637×10^{-5}	3.3560×10^{-6}	3.7122×10^{-6}
2048	1/1024	5.7811×10^{-3}	5.1173×10^{-6}	1.1785×10^{-6}	1.3031×10^{-6}

Table 4.5. Rate of convergence p for $\bar{\tau}^s / \bar{a} = 1$ and $\bar{t}_o = 1$.

Number of elements	h	The rate of convergence p			
		Type-1	Type-2	Type-3	Type-4
2	1	0.826	1.070	1.402	1.458
4	1/2	0.863	1.260	1.483	1.479
8	1/4	0.912	1.376	1.528	1.522
16	1/8	0.948	1.446	1.538	1.536
32	1/16	0.970	1.485	1.532	1.532
64	1/32	0.984	1.504	1.522	1.523
128	1/64	0.991	1.511	1.514	1.515
256	1/128	0.995	1.512	1.510	1.510
512	1/256	0.997	1.511	1.516	1.515
1024	1/512	0.999	1.516	1.510	1.510

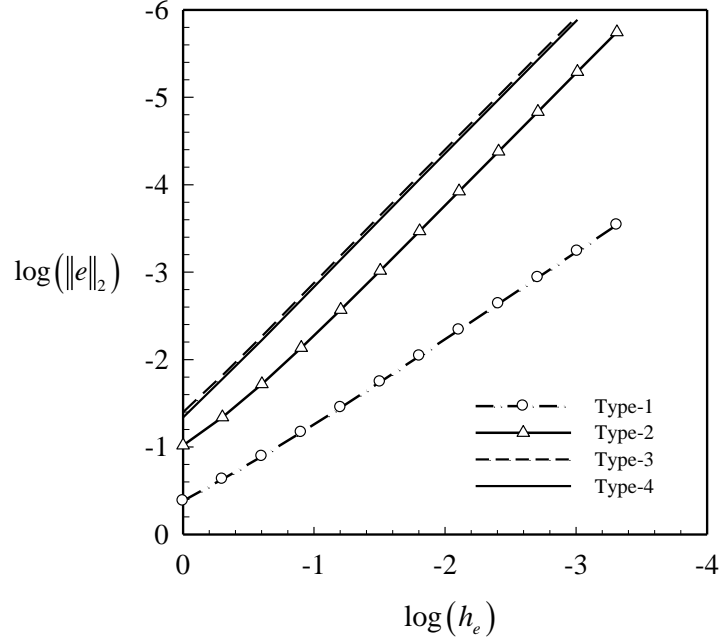


Figure 4.4. Log-log plots of L_2 -norm error $\|e\|_2$ versus the element size h_e for $\bar{\tau}^s / \bar{a} = 1$ and $\bar{t}_o = 1$.

The classical case (i.e., $\bar{\tau}^s = 0$) is also considered in the present study where results can be used not only in the verification of the formulation and implementations but also in the comparison of results to demonstrate the role of the residual surface tension. The normalized crack opening displacement $\Delta \bar{u} / \bar{t}_o$ and the normalized normal stress components $\bar{\sigma}_{11}^b / \bar{t}_o = \bar{\sigma}_{22}^b / \bar{t}_o$ with $\bar{t}_o = t_o / \mu$ for $\bar{a} = 10$ are obtained using a mesh with 512 elements of type-4 and reported in Figures 4.5. It can be seen that the obtained results for the classical case (without the residual surface tension), the crack-face displacement and the near-tip stress field agree very well with the available exact solution (e.g., Tada *et al.*, 2000) when the mesh is sufficiently refined.

4.1.2 Parametric study

From an extensive survey of literatures, the residual surface tension has been found to play an important role in characterizing the properties of nano-materials and many researchers have attempted to collect such parameter for various types of materials.

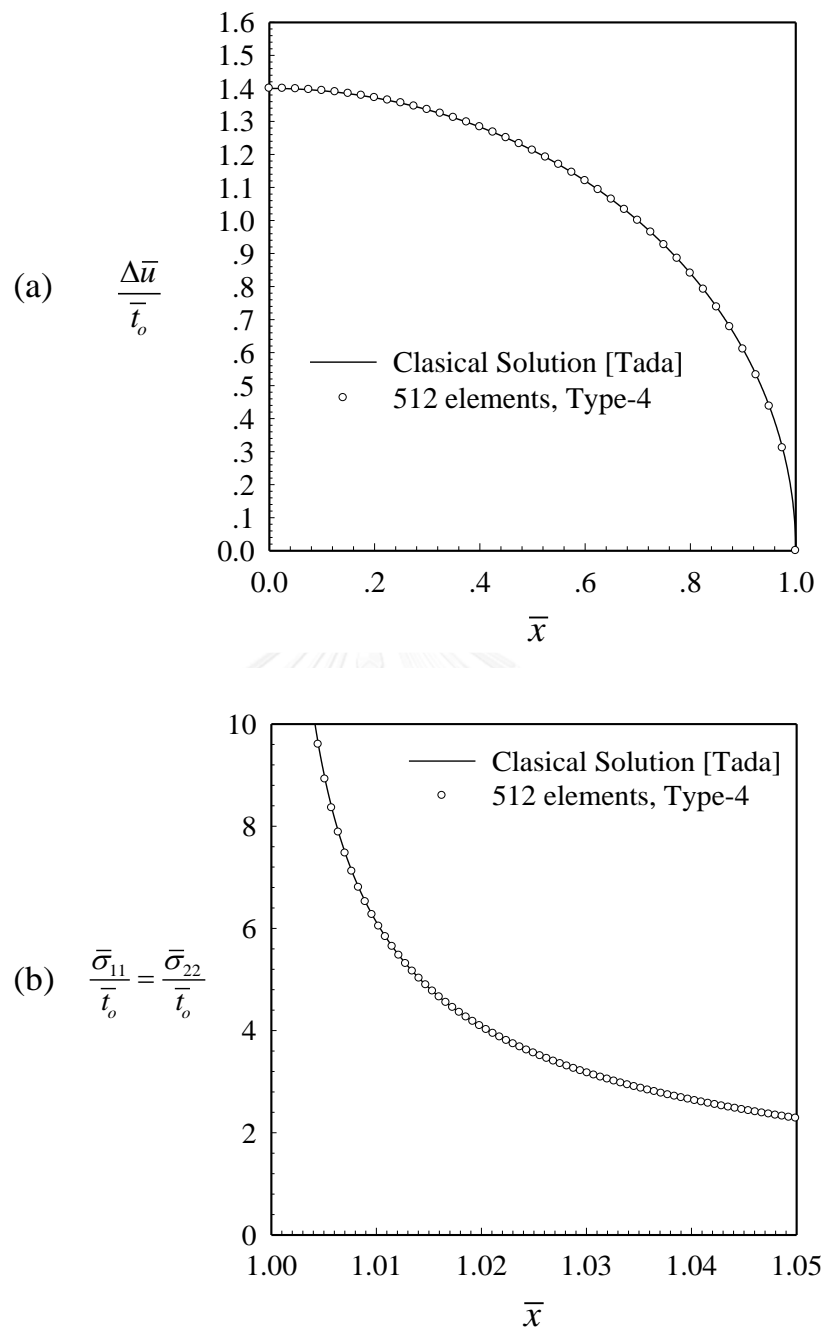


Figure 4.5. (a) Normalized crack opening displacement and (b) normalized normal stress components along the x_1 -axis for crack under uniformly distributed normal traction without the residual surface tension and for $E = 89.5 \text{ GPa}$, $\nu = 0.3$.

For instance, Keene (1993) published a review of the residual surface tension data for various metallic materials; Vinet et al. (2002) have given reference values for the elements; and, more recently, Mills and Su (2006) reviewed the residual surface tension

data for pure metals. The residual surface tension data is available for a family of metals such as Al, Cu, Co, Cr, Fe, Gd, Ge, Hf, Ir, Mo, Mn, Nb, Ni, Os, Pd, Pt, Pl, Re, Rh, Ro, Si, Ta, Ti, U, W, V, and Zr. Existing data of the residual surface tension have indicated its range from 0.007 N/m to 2.6 N/m. In the present investigation, the range of the normalized residual surface tension $\bar{\tau}^s$ is taken as follows:

$$0.005 < \bar{\tau}^s = \frac{\tau^s}{\tau^{so}} < 2 \quad (4.10)$$

where $\tau^{so} = 1.3 \text{ N/m}$ and $0.007 \text{ N/m} \leq \tau^s \leq 2.6 \text{ N/m}$.

Within the context of nano-structured materials, the study of nano-scale fracture mechanisms has been discussed in various literatures (e.g., Wunderlich and Awaji, 2001; Celarie et al., 2003; Gao et al., 2003; Sharma et al., 2003; Guin and Wiederhorn, 2004). Wunderlich and Awaji (2001) used the molecular dynamics simulation to estimate the fracture toughness of Al_2O_3 with an initial crack of length $2a \approx 1 \text{ nm}$. Moreover, Sharma *et al.* (2003) showed that for structures with their size greater than 100 nm, the surface-to-volume ratio is typically negligible and the effective properties are sufficiently governed by a classical bulk material with given Young's modulus and Poisson's ratio. In the present study, the following range of normalized crack length $\bar{a} = a / \Lambda$ was used:

$$10 < \bar{a} = \frac{a}{\Lambda} < 2500 \quad (4.11)$$

where $\Lambda = \tau^{so} / \mu = 0.03864 \text{ nm}$ and $0.5 \text{ nm} \leq a \leq 100 \text{ nm}$.

To demonstrate the role of the residual surface tension, the normalized crack-face displacement and normalized near-tip stress for $\bar{a} = 10$ and five different values of the normalized residual surface tension $\bar{\tau}^s$ ranging from 0.005 to 2 are generated and reported in Figure 4.6. As the residual surface tension increases, the value of $\Delta\bar{u} / \bar{t}_o$ increases in the range of $1.1 < \Delta\bar{u} / \bar{t}_o < 1.4$, as shown in Figure 4.6(a). In addition, the normalized normal stress along the x_1 -axis is significantly less than that of the classical case when $\bar{\tau}^s$ increases in range of $0 < \bar{\tau}^s < 0.5$ (see Figure 4.6(b)). It can be concluded from these results that the residual surface tension not only significantly reduces the crack-face displacement over the whole crack line and the near-tip stress

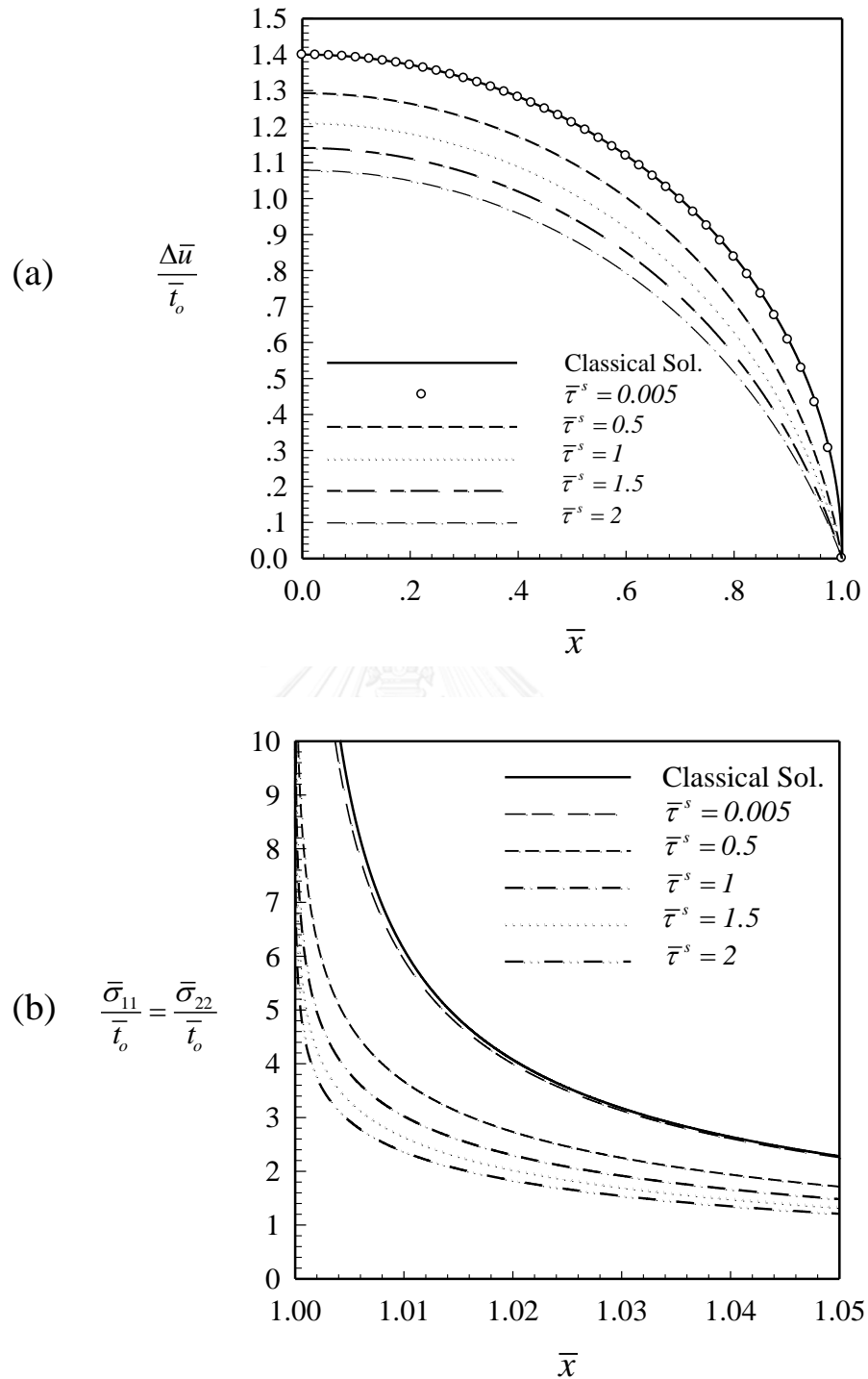
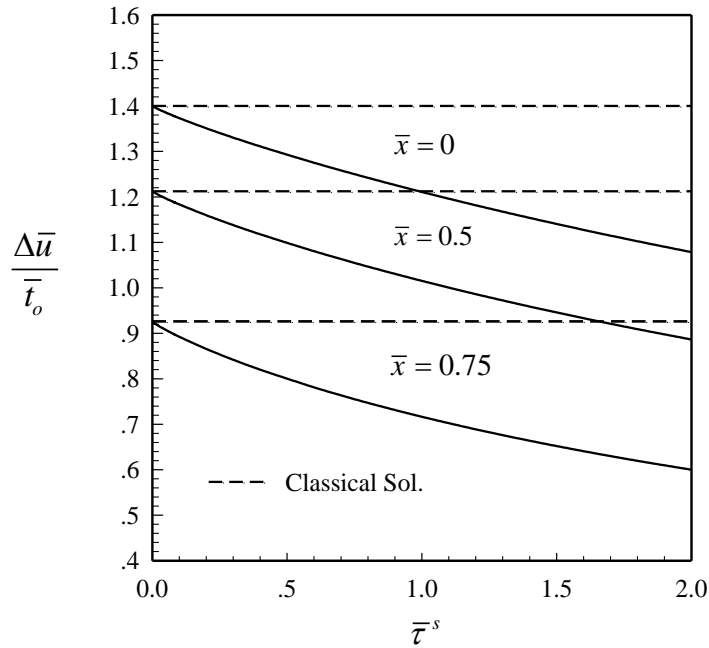
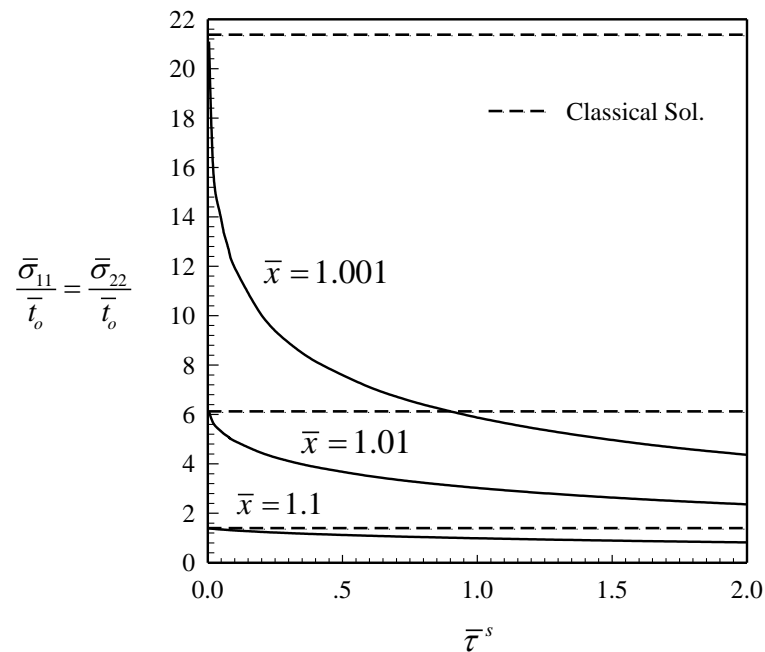


Figure 4.6. (a) Normalized crack opening displacement and (b) normalized normal stress components along the x_1 -axis of straight crack under uniformly distributed normal traction for five different values of $\bar{\tau}^s$ ranging from 0.005 to 2 and for $E = 89.5 \text{ GPa}$ and $\nu = 0.3$.



Figures 4.7. Normalized crack opening displacement $\Delta \bar{u} / \bar{t}_o$ for $\bar{x} = 0, 0.5, 0.75$ versus normalized residual surface tension $\bar{\tau}^s$ of straight crack under uniformly distributed normal traction for $E = 89.5 \text{ GPa}$, $\nu = 0.3$ and $\bar{a} = 10$.



Figures 4.8. Normalized normal stress components $\bar{\sigma}_{11} / \bar{t}_o = \bar{\sigma}_{22} / \bar{t}_o$ for $\bar{x} = 1.001, 1.01, 1.1$ versus normalized residual surface tension $\bar{\tau}^s$ of straight crack under uniformly distributed normal traction for $E = 89.5 \text{ GPa}$, $\nu = 0.3$ and $\bar{a} = 10$.

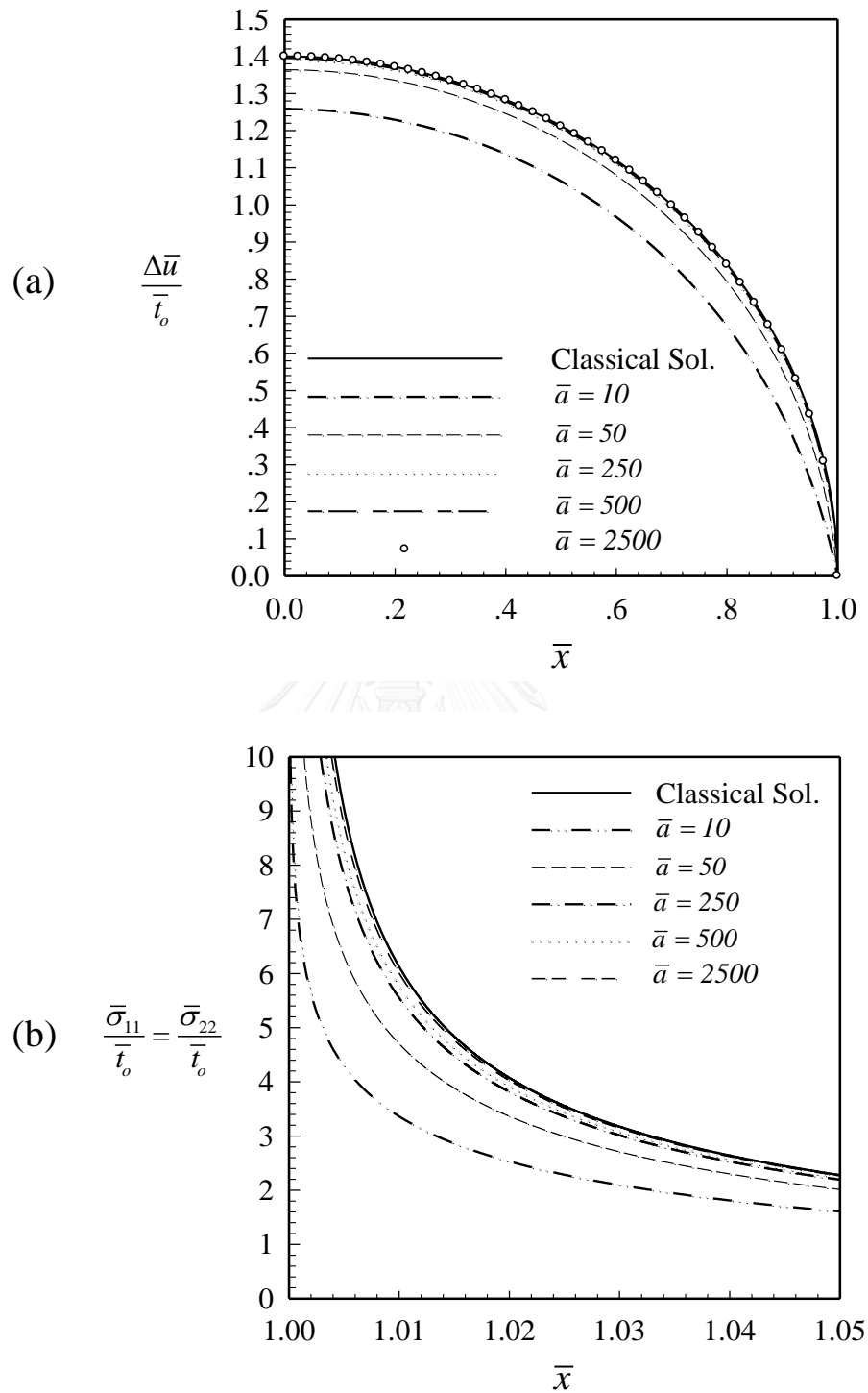
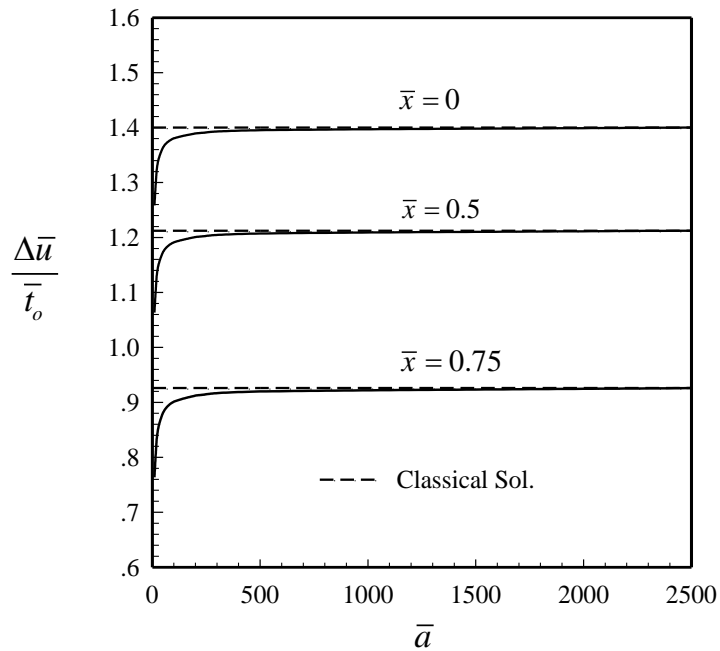
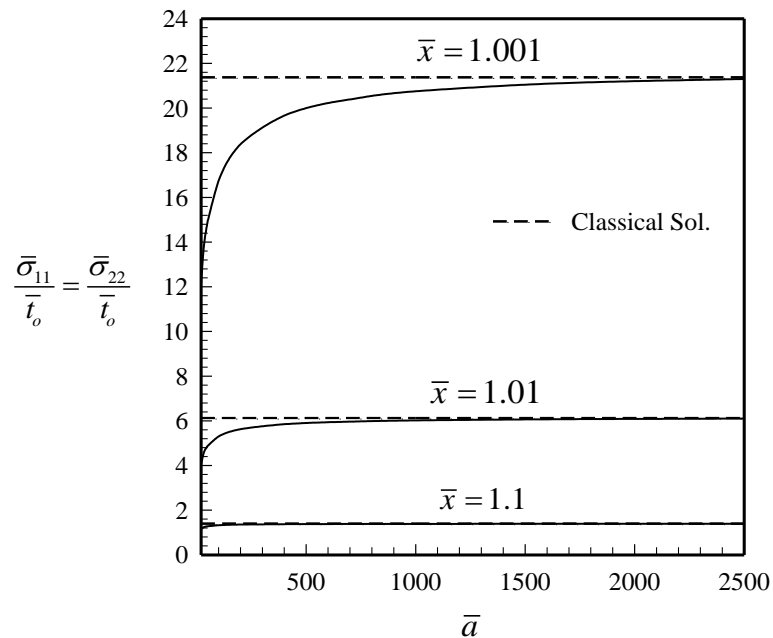


Figure 4.9. (a) Normalized crack opening displacement and (b) normalized normal stress components along the x_1 -axis for straight crack under uniformly distributed normal for five different values of $\bar{a} = a/\Lambda = 10, 50, 250, 500, 2500$ and for $E = 89.5 \text{ GPa}$ and $\nu = 0.3$.



Figures 4.10. Normalized crack opening displacement $\Delta \bar{u} / \bar{t}_o$ for $\bar{x} = 0, 0.5, 0.75$ versus normalized crack length \bar{a} of straight crack under uniformly distributed normal traction for $E = 89.5 \text{ GPa}$, $\nu = 0.3$ and $\bar{\tau}^s = 0.7$.



Figures 4.11. Normalized normal stress components $\bar{\sigma}_{11} / \bar{t}_o = \bar{\sigma}_{22} / \bar{t}_o$ for $\bar{x} = 1.001, 1.01, 1.1$ versus normalized crack length \bar{a} of straight crack under uniformly distributed normal traction for $E = 89.5 \text{ GPa}$, $\nu = 0.3$ and $\bar{\tau}^s = 0.7$.

but also alters the crack-tip stress singularity; i.e., the classical square-root singularity is weakened. In particular, when $\bar{\tau}^s$ becomes greater, the deviation of predicted solutions from those of the classical case (i.e., $\bar{\tau}^s = 0$) is more significant and, clearly, presence of the residual surface tension renders the elastic medium much stiffer.

Figure 4.7 reports the relation between the normalized crack-face displacement and the normalized residual surface tension $\bar{\tau}^s$ for $\bar{a} = 10$. With the increasing of $\bar{\tau}^s$ ranging from 0 to 2, values of the normalized crack-face displacement decrease evidently. The normalized crack-face displacements essentially approach those of the classical case when the residual surface tension becomes negligible ($\bar{\tau}^s = 0$). It is also seen that presence of the residual surface tension, the normalized near-tip stress at $\bar{x} = 1.001, 1.01, 1.1$ significantly reduces from that of the classical case (without the residual surface tension), as illustrated in Figure 4.8. In particular, the magnitude of $\bar{\sigma}_{11} / \bar{t}_o = \bar{\sigma}_{22} / \bar{t}_o$ in the neighborhood of the crack-tip at $\bar{x} = 1.001$ is much larger than that of $\bar{\sigma}_{11} / \bar{t}_o = \bar{\sigma}_{22} / \bar{t}_o$ at $\bar{x} = 1.001, 1.01$. It can then be concluded that the residual surface tension plays an important role in the reduction of the crack-face displacement and the near-tip stress of nano-sized cracks.

To further examine the size-dependent characteristics of the predicted solutions, the normalized relative crack-face displacement and normalized near-tip stress for five different values of normalized crack length $\bar{a} = 10, 50, 250, 500, 2500$ are reported in Figure 4.9 for both the classical case and that associated with $\bar{\tau}^s = 0.9108/1.3 = 0.7$. It can be seen that, unlike the classical case, the normalized crack opening displacement and normalized normal stress near the crack tip for $\bar{\tau}^s = 0.7$ exhibit strong size dependence. For instance, while the difference between normalized crack opening displacement for $\bar{a} = 250, 500, 2500$ cannot be well recognized, the value of the normalized crack opening displacement decreases rapidly when \bar{a} increases from 10 to 50 (see Figure 4.9(a)). Moreover, when the crack-size increases, the influence of the residual surface tension on the near-tip stress becomes less significant and results clearly approach those of the classical case as indicated in Figure 4.9(b). In other words, when the crack-size reduces to the nano-scale, the influence of the residual surface tension on the elastic responses can be remarkable.

Results shown in Figure 4.10 provide the information of the relationship between the normalized crack opening displacement and the normalized crack length \bar{a} . While the value of the normalized crack opening displacement for $\bar{\tau}^s = 0.7$ at $\bar{x} = 0, 0.5, 0.75$ increases rapidly when \bar{a} increasing from 0 to 500, the values rapidly approach the classical solution when \bar{a} increases from 500 to 2500. In particular, when the crack length increases to a certain value, the influence of the residual surface tension on the crack deformation becomes weak or even insignificant. Furthermore, the relation between the normalized normal stress components $\bar{\sigma}_{11} / \bar{t}_o = \bar{\sigma}_{22} / \bar{t}_o$ and the normalized crack length \bar{a} is also reported in Figure 4.11. For three different values of $\bar{x} = 1.001, 1.01, 1.1$, the classical case (i.e., $\bar{\tau}^s = 0$) yields the maximum value of the normalized near-tip stress. With the decrease of the crack length to a nano-scale, it can be remarked that the effect of the residual surface tension on the near-tip stress becomes significant.

4.2 Crack under Linear Normal Traction

In this section, a straight crack under a self-equilibrated, linearly distributed normal traction $t_2^o = t_o(|x|/a)$ as shown schematically in Figure 4.12 is investigated. Similar to the previous problem, the crack opening displacement for the entire crack line and the non-zero stress components along the x_1 -axis are quantities of interest. In the numerical study, a mesh containing 512 elements of type-4 is utilized to obtain the numerical results. The classical solution of the crack opening displacement, for this particular case, can be found in Tada *et al.* (2000) and the converged near-tip stress for $\bar{\tau}^s = 0$ obtained from a mesh with the type-4 elements is used to compare with present results. By using the same non-dimensional parameters shown in chapter II, the solution of the crack opening displacement in Tada *et al.* (2000) can be given by

$$\Delta \bar{u}_2(\bar{x}) = \frac{2\bar{t}_o(1-\nu)}{\pi} \left\{ \sqrt{1-\bar{x}^2} + \bar{x}^2 \cosh^{-1}\left(\frac{1}{\bar{x}}\right) \right\} \quad (4.12)$$

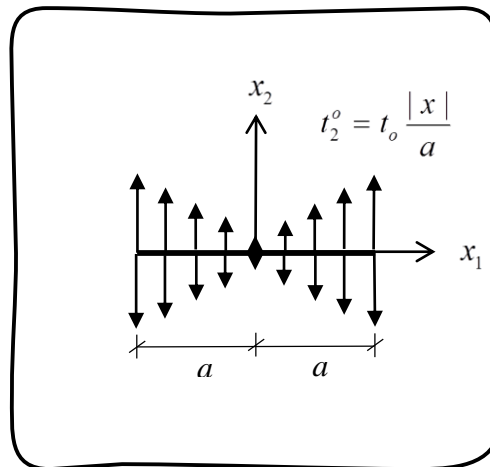


Figure 4.12. Schematic of straight crack of length $2a$ under self-equilibrated linearly distributed normal traction.

To further examine the role of the residual surface tension, the normalized crack opening displacement and normalized near-tip stress for $\bar{a} = 10$ and five different values of the normalized residual surface tension $\bar{\tau}^s$ ranging from 0.005 to 2 are considered. Results of the normalized crack opening displacement and the normalized normal stress components along the x_1 -axis are shown in Figure 4.13. The finding agrees very well with the available exact solution (e.g., Tada et al., 2000) for the classical case. As can be seen in the Figure 4.13(a), when the residual surface tension increases, the crack opening displacement profile increasingly deviates from the classical solution. For instance, when $\bar{\tau}^s = 2$, the normalized crack opening displacement is substantially less than that of the classical case. Moreover, with increasing of $\bar{\tau}^s$, the influence of the residual surface tension on near-tip stress becomes more significant. According to Figure 4.13(b), when $\bar{\tau}^s$ is greater than 0.5, the stresses very different from the case without residual surface tension ($\bar{\tau}^s = 0$). In conclusion, when $\bar{\tau}^s$ increases, the influence of the residual surface tension is quite significant and the medium becomes locally stiffer.

As clearly discussed in the section 4.1.1, the range of normalized residual surface tension $\bar{\tau}^s$ and normalized crack length \bar{a} are taken from (4.10) and (4.11). The relation between the normalized crack opening displacement and the normalized residual surface tension $\bar{\tau}^s$ for $\bar{a} = 10$ is displayed in Figure 4.14. Similar to the straight

crack under uniformly distributed normal traction, when $\bar{\tau}^s = 0$ (i.e., the classical case), the normalized crack opening displacement at $\bar{x} = 0, 0.5, 0.75$ always attains its maximum value. As the residual surface tension increases, the normalized crack opening displacement $\Delta\bar{u} / \bar{t}_o$ for each case increases in the range of $\bar{x} < 0.55$ but decreases in the range of $0.55 < \bar{x} < 1$. Furthermore, the relationship between the normalized near-tip stress at $\bar{x} = 1.001, 1.01, 1.1$ and the normalized residual surface tension $\bar{\tau}^s$ is also reported in Figure 4.15. This set of results reveals that the role of the residual surface tension on the stress field around the crack-tip becomes increasingly important when $\bar{\tau}^s$ increases from 0 to 2. Based on results from Figure 4.14 and Figure 4.15, it is clearly shown that the residual surface tension can considerably reduce the crack opening displacement over the entire crack face and corresponding stress at the crack-tip.

In order to investigate the size-dependent behavior of the predicted solutions, the normalized crack opening displacement and normalized near-tip stress for normalized crack length $\bar{a} = 10, 50, 250, 500, 2500$ are shown in Figure 4.16 for both the classical case ($\bar{\tau}^s = 0$) and that associated with $\bar{\tau}^s = 0.7$. Among the entire normalized crack opening displacements reported in Figure 4.16(a), the value of $\Delta\bar{u} / \bar{t}_o$ at $\bar{a} = 10$ is the minimum and is very different from the classical solution. From the obtained relationship between the normalized crack opening displacement and the normalized crack length \bar{a} , when the crack-size increases, the influence of the residual surface tension on crack-face displacement becomes less significant and results clearly approach those of the classical case. In the other hand, with the decreasing crack-size from 2500 to 10, the effect of residual surface tension on the crack-tip stress is strongly significant, as indicated by Figure 4.16(b).

For a particular value of the residual surface tension $\bar{\tau}^s = 0.7$, the ratio $\bar{\tau}^s / \bar{a}$ is controlled by the difference crack size and it is also indicated that the crack opening displacement and the near-tip stress are strongly dependent on the crack size. When the normalized crack length \bar{a} increases, the values of the normalized crack opening displacement at $\bar{x} = 0, 0.5, 0.75$ increase rapidly in the range of $0 < \bar{a} < 500$ whereas results of the crack opening displacement asymptotically approach the classical solution when \bar{a} increases from 500 to 2500 as indicated in Figure 4.17. The relation between

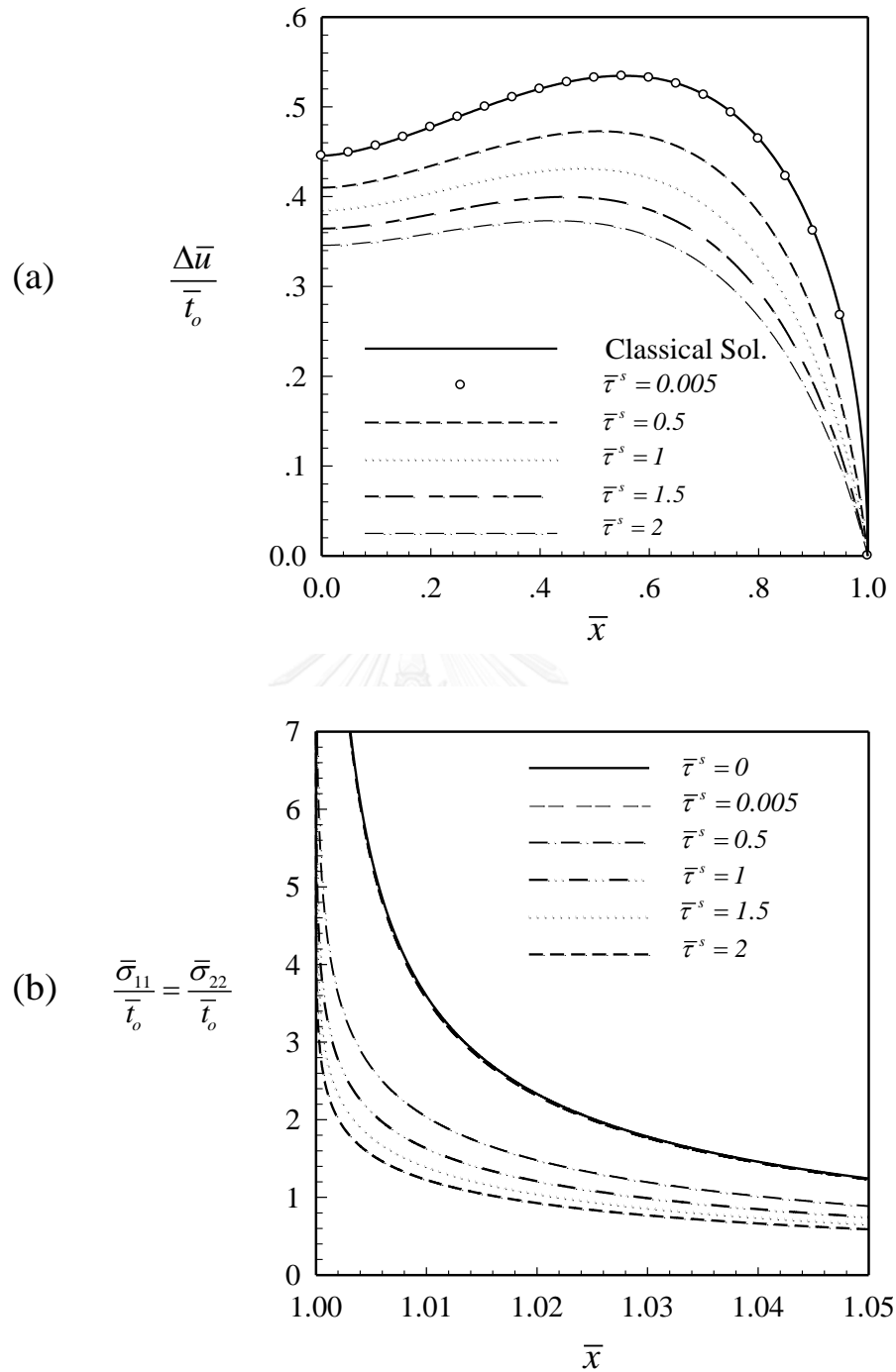
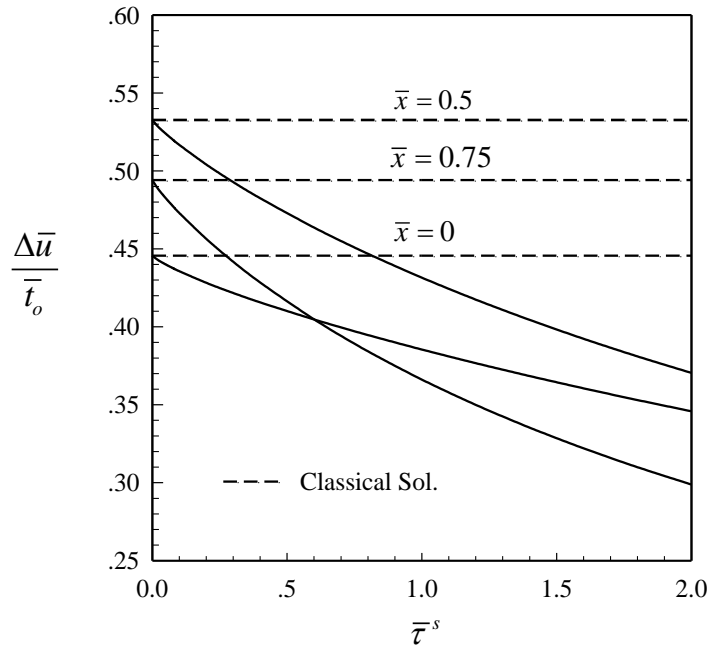
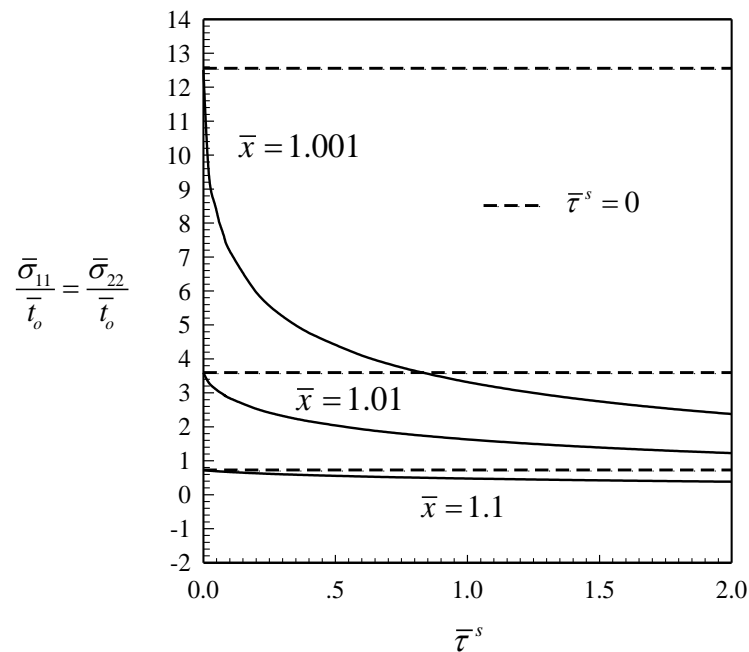


Figure 4.13. (a) Normalized crack opening displacement and (b) normalized normal stress components along the x_1 -axis of straight crack under linearly distributed normal traction for five different values of $\bar{\tau}^s$ ranging from 0.005 to 2 and for $E = 89.5 \text{ GPa}$ and $\nu = 0.3$.



Figures 4.14. Normalized crack opening displacement $\Delta\bar{u}/\bar{t}_o$ for $\bar{x} = 0, 0.5, 0.75$ versus normalized residual surface tension $\bar{\tau}^s$ of straight crack under linearly distributed normal traction for $E = 89.5 \text{ GPa}$, $\nu = 0.3$ and $\bar{a} = 10$.



Figures 4.15. Normalized normal stress components $\bar{\sigma}_{11}/\bar{t}_o = \bar{\sigma}_{22}/\bar{t}_o$ for $\bar{x} = 1.001, 1.01, 1.1$ versus normalized residual surface tension $\bar{\tau}^s$ of straight crack under linearly distributed normal traction for $E = 89.5 \text{ GPa}$, $\nu = 0.3$ and $\bar{a} = 10$.

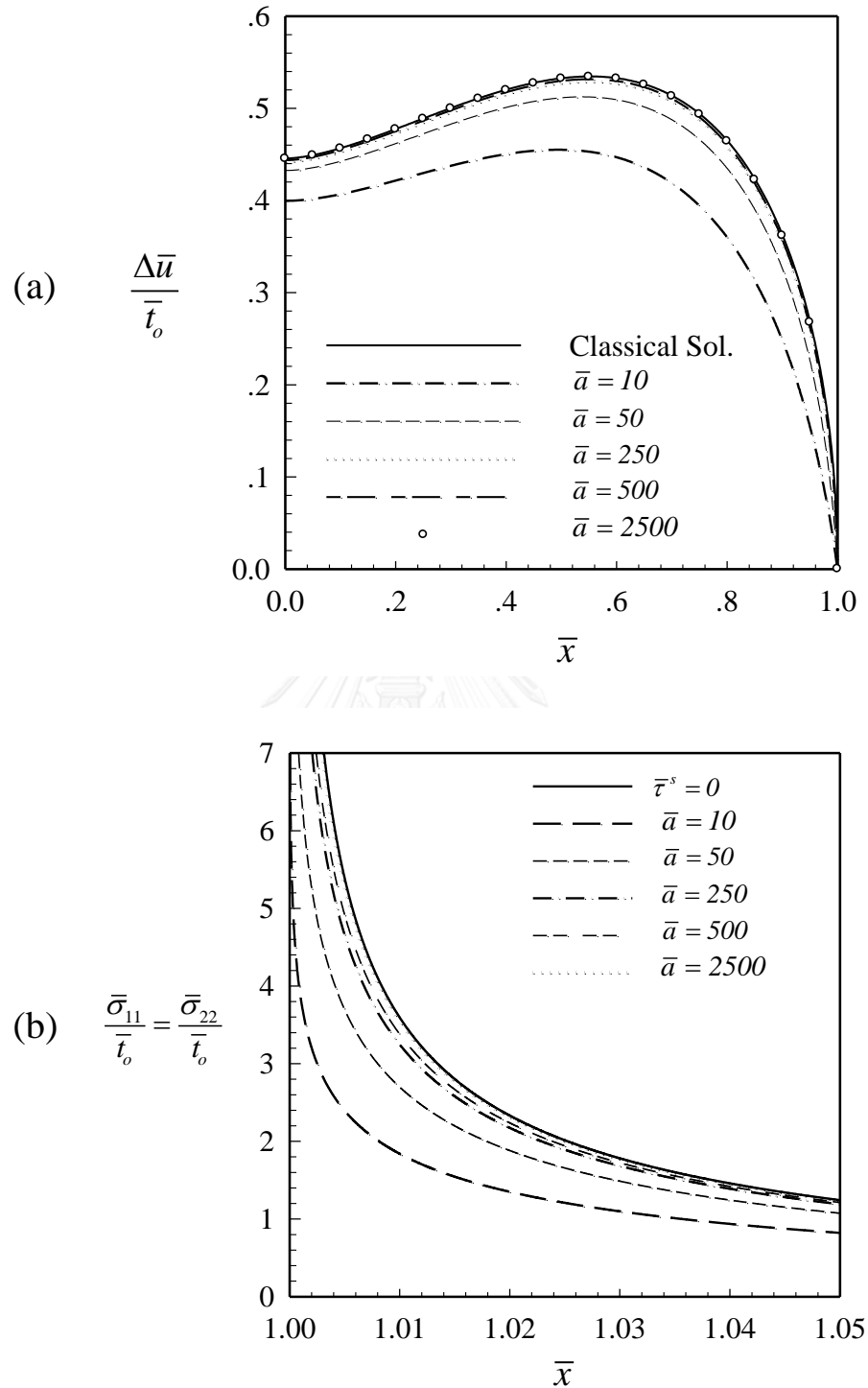
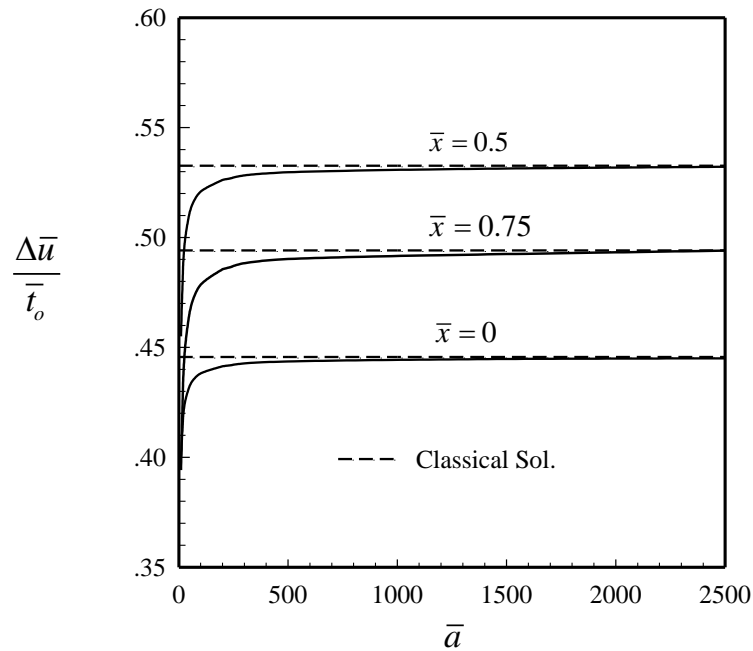
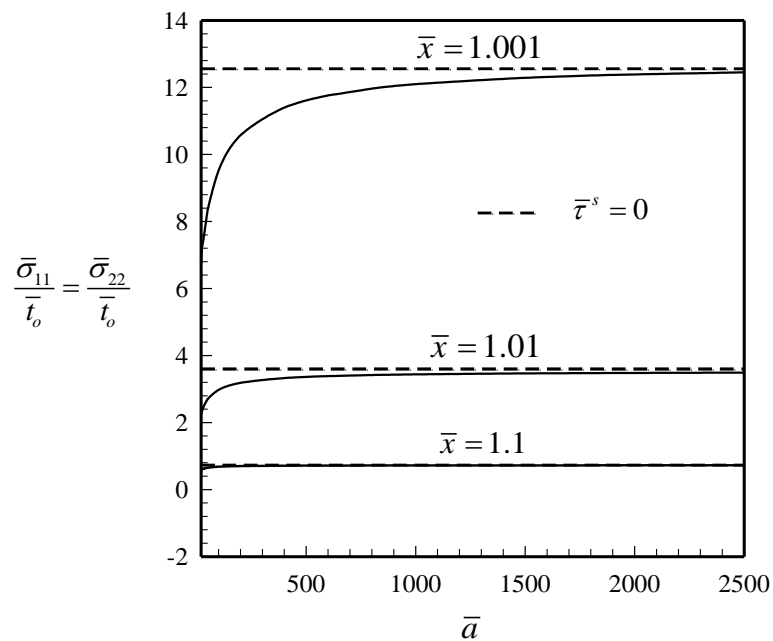


Figure 4.16. (a) Normalized crack opening displacement and (b) normalized normal stress components along the x_1 -axis of straight crack under linearly distributed normal traction for five different values of $\bar{a} = a/\Lambda = 10, 50, 250, 500, 2500$ and for $E = 89.5 \text{ GPa}$ and $\nu = 0.3$.



Figures 4.17. Normalized crack opening displacement $\Delta \bar{u} / \bar{t}_o$ for $\bar{x} = 0, 0.5, 0.75$ versus normalized crack length \bar{a} of straight crack under linearly distributed normal traction for $E = 89.5 \text{ GPa}$, $\nu = 0.3$ and $\bar{\tau}^s = 0.7$.



Figures 4.18. Normalized normal stress components $\bar{\sigma}_{11} / \bar{t}_o = \bar{\sigma}_{22} / \bar{t}_o$ for $\bar{x} = 1.001, 1.01, 1.1$ versus normalized crack length \bar{a} of straight crack under linearly distributed normal traction for $E = 89.5 \text{ GPa}$, $\nu = 0.3$ and $\bar{\tau}^s = 0.7$.

the normalized near-tip stress and the normalized crack length \bar{a} is also illustrated in Figure 4.18. It is evident from these results that the normalized near-tip stress for $\bar{x} = 1.001$ increases rapidly in comparison with those associated with $\bar{x} = 1.01, 1.1$ as can be seen in Figure 4.18.

4.2 Crack under Quadratic Normal Traction

As a final example to demonstrate capability of the proposed Galerkin technique in the analysis of nano-sized cracks, let us consider a straight crack of length $2a$ subjected to a self-equilibrated, quadratic normal traction $t_2^o = t_o(1 - x^2/a^2)$ as shown schematically in Figure 4.19. The constituting material is taken as Al [111] where Young's modulus and Poisson's ratio for the bulk material and the residual surface tension are given by $E = 89.5 \text{ GPa}$, $\nu = 0.3$ and $\tau^s = 0.9108 \text{ N/m}$, respectively.

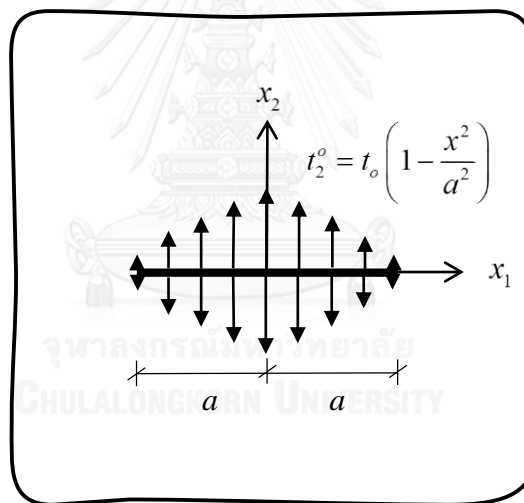


Figure 4.19. Schematic of straight crack of length $2a$ under self-equilibrated, quadratic normal traction.

Since the closed-form solution for the classical case (i.e., $\bar{\tau}^s = 0$) does not exist in the literature, the crack opening displacement and the stress components along the x_1 -axis are obtained directly from the dislocation theory as follows:

$$\Delta \bar{u}_2(\bar{x}) = -\frac{1}{\pi \bar{\kappa}} \sum_{i=1}^{\infty} \left(\int_{-1}^{\bar{x}_1} \frac{1}{\sqrt{1-\bar{\xi}^2}} T_i(\bar{\xi}) d\bar{\xi} \right) \lambda_{i-1}^{\alpha} \quad (4.13)$$

$$\frac{d(\Delta\bar{u}_2)}{d\bar{\xi}} = -\frac{1}{\pi\bar{\kappa}\sqrt{1-\bar{\xi}^2}} \sum_{i=1}^{\infty} \lambda_{i-1}^{\alpha} T_i(\bar{\xi}) \quad (4.14)$$

where $T_i(\bar{\xi})$ is the Chebyshev polynomial of the first kind and the coefficient λ_i^{α} can be obtained explicitly from

$$\lambda_{i-1}^{\alpha} = \frac{2}{\pi} \int_{-1}^1 \frac{t_o}{\mu} \delta_{\alpha 2} (1-\bar{x}^2) U_i(\bar{x}_1) \sqrt{1-\bar{x}^2} d\bar{x}_1 = -\frac{\delta_{\alpha 2}}{4\pi\mu} (\delta_{i2} - 3\delta_{i0}) \quad (4.15)$$

The relative crack-face displacement and its gradient become

$$\begin{aligned} \Delta\bar{u}_2(\bar{x}) &= \frac{t_o}{4\pi\mu\bar{\kappa}} \left(\int_{-1}^{\bar{x}_1} \frac{1}{\sqrt{1-\bar{\xi}^2}} (T_3(\bar{\xi}) - 3T_1(\bar{\xi})) d\bar{\xi} \right) \\ &= \frac{t_o}{4\pi\mu\bar{\kappa}} \left(\int_{-1}^{\bar{x}_1} \frac{1}{\sqrt{1-\bar{\xi}^2}} (4\bar{\xi}^3 - 6\bar{\xi}) d\bar{\xi} \right) = \frac{\bar{t}_o}{6\pi\bar{\kappa}} (5 - 2\bar{x}^2) \sqrt{1-\bar{x}^2} \end{aligned} \quad (4.16)$$

$$\frac{d(\Delta\bar{u}_2)}{d\bar{\xi}} = \frac{t_o}{4\pi\mu\bar{\kappa}} \frac{T_3(\bar{\xi}) - 3T_1(\bar{\xi})}{\sqrt{1-\bar{\xi}^2}} = \frac{\bar{t}_o}{4\pi\bar{\kappa}} \frac{4\bar{\xi}^3 - 6\bar{\xi}}{\sqrt{1-\bar{\xi}^2}} \quad (4.17)$$

The non-zero stress components at any point $(x_1, 0)$, $|x_1| > a$ can readily be obtained from

$$\begin{aligned} \bar{\sigma}_{11}^b(x_1, 0) = \bar{\sigma}_{22}^b(x_1, 0) &= -\bar{\kappa} \int_{-1}^1 \frac{1}{\bar{x} - \bar{\xi}} \frac{d\Delta\bar{u}_2}{d\bar{\xi}} d\bar{\xi} = -\frac{\bar{t}_o}{4\pi} \int_{-1}^1 \frac{1}{\bar{x} - \bar{\xi}} \frac{4\bar{\xi}^3 - 6\bar{\xi}}{\sqrt{1-\bar{\xi}^2}} d\bar{\xi} \\ &= \bar{t}_o \left(\bar{x}^2 - 1 + \frac{3|\bar{x}|}{2\sqrt{\bar{x}^2 - 1}} - \frac{|\bar{x}^3|}{\sqrt{\bar{x}^2 - 1}} \right) \end{aligned} \quad (4.18)$$

where $\bar{\kappa} = 2/\pi(\kappa + 1)$, $\bar{t}_o = t_o/\mu$.

To investigate the role of the residual surface tension on responses of the crack under this particular loading condition, the normalized crack opening displacement and the normalized near-tip stress for $\bar{a} = 10$ and different values of the normalized residual surface tension $\bar{\tau}^s$ ranging from 0.005 to 2 are reported in Figure 4.20. It can be seen that when $\bar{\tau}^s$ increases from 0.005 to 2, the value of $\Delta\bar{u}/\bar{t}_o$ decreases rapidly in the range $0.9 < \Delta\bar{u}/\bar{t}_o < 1.2$ and the maximum value of $\Delta\bar{u}/\bar{t}_o$ for $\bar{\tau}^s = 2$ is 25% below the classical solution, as indicated in Figure 4.20(a). It can be deduced from Figure 4.20(b) that the classical solution for $\bar{\sigma}_{11}/\bar{t}_o = \bar{\sigma}_{22}/\bar{t}_o$ is slightly greater than that for

$\bar{\tau}^s = 0.005$ whereas such discrepancy of the predicted solutions become more evident when $\bar{\tau}^s = 0.5, 1, 1.5, 2$.

To demonstrate the size-dependent behavior of the predicted solution for this loading case, the normalized crack opening displacement and the normalized near-tip stress for the normalized crack length \bar{a} ranging from 10 to 2500 are obtained and reported in Figure 4.23 for $\bar{\tau}^s = 0.7$. It can be seen from results in Figure 4.23(a) that the normalized crack opening displacement exhibits strongly size-dependent. In particular, $\Delta\bar{u} / \bar{t}_o$ is the minimum at for $\bar{a} = 10$ and takes approximately 12.5% of the classical solution. Furthermore, when the crack-size decreases, the influence of the residual surface tension on the near-tip stress behavior becomes increasingly significant, as clearly evident in Figure 4.23(b). In the other words, when the crack length increases, the influence of the residual surface tension on the elastic responses (e.g., the crack-face displacement and near-tip stress) becomes less significant and results clearly approach that of the classical case.

In order to investigate the influence of the residual surface tension and the role of the crack size, the behavior of the crack opening displacement and the near-tip stress field are also observed. The behavior of the normalized crack opening displacement and the normalized near-tip stress are shown in Figure 4.21 and Figure 4.22, respectively. Similar to the straight crack under uniformly and linear distributed normal tractions, the residual surface tension significantly reduces the crack opening displacement and the near-tip stress when $\bar{\tau}^s$ becomes larger. Figure 4.24 and Figure 4.25 displayed the normalized crack opening displacement $\Delta\bar{u} / \bar{t}_o$ and the normalized normal stress components $\bar{\sigma}_{11} / \bar{t}_o = \bar{\sigma}_{22} / \bar{t}_o$ versus the normalized crack length \bar{a} , respectively. It can be concluded from these numerical solutions that the crack opening displacement and the near-tip stress field exhibit strong dependence on the crack size.

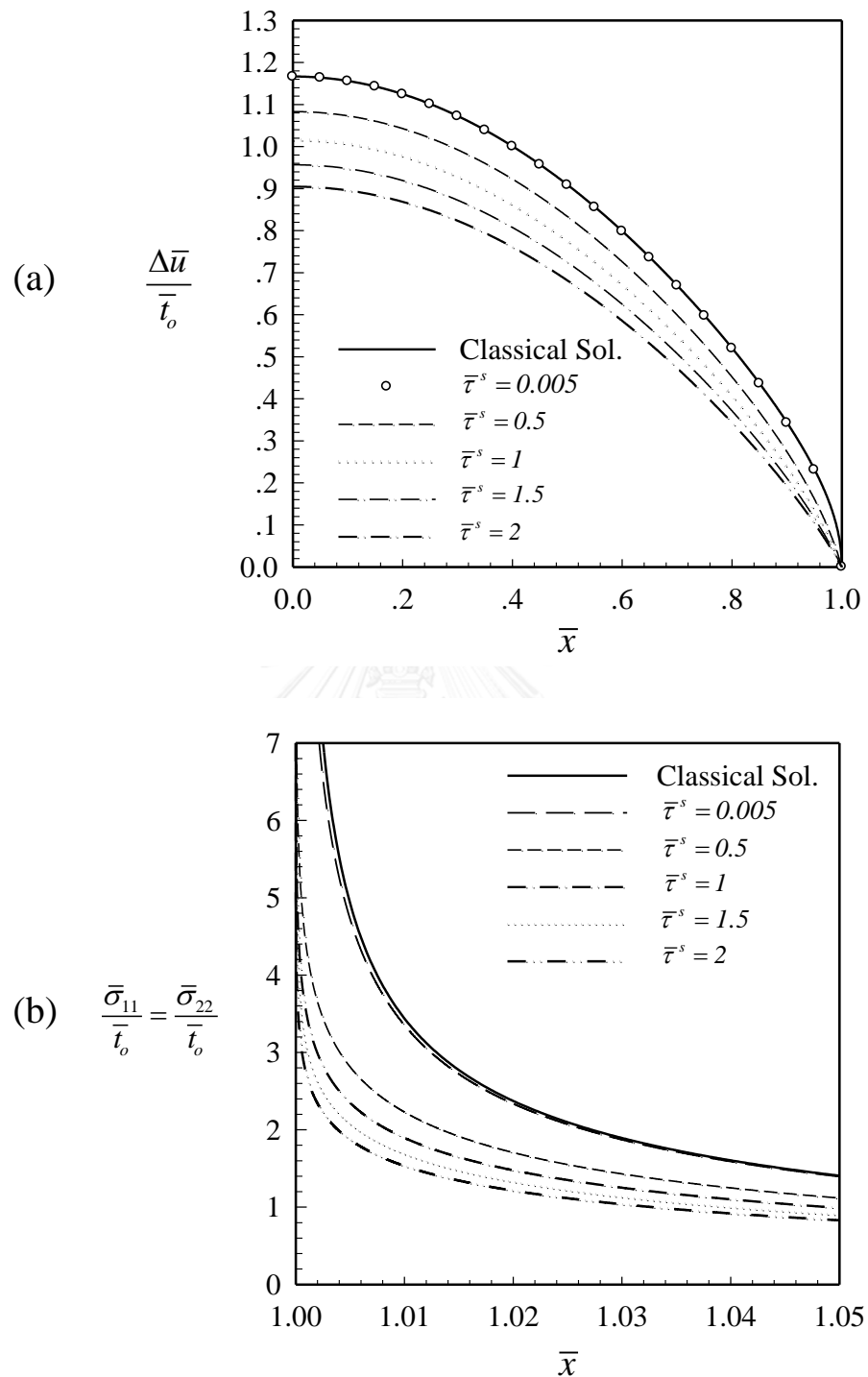
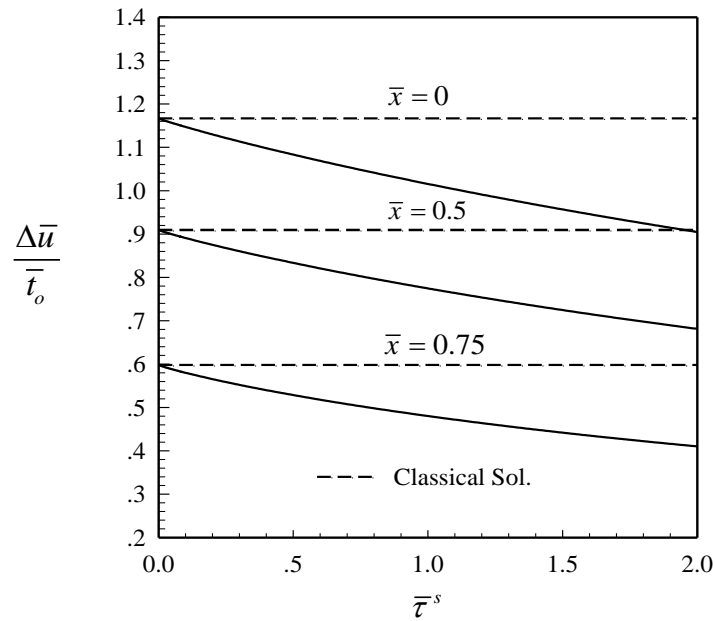
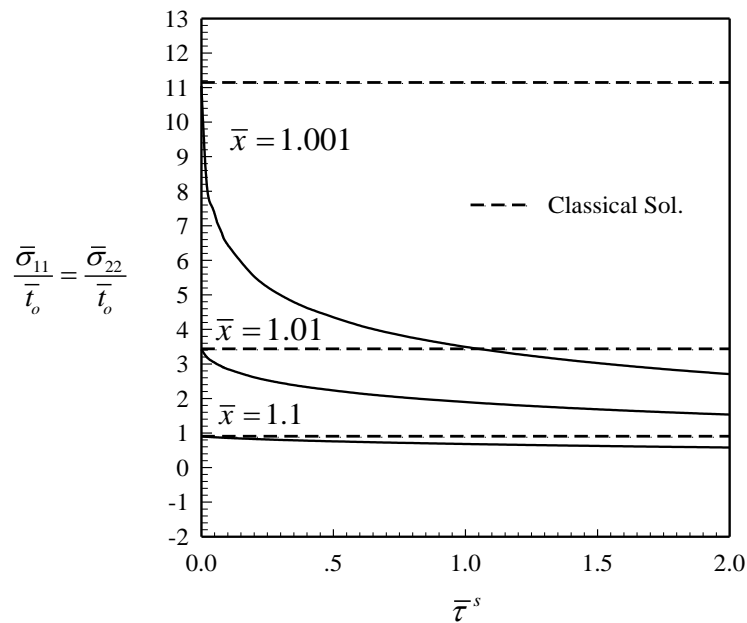


Figure 4.20. (a) Normalized crack opening displacement and (b) normalized normal stress components along the x_1 -axis of straight crack under quadratic normal traction for five different values of $\bar{\tau}^s$ ranging from 0.005 to 2 and for $E = 89.5 \text{ GPa}$ and $\nu = 0.3$.



Figures 4.21. Normalized crack opening displacement $\Delta \bar{u} / \bar{t}_o$ for $\bar{x} = 0, 0.5, 0.75$ versus normalized residual surface tension $\bar{\tau}^s$ of straight crack under quadratic normal traction for $E = 89.5 \text{ GPa}$, $\nu = 0.3$ and $\bar{a} = 10$.



Figures 4.22. Normalized normal stress components $\bar{\sigma}_{11} / \bar{t}_o = \bar{\sigma}_{22} / \bar{t}_o$ for $\bar{x} = 1.001, 1.01, 1.1$ versus normalized residual surface tension $\bar{\tau}^s$ of straight crack under quadratic normal traction for $E = 89.5 \text{ GPa}$, $\nu = 0.3$ and $\bar{a} = 10$.

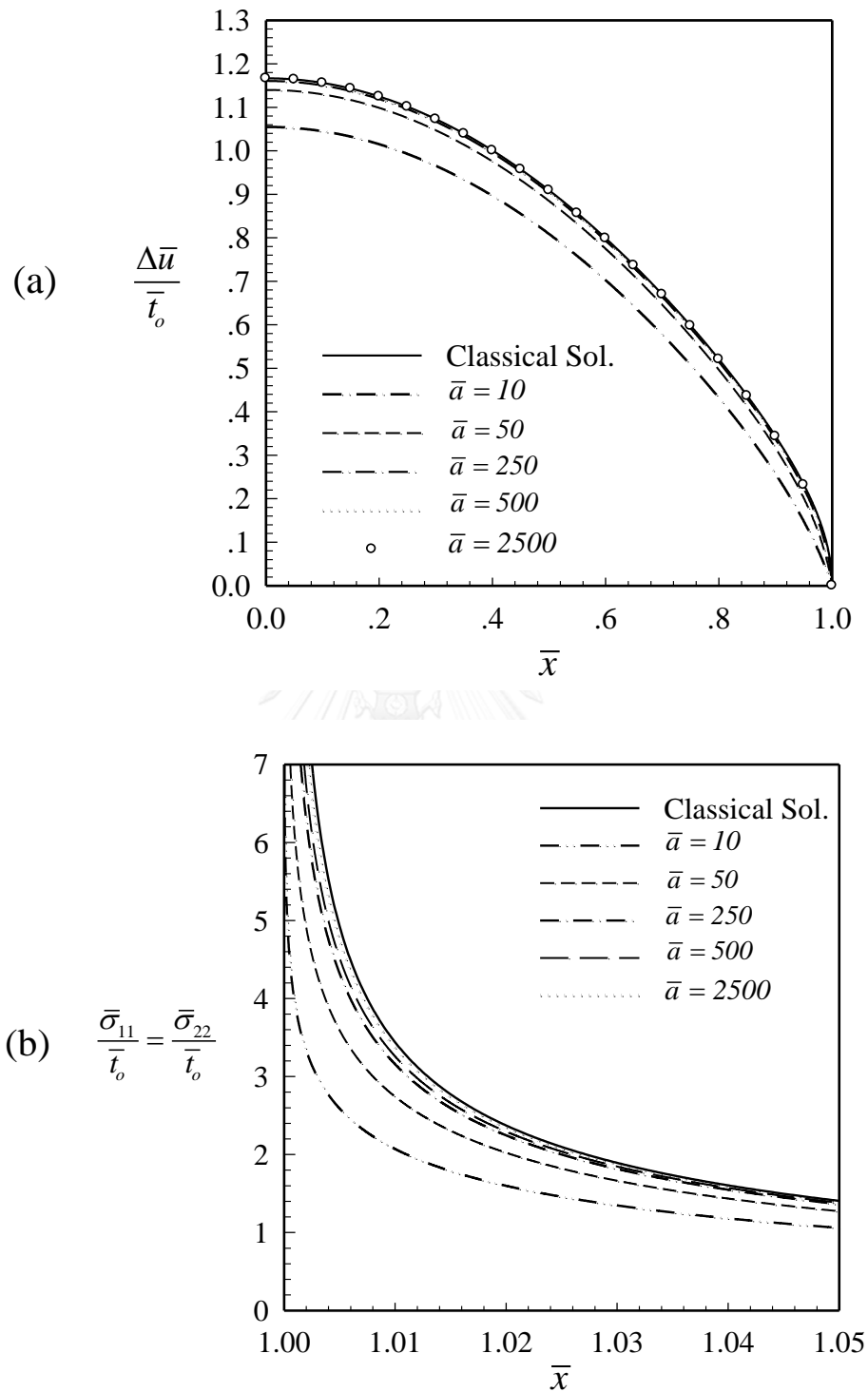
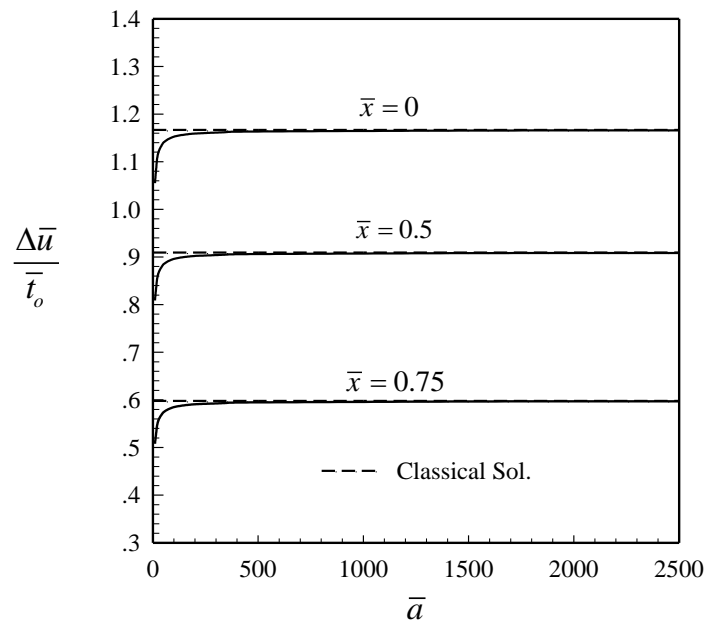
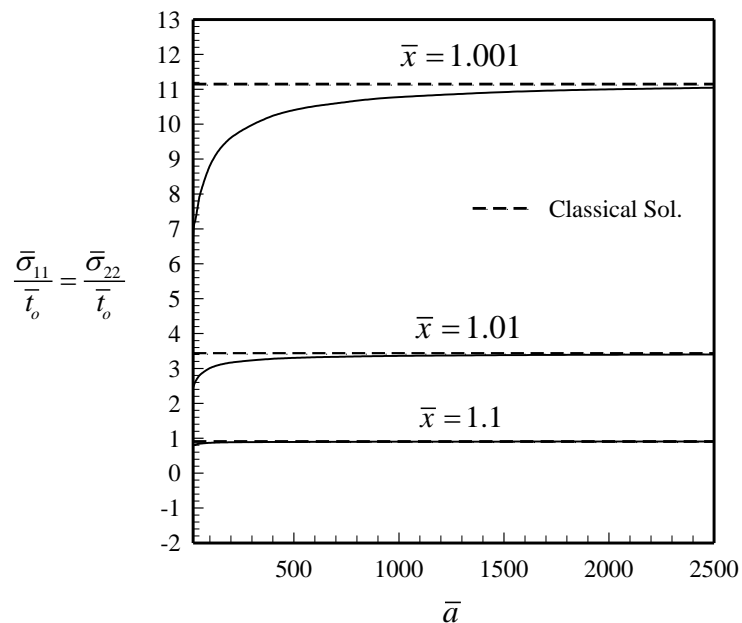


Figure 4.23. (a) Normalized crack opening displacement and (b) normalized normal stress components along the x_1 -axis of straight crack under quadratic normal traction for five different values of $\bar{a} = a/\Lambda = 10, 50, 250, 500, 2500$ and for $E = 89.5 \text{ GPa}$ and $\nu = 0.3$.



Figures 4.24. Normalized crack opening displacement $\Delta \bar{u} / \bar{t}_o$ for $\bar{x} = 0, 0.5, 0.75$ versus normalized crack length \bar{a} of straight crack under quadratic normal traction for $E = 89.5 \text{ GPa}$, $\nu = 0.3$ and $\bar{\tau}^s = 0.7$.



Figures 4.25. Normalized normal stress components $\bar{\sigma}_{11} / \bar{t}_o = \bar{\sigma}_{22} / \bar{t}_o$ for $\bar{x} = 1.001, 1.01, 1.1$ versus normalized crack length \bar{a} of straight crack under quadratic normal traction for $E = 89.5 \text{ GPa}$, $\nu = 0.3$ and $\bar{\tau}^s = 0.7$.

CHAPTER V

CONCLUSIONS

5.1 Summary

An accurate and computationally efficient numerical technique capable of modeling a two-dimensional elastic medium containing a straight, sharp crack under pure mode-I loading condition and the effect of the residual surface tension has been developed. The key governing equation has been derived based on the classical linear theory of elasticity for the bulk material and the Gurtin-Murdoch surface elasticity theory with only non-zero residual surface for the crack surfaces. Galerkin method has been adopted to solve the resulting weakly singular, weak-form equation. Standard basis functions constructed locally via the finite element mesh have been employed in the solution discretization and a selected efficient quadrature has been adopted to form a set of discretized linear algebraic equations.

The obtained results from extensive numerical experiments have been compared with available benchmark solutions (e.g., Tada *et al.*, 2000; Sendova and Walton, 2010) to demonstrate both the theoretical consideration and the solution procedure of the proposed technique. The rate of convergence of numerical solutions has been fully explored and it has been found that approximations using quadratic, cubic and Hermite shape functions yield about the same rate of convergence that is higher than that of the linear case and the derivative of the relative crack-face displacement becomes finite at the crack-tip for non-zero residual surface tension. In addition, the fundamental solutions of a straight crack under different types of traction are presented when the residual surface tension is treated.

The behavior of the crack opening displacement and the near-tip stress field has been fully investigated when the residual surface tension and crack size are treated. It has been found from an extensive numerical study that the residual surface tension appearing in Gurtin-Murdoch model plays a significant role on the response prediction. In particular, the residual surface tension effectively reduces the crack opening displacement and the near-tip stress. In addition, the crack length controls the behavior

of the elastic responses predicted. With the decreasing crack length to the range of a nano-scale, the influence of the residual surface tension on the crack-face displacement and near-tip stress becomes increasingly significant.

Results from an extensive numerical study have also indicated that the proposed technique is computationally robust and promising for the modeling of cracks under the pure mode-I loading condition and influence of residual surface tension. It has also been shown that the residual surface tension strongly affects the elastic responses of the crack. In particular, the crack opening displacement on the entire crack face and the near-tip stress is substantially reduced from those of the classical case (without the residual surface tension). Integration of the residual surface tension on the crack surface into the mathematical model not only weakens the crack-tip stress singularity but also renders the predicted solutions strongly size-dependent.

5.2 Potential Extensions

The present work has directly offered the fundamental insight of the crack opening displacement and the near-tip stress field when the residual surface tension is taken into account. However, the role of the residual surface tension on the near-tip field of nano-size cracks is still not fully established, the conclusion about singularity and boundedness of the crack-tip stresses and strains still requires further investigations. In addition, the extension of the current work to treat the influence of the surface elastic constants and the mixed-mode loading conditions is also significant.

REFERENCES

- Abdou, M. 2003. Fredholm–Volterra integral equation with singular kernel. Applied Mathematics and Computation 137: 231-243.
- Adnan, A., and Sun, C. T. 2010. Evolution of nanoscale defects to planar cracks in a brittle solid. Journal of the Mechanics and Physics of Solids 58: 983-1000.
- Atkinson, K. E. 1997. The numerical solution of integral equations of the second kind. Cambridge university press.
- Badr, A. 2001. Integro-differential equation with Cauchy kernel. Journal of Computational and Applied Mathematics 134: 191-199.
- Barber, J. R. 1992. Elasticity. Springer.
- Bathe, K.-J. 2006. Finite element procedures. Klaus-Jurgen Bathe.
- Becker, E. B., Carey, G. F., and Oden, J. T. 1981. Finite Elements, An Introduction: Volume I. ..258: 1981.
- Buehler, M. J., Abraham, F. F., and Gao, H. 2003. Hyperelasticity governs dynamic fracture at a critical length scale. Nature 426: 141-146.
- Buehler, M. J., and Gao, H. 2006. Dynamical fracture instabilities due to local hyperelasticity at crack tips. Nature 439: 307-310.
- Cammarata, R. C. 1997. Surface and interface stress effects on interfacial and nanostructured materials. Materials Science and Engineering: A 237: 180-184.
- Chen, Q., Chasiotis, I., Chen, C., and Roy, A. 2008. Nanoscale and effective mechanical behavior and fracture of silica nanocomposites. Composites Science and Technology 68: 3137-3144.
- Cuenot, S., Frétiigny, C., Demoustier-Champagne, S., and Nysten, B. 2004. Surface tension effect on the mechanical properties of nanomaterials measured by atomic force microscopy. Physical Review B 69: 165410.
- Dingreville, R., Qu, J., and Mohammed, C. 2005. Surface free energy and its effect on the elastic behavior of nano-sized particles, wires and films. Journal of the Mechanics and Physics of Solids 53: 1827-1854.

- Duan, H., Wang, J., Huang, Z., and Karihaloo, B. 2005a. Size-dependent effective elastic constants of solids containing nano-inhomogeneities with interface stress. Journal of the Mechanics and Physics of Solids 53: 1574-1596.
- Duan, H., Wang, J., Huang, Z., and Karihaloo, B. L. 2005b. Eshelby formalism for nano-inhomogeneities. Proceedings of the Royal Society A: Mathematical, Physical and Engineering Science 461: 3335-3353.
- Fang, Q. H., Liu, Y., Liu, Y. W., and Huang, B. Y. 2009. Dislocation emission from an elliptically blunted crack tip with surface effects. Physica B: Condensed Matter 404: 3421-3424.
- Frankel, J. I. 1995. A Galerkin solution to a regularized Cauchy singular integro-differential equation. Quarterly of Applied Mathematics 53: 245-258.
- Fu, X. L., Wang, G. F., and Feng, X. Q. 2008. Surface effects on the near-tip stress fields of a mode-II crack. International Journal of Fracture 151: 95-106.
- Fu, X. L., Wang, G. F., and Feng, X. Q. 2010. Surface effects on mode-I crack tip fields: A numerical study. Engineering Fracture Mechanics 77: 1048-1057.
- Guin, J.-P., Wiederhorn, S. M., and Fett, T. 2005. Crack-Tip Structure in Soda-Lime-Silicate Glass. Journal of the American Ceramic Society 88: 652-659.
- Gurtin, M., and Ian Murdoch, A. 1975. A continuum theory of elastic material surfaces. Archive for Rational Mechanics and Analysis 57: 291-323.
- Gurtin, M. E., and Ian Murdoch, A. 1978. Surface stress in solids. International Journal of Solids and Structures 14: 431-440.
- Gurtin, M. E., Weissmüller, J., and Larché, F. 1998. A general theory of curved deformable interfaces in solids at equilibrium. Philosophical Magazine A 78: 1093-1109.
- Hirth, J. P., and Lothe, J. 1982. Theory of dislocations.
- Huang, S., Zhang, S., Belytschko, T., Terdalkar, S. S., and Zhu, T. 2009. Mechanics of nanocrack: Fracture, dislocation emission, and amorphization. Journal of the Mechanics and Physics of Solids 57: 840-850.

- Iijima, S. 1991. Helical microtubules of graphitic carbon. nature 354: 56-58.
- Iijima, S., and Ichihashi, T. 1993. Single-shell carbon nanotubes of 1-nm diameter. Nature 363: 603-605.
- Jing, G., Duan, H., Sun, X., Zhang, Z., Xu, J., Li, Y., Wang, J., and Yu, D. 2006. Surface effects on elastic properties of silver nanowires: contact atomic-force microscopy. Physical Review B 73: 235409.
- Karimi, A., Wang, Y., Cselle, T., and Morstein, M. 2002. Fracture mechanisms in nanoscale layered hard thin films. Thin Solid Films 420–421: 275-280.
- Kawai, E., Sanada, K., Sumigawa, T., and Kitamura, T. 2014. Delamination crack initiation from copper/silicon nitride interface edge with nanoscale singular stress field. Engineering Fracture Mechanics 120: 60-66.
- Keene, B. J. 1993. Review of data for the surface tension of pure metals. International Materials Reviews 38: 157-192.
- Kim, C., Ru, C.-Q., and Schiavone, P. 2013. A clarification of the role of crack-tip conditions in linear elasticity with surface effects. Mathematics and Mechanics of Solids 18: 59-66.
- Kim, C. I., Schiavone, P., and Ru, C. Q. 2010. Analysis of a mode-III crack in the presence of surface elasticity and a prescribed non-uniform surface traction. Zeitschrift für angewandte Mathematik und Physik 61: 555-564.
- Kim, C. I., Schiavone, P., and Ru, C. Q. 2011a. Analysis of Plane-Strain Crack Problems (Mode-I & Mode-II) in the Presence of Surface Elasticity. Journal of Elasticity 104: 397-420.
- Kim, C. I., Schiavone, P., and Ru, C. Q. 2011b. The effect of surface elasticity on a Mode-III interface crack. Archives of Mechanics 63: 267-286.
- Liu, D. S., Zhao, C. W., and Du, W. H. 2013. Nanoscale deformation analysis near crack-tip under residual stress in Si by high-resolution transmission electron microscopy. Journal of Materials Science: Materials in Electronics 24: 933-937.
- Masuda-Jindo, K., Hung, V. V., and Menon, M. 2009. Fracture and mechanical properties of nanotubes and nanowires. Procedia Engineering 1: 163-166.

- Miller, R. E., and Shenoy, V. B. 2000. Size-dependent elastic properties of nanosized structural elements. Nanotechnology 11: 139.
- Mills, K. C., and Su, Y. C. 2006. Review of surface tension data for metallic elements and alloys: Part 1 – Pure metals. International Materials Reviews 51: 329-351.
- Nan, H., and Wang, B. 2012. Effect of residual surface stress on the fracture of nanoscale materials. Mechanics Research Communications 44: 30-34.
- Nan, H. S., and Wang, B. L. 2013. Effect of crack face residual surface stress on nanoscale fracture of piezoelectric materials. Engineering Fracture Mechanics 110: 68-80.
- Nazmus Sakib, A. R., and Adnan, A. 2012. On the size-dependent critical stress intensity factor of confined brittle nanofilms. Engineering Fracture Mechanics 86: 13-22.
- Oh, E.-S., Walton, J. R., and Slattery, J. C. 2006. A theory of fracture based upon an extension of continuum mechanics to the nanoscale. Journal of applied mechanics 73: 792-798.
- Ou, Z. Y., Wang, G. F., and Wang, T. J. 2008. Effect of residual surface tension on the stress concentration around a nanosized spheroidal cavity. International Journal of Engineering Science 46: 475-485.
- Peng, B., Locascio, M., Zapol, P., Li, S., Mielke, S. L., Schatz, G. C., and Espinosa, H. D. 2008. Measurements of near-ultimate strength for multiwalled carbon nanotubes and irradiation-induced crosslinking improvements. Nat Nano 3: 626-631.
- Pugno, N., Carpinteri, A., Ippolito, M., Mattoni, A., and Colombo, L. 2008. Atomistic fracture: QFM vs. MD. Engineering Fracture Mechanics 75: 1794-1803.
- Rafii-Tabar, H., Shodja, H. M., Darabi, M., and Dahi, A. 2006. Molecular dynamics simulation of crack propagation in fcc materials containing clusters of impurities. Mechanics of Materials 38: 243-252.
- Reddy, J. N. 1993. An introduction to the finite element method. McGraw-Hill New York.

- Saranen, J., and Vainikko, G. 2013. Periodic integral and pseudodifferential equations with numerical approximation. Springer Science & Business Media.
- Sendova, T., and Walton, J. 2010. A New Approach to the Modeling and Analysis of Fracture through Extension of Continuum Mechanics to the Nanoscale. Mathematics and Mechanics of Solids.
- Sharma, P., and Ganti, S. 2004. Size-Dependent Eshelby's Tensor for Embedded Nano-Inclusions Incorporating Surface/Interface Energies. Journal of Applied Mechanics 71: 663-671.
- Sharma, P., Ganti, S., and Bhate, N. 2003. Effect of surfaces on the size-dependent elastic state of nano-inhomogeneities. Applied Physics Letters 82: 535-537.
- Shenoy, V. B. 2005. Atomistic calculations of elastic properties of metallic fcc crystal surfaces. Physical Review B 71: 094104.
- Tada, H., Paris, P., and Irwin, G. 2000. The analysis of cracks handbook. New York: ASME Press.
- Tian, L., and Rajapakse, R. K. N. D. 2006. Analytical Solution for Size-Dependent Elastic Field of a Nanoscale Circular Inhomogeneity. Journal of Applied Mechanics 74: 568-574.
- Tian, L., and Rajapakse, R. K. N. D. 2007. Elastic field of an isotropic matrix with a nanoscale elliptical inhomogeneity. International Journal of Solids and Structures 44: 7988-8005.
- Vinet, B., Magnusson, L., Fredriksson, H., and Desré, P. J. 2002. Correlations between surface and interface energies with respect to crystal nucleation. Journal of colloid and interface science 255: 363-374.
- Walton, J. R. 2014. Plane-strain fracture with curvature-dependent surface tension: mixed-mode loading. Journal of Elasticity 114: 127-142.
- Wang, G.-F., and Feng, X.-Q. 2007. Effects of surface elasticity and residual surface tension on the natural frequency of microbeams. Applied Physics Letters 90: -.

- Wang, G.-F., and Feng, X.-Q. 2009. Timoshenko beam model for buckling and vibration of nanowires with surface effects. Journal of physics D: applied physics 42: 155411.
- Wang, G.-F., and Yang, F. 2011. Postbuckling analysis of nanowires with surface effects. Journal of Applied Physics 109: -.
- Wang, G., and Li, Y. 2013. Influence of surface tension on mode-I crack tip field. Engineering Fracture Mechanics 109: 290-301.
- Wang, G. F., and Wang, T. J. 2006. Deformation around a nanosized elliptical hole with surface effect. Applied Physics Letters 89: -.
- Wang, J.-S., Feng, X.-Q., Wang, G.-F., and Yu, S.-W. 2008. Twisting of nanowires induced by anisotropic surface stresses. Applied Physics Letters 92: -.
- Wang, K., and Wang, B. 2012. Effects of residual surface stress and surface elasticity on the nonlinear free vibration of nanoscale plates. Journal of Applied Physics 112: 013520.
- Wu, C. H. 1999. The effect of surface stress on the configurational equilibrium of voids and cracks. Journal of the Mechanics and Physics of Solids 47: 2469-2492.
- Wu, C. H., and Wang, M. L. 2000. The effect of crack-tip point loads on fracture. Journal of the Mechanics and Physics of Solids 48: 2283-2296.
- Wu, C. H., and Wang, M. L. 2001. Configurational equilibrium of circular-arc cracks with surface stress. International Journal of Solids and Structures 38: 4279-4292.
- Wunderlich, W., and Awaji, H. 2001. Molecular dynamics — simulations of the fracture toughness of sapphire. Materials & Design 22: 53-59.
- Yamakov, V. I., Warner, D. H., Zamora, R. J., Saether, E., Curtin, W. A., and Glaessgen, E. H. 2014. Investigation of crack tip dislocation emission in aluminum using multiscale molecular dynamics simulation and continuum modeling. Journal of the Mechanics and Physics of Solids 65: 35-53.

- Yan, Y., Sumigawa, T., Shang, F., and Kitamura, T. 2011. Cohesive zone criterion for cracking along the Cu/Si interface in nanoscale components. Engineering Fracture Mechanics 78: 2935-2946.
- Yang, Z., Zhou, Y., Wang, T., Liu, Q., and Lu, Z. 2014. Crack propagation behaviors at Cu/SiC interface by molecular dynamics simulation. Computational Materials Science 82: 17-25.
- Zhang, S., Mielke, S. L., Khare, R., Troya, D., Ruoff, R. S., Schatz, G. C., and Belytschko, T. 2005. Mechanics of defects in carbon nanotubes: Atomistic and multiscale simulations. Physical Review B 71: 115403.
- Zhao, C. W., and Xing, Y. M. 2008. Nanoscale experimental study of a micro-crack in silicon. Physica B: Condensed Matter 403: 4202-4204.
- Zhao, C. W., and Xing, Y. M. 2010. Nanoscale deformation analysis of a crack-tip in silicon by geometric phase analysis and numerical moiré method. Optics and Lasers in Engineering 48: 1104-1107.
- Zhao, X. J., and Rajapakse, R. K. N. D. 2009. Analytical solutions for a surface-loaded isotropic elastic layer with surface energy effects. International Journal of Engineering Science 47: 1433-1444.

APPENDIX



จุฬาลงกรณ์มหาวิทยาลัย
CHULALONGKORN UNIVERSITY

The closed-form expressions for Γ_{ji}^e , Γ_{ji}^{pq} and P_j^e with $\Omega^e = (\bar{x}_1, \bar{x}_2)$, $\Omega^p = (\bar{x}_1, \bar{x}_2)$, $\Omega^q = (\bar{x}_3, \bar{x}_4)$ for all four types of elements are given below.

A.1 Explicit Expression for P_j^e for Uniform Normal Traction \bar{t}_0

Type-1: $\mathbf{P}^e = \bar{t}_0 \{\bar{x}_2 - \bar{x}_1 \quad \bar{x}_2 - \bar{x}_1\}^T$

Type-2: $\mathbf{P}^e = \bar{t}_0 \left\{ \frac{\bar{x}_2 - \bar{x}_1}{3} \quad \frac{1}{3}(-4)(\bar{x}_1 - \bar{x}_2) \quad \frac{\bar{x}_2 - \bar{x}_1}{3} \right\}^T$

Type-3: $\mathbf{P}^e = \bar{t}_0 \left\{ \frac{1}{4}(\bar{x}_2 - \bar{x}_1) \quad -\frac{3}{4}(\bar{x}_1 - \bar{x}_2) \quad -\frac{3}{4}(\bar{x}_1 - \bar{x}_2) \quad \frac{1}{4}(\bar{x}_2 - \bar{x}_1) \right\}^T$

Type-4: $\mathbf{P}^e = \bar{t}_0 \begin{pmatrix} \frac{1}{15}(\bar{x}_1 - \bar{x}_2)(8\bar{x}_1^2 + 5\bar{x}_2\bar{x}_1 + 2\bar{x}_2^2 - 15) \\ -\frac{1}{30}(\bar{x}_1 - \bar{x}_2)^2(2\bar{x}_1^2 + 2\bar{x}_2\bar{x}_1 + \bar{x}_2^2 - 5) \\ \frac{1}{15}(\bar{x}_1 - \bar{x}_2)(2\bar{x}_1^2 + 5\bar{x}_2\bar{x}_1 + 8\bar{x}_2^2 - 15) \\ \frac{1}{30}(\bar{x}_1 - \bar{x}_2)^2(\bar{x}_1^2 + 2\bar{x}_2\bar{x}_1 + 2\bar{x}_2^2 - 5) \end{pmatrix}$

A.2 Explicit Expression for Γ_{ji}^e

Type-1: $\mathbf{\Gamma}^e = \frac{\bar{\tau}^s}{\bar{a}} \begin{pmatrix} \frac{1}{\bar{x}_2 - \bar{x}_1} & -\frac{1}{\bar{x}_2 - \bar{x}_1} \\ -\frac{1}{\bar{x}_2 - \bar{x}_1} & \frac{1}{\bar{x}_2 - \bar{x}_1} \end{pmatrix}$

Type-2: $\mathbf{\Gamma}^e = \frac{\bar{\tau}^s}{\bar{a}} \begin{pmatrix} \frac{7}{3(\bar{x}_2 - \bar{x}_1)} & \frac{8}{3(\bar{x}_1 - \bar{x}_2)} & \frac{1}{3(\bar{x}_2 - \bar{x}_1)} \\ \frac{8}{3(\bar{x}_1 - \bar{x}_2)} & \frac{16}{3(\bar{x}_2 - \bar{x}_1)} & \frac{8}{3(\bar{x}_1 - \bar{x}_2)} \\ \frac{1}{3(\bar{x}_2 - \bar{x}_1)} & \frac{8}{3(\bar{x}_1 - \bar{x}_2)} & \frac{7}{3(\bar{x}_2 - \bar{x}_1)} \end{pmatrix}$

Type-3: $\mathbf{\Gamma}^e = \frac{\bar{\tau}^s}{\bar{a}} \begin{pmatrix} \frac{37}{10(\bar{x}_2 - \bar{x}_1)} & \frac{189}{40(\bar{x}_1 - \bar{x}_2)} & \frac{27}{20(\bar{x}_2 - \bar{x}_1)} & \frac{13}{40(\bar{x}_1 - \bar{x}_2)} \\ \frac{189}{40(\bar{x}_1 - \bar{x}_2)} & \frac{54}{5(\bar{x}_2 - \bar{x}_1)} & \frac{297}{40(\bar{x}_1 - \bar{x}_2)} & \frac{27}{20(\bar{x}_2 - \bar{x}_1)} \\ \frac{27}{20(\bar{x}_2 - \bar{x}_1)} & \frac{297}{40(\bar{x}_1 - \bar{x}_2)} & \frac{54}{5(\bar{x}_2 - \bar{x}_1)} & \frac{189}{40(\bar{x}_1 - \bar{x}_2)} \\ \frac{13}{40(\bar{x}_1 - \bar{x}_2)} & \frac{27}{20(\bar{x}_2 - \bar{x}_1)} & \frac{189}{40(\bar{x}_1 - \bar{x}_2)} & \frac{37}{10(\bar{x}_2 - \bar{x}_1)} \end{pmatrix}$

Type-4: $\mathbf{\Gamma}^e = \frac{\bar{\tau}^s}{\bar{a}} \begin{pmatrix} -\frac{6}{5(\bar{x}_1 - \bar{x}_2)} & \frac{1}{10} & \frac{6}{5(\bar{x}_1 - \bar{x}_2)} & \frac{1}{10} \\ \frac{1}{10} & \frac{2\bar{x}_2}{15} - \frac{2\bar{x}_1}{15} & -\frac{1}{10} & \frac{\bar{x}_1}{30} - \frac{\bar{x}_2}{30} \\ \frac{6}{5(\bar{x}_1 - \bar{x}_2)} & -\frac{1}{10} & -\frac{6}{5(\bar{x}_1 - \bar{x}_2)} & -\frac{1}{10} \\ \frac{1}{10} & \frac{\bar{x}_1}{30} - \frac{\bar{x}_2}{30} & -\frac{1}{10} & \frac{2\bar{x}_2}{15} - \frac{2\bar{x}_1}{15} \end{pmatrix}$

A.3 Explicit Expression for Γ_{ji}^{pp}

$$\text{Type-1: } \Gamma^{pp} = -\bar{\kappa} \begin{pmatrix} \log(\bar{x}_2 - \bar{x}_1) - \frac{3}{2} & \frac{3}{2} - \log(\bar{x}_2 - \bar{x}_1) \\ \frac{3}{2} - \log(\bar{x}_2 - \bar{x}_1) & \log(\bar{x}_2 - \bar{x}_1) - \frac{3}{2} \end{pmatrix}$$

$$\text{Type-2: } \Gamma^{pp} = -\bar{\kappa} \begin{pmatrix} \log(\bar{x}_2 - \bar{x}_1) - \frac{5}{2} & 2 & \frac{1}{2} - \log(\bar{x}_2 - \bar{x}_1) \\ 2 & -4 & 2 \\ \frac{1}{2} - \log(\bar{x}_2 - \bar{x}_1) & 2 & \log(\bar{x}_2 - \bar{x}_1) - \frac{5}{2} \end{pmatrix}$$

$$\text{Type-3: } \Gamma^{pp} = -\bar{\kappa} \begin{pmatrix} \log(\bar{x}_2 - \bar{x}_1) - \frac{45}{16} & \frac{63}{32} & \frac{9}{16} & \frac{9}{32} - \log(\bar{x}_2 - \bar{x}_1) \\ \frac{63}{32} & -\frac{81}{16} & \frac{81}{32} & \frac{9}{16} \\ \frac{9}{16} & \frac{81}{32} & -\frac{81}{16} & \frac{63}{32} \\ \frac{9}{32} - \log(\bar{x}_2 - \bar{x}_1) & \frac{9}{16} & \frac{63}{32} & \log(\bar{x}_2 - \bar{x}_1) - \frac{45}{16} \end{pmatrix}$$

$$\text{Type-4: } \Gamma^{pp} = -\bar{\kappa} \begin{pmatrix} \log(\bar{x}_2 - \bar{x}_1) - \frac{7}{4} & \frac{1}{12}(\bar{x}_1 - \bar{x}_2) & \frac{7}{4} - \log(\bar{x}_2 - \bar{x}_1) & \frac{1}{12}(\bar{x}_1 - \bar{x}_2) \\ \frac{1}{12}(\bar{x}_1 - \bar{x}_2) & -\frac{1}{12}(\bar{x}_1 - \bar{x}_2)^2 & \frac{1}{12}(\bar{x}_2 - \bar{x}_1) & \frac{1}{24}(\bar{x}_1 - \bar{x}_2)^2 \\ \frac{7}{4} - \log(\bar{x}_2 - \bar{x}_1) & \frac{1}{12}(\bar{x}_2 - \bar{x}_1) & \log(\bar{x}_2 - \bar{x}_1) - \frac{7}{4} & \frac{1}{12}(\bar{x}_2 - \bar{x}_1) \\ \frac{1}{12}(\bar{x}_1 - \bar{x}_2) & \frac{1}{24}(\bar{x}_1 - \bar{x}_2)^2 & \frac{1}{12}(\bar{x}_2 - \bar{x}_1) & -\frac{1}{12}(\bar{x}_1 - \bar{x}_2)^2 \end{pmatrix}$$

A.4 Explicit Expression for Γ_{ji}^{pq} with $p \neq q$

Type-1:

$$\Gamma_{11}^{pq} = -\bar{\kappa} \left(\frac{-2(\bar{x}_1 - \bar{x}_3)^2 \log|\bar{x}_1 - \bar{x}_3| + 2(\bar{x}_1 - \bar{x}_4)^2 \log|\bar{x}_1 - \bar{x}_4| + 2(\bar{x}_2 - \bar{x}_3)^2 \log|\bar{x}_2 - \bar{x}_3| - 2(\bar{x}_2 - \bar{x}_4)^2 \log|\bar{x}_2 - \bar{x}_4| - 6\bar{x}_1\bar{x}_3 + 6\bar{x}_1\bar{x}_4 + 6\bar{x}_2\bar{x}_3 - 6\bar{x}_2\bar{x}_4}{4(\bar{x}_1 - \bar{x}_2)^2} \right)$$

$$\Gamma_{12}^{pq} = -\bar{\kappa} \left(\frac{2(\bar{x}_1 - \bar{x}_3)^2 \log|\bar{x}_1 - \bar{x}_3| - 2(\bar{x}_1 - \bar{x}_4)^2 \log|\bar{x}_1 - \bar{x}_4| - 2(\bar{x}_2 - \bar{x}_3)^2 \log|\bar{x}_2 - \bar{x}_3| + 2(\bar{x}_2 - \bar{x}_4)^2 \log|\bar{x}_2 - \bar{x}_4| + 6\bar{x}_1\bar{x}_3 - 6\bar{x}_1\bar{x}_4 - 6\bar{x}_2\bar{x}_3 + 6\bar{x}_2\bar{x}_4}{4(\bar{x}_1 - \bar{x}_2)^2} \right)$$

$$\Gamma_{22}^{pq} = -\bar{\kappa} \left(\frac{-2(\bar{x}_1 - \bar{x}_3)^2 \log|\bar{x}_1 - \bar{x}_3| + 2(\bar{x}_1 - \bar{x}_4)^2 \log|\bar{x}_1 - \bar{x}_4| + 2(\bar{x}_2 - \bar{x}_3)^2 \log|\bar{x}_2 - \bar{x}_3| - 2(\bar{x}_2 - \bar{x}_4)^2 \log|\bar{x}_2 - \bar{x}_4| - 6\bar{x}_1\bar{x}_3 + 6\bar{x}_1\bar{x}_4 + 6\bar{x}_2\bar{x}_3 - 6\bar{x}_2\bar{x}_4}{4(\bar{x}_1 - \bar{x}_2)^2} \right)$$

Type-2:

$$\Gamma_{11}^{pq} = -\bar{\kappa} \left[\begin{aligned} & -\frac{1}{12(\bar{x}_1 - \bar{x}_2)^2 (\bar{x}_3 - \bar{x}_4)^2} (2(\bar{x}_1 - \bar{x}_2)(\bar{x}_3 - \bar{x}_4)(8\bar{x}_1^2 - (4\bar{x}_2 + \bar{x}_3 + 11\bar{x}_4)\bar{x}_1 + 8\bar{x}_3^2 - 11\bar{x}_2\bar{x}_3 + 15\bar{x}_2\bar{x}_4 - 4\bar{x}_3\bar{x}_4) + \\ & (\bar{x}_1 - \bar{x}_3)^2 (8\bar{x}_1^2 - 12\bar{x}_2\bar{x}_1 + 11\bar{x}_3\bar{x}_1 + 8\bar{x}_3^2 - 15\bar{x}_2\bar{x}_3 - 3\bar{x}_4(5\bar{x}_1 - 9\bar{x}_2 + 4\bar{x}_3)) (\log(\bar{x}_1 - \bar{x}_3))^2 - \\ & (\bar{x}_1 - \bar{x}_4)^2 \log((\bar{x}_1 - \bar{x}_4)^2) (8\bar{x}_1^2 + \bar{x}_1(-12\bar{x}_2 - 5\bar{x}_3 + \bar{x}_4) + 9\bar{x}_2\bar{x}_3 + 3\bar{x}_2\bar{x}_4 - 4\bar{x}_3\bar{x}_4) - \\ & (\bar{x}_2 - \bar{x}_3)^2 \log((\bar{x}_2 - \bar{x}_3)^2) (\bar{x}_1(-4\bar{x}_2 - 5\bar{x}_3 + 9\bar{x}_4) + 3\bar{x}_4(\bar{x}_2 - 4\bar{x}_3) + \bar{x}_3(\bar{x}_2 + 8\bar{x}_3)) + \\ & (\bar{x}_2 - \bar{x}_4)^2 \log((\bar{x}_2 - \bar{x}_4)^2) (\bar{x}_1(-4\bar{x}_2 + 3\bar{x}_3 + \bar{x}_4) + \bar{x}_2\bar{x}_3 + 3\bar{x}_2\bar{x}_4 - 4\bar{x}_3\bar{x}_4) \end{aligned} \right]$$

$$\begin{aligned}
& \left[\frac{2}{3(\bar{x}_1 - \bar{x}_2)^2 (\bar{x}_3 - \bar{x}_4)^2} ((\bar{x}_1 - \bar{x}_3)^2 \log(|\bar{x}_1 - \bar{x}_3|) (4\bar{x}_1^2 + \bar{x}_1(-6\bar{x}_2 + 3\bar{x}_3 - 5\bar{x}_4) - 3\bar{x}_2(\bar{x}_3 - 3\bar{x}_4) + 2\bar{x}_3(\bar{x}_3 - 2\bar{x}_4)) - \right. \\
& (\bar{x}_1 - \bar{x}_4)^2 \log(|\bar{x}_1 - \bar{x}_4|) (4\bar{x}_1^2 + \bar{x}_1(-6\bar{x}_2 - 5\bar{x}_3 + 3\bar{x}_4) + \bar{x}_2(9\bar{x}_3 - 3\bar{x}_4) + 2\bar{x}_4(\bar{x}_4 - 2\bar{x}_3)) - \\
\Gamma_{12}^{pq} = & \bar{\kappa} \left. (\bar{x}_2 - \bar{x}_3)^2 \log|\bar{x}_2 - \bar{x}_3| (-\bar{x}_1(2\bar{x}_2 + \bar{x}_3 - 3\bar{x}_4) + \bar{x}_2(\bar{x}_3 + \bar{x}_4) + 2\bar{x}_3(\bar{x}_3 - 2\bar{x}_4)) + \right. \\
& (\bar{x}_2 - \bar{x}_4)^2 \log(|\bar{x}_2 - \bar{x}_4|) (-\bar{x}_1(2\bar{x}_2 - 3\bar{x}_3 + \bar{x}_4) + \bar{x}_2(\bar{x}_3 + \bar{x}_4) + 2\bar{x}_4(\bar{x}_4 - 2\bar{x}_3)) + \\
& \left. (\bar{x}_1 - \bar{x}_2)(\bar{x}_3 - \bar{x}_4) (4\bar{x}_1^2 - \bar{x}_1(2\bar{x}_2 + 3(\bar{x}_3 + \bar{x}_4)) + \bar{x}_2(\bar{x}_3 + \bar{x}_4) + 2(\bar{x}_3^2 - \bar{x}_3\bar{x}_4 + \bar{x}_4^2)) \right) \\
& \left[\frac{1}{12(\bar{x}_1 - \bar{x}_2)^2 (\bar{x}_3 - \bar{x}_4)^2} (2(\bar{x}_1 - \bar{x}_2)(\bar{x}_3 - \bar{x}_4) (-8\bar{x}_1^2 + (4\bar{x}_2 + 11\bar{x}_3 + \bar{x}_4)\bar{x}_1 - 8\bar{x}_4^2 - 15\bar{x}_2\bar{x}_3 + 11\bar{x}_2\bar{x}_4 + 4\bar{x}_3\bar{x}_4) + \right. \\
& (\bar{x}_1 - \bar{x}_4)^2 \log((\bar{x}_1 - \bar{x}_4)^2) (8\bar{x}_1^2 + \bar{x}_1(-12\bar{x}_2 - 15\bar{x}_3 + 11\bar{x}_4) - 3\bar{x}_4(5\bar{x}_2 + 4\bar{x}_3) + 27\bar{x}_2\bar{x}_3 + 8\bar{x}_4^2) + \\
\Gamma_{13}^{pq} = & \bar{\kappa} \left. (\bar{x}_1 - \bar{x}_3)^2 (-8\bar{x}_1^2 + (-12\bar{x}_2 + \bar{x}_3 - 5\bar{x}_4)\bar{x}_1 + 3\bar{x}_2\bar{x}_3 + 9\bar{x}_2\bar{x}_4 - 4\bar{x}_3\bar{x}_4) (\log(\bar{x}_1 - \bar{x}_3)^2) - \right. \\
& (\bar{x}_2 - \bar{x}_4)^2 (8\bar{x}_4^2 + (-5\bar{x}_1 + \bar{x}_2 - 12\bar{x}_3)\bar{x}_4 - 4\bar{x}_1\bar{x}_2 + 9\bar{x}_1\bar{x}_3 + 3\bar{x}_2\bar{x}_3) (\log(\bar{x}_2 - \bar{x}_4)^2) + \\
& \left. (\bar{x}_2 - \bar{x}_3)^2 (3\bar{x}_2\bar{x}_3 - 4\bar{x}_4\bar{x}_3 + \bar{x}_2\bar{x}_4 + \bar{x}_1(-4\bar{x}_2 + \bar{x}_3 + 3\bar{x}_4)) (\log(\bar{x}_2 - \bar{x}_3)^2) \right) \\
& \left[\frac{4}{3(\bar{x}_1 - \bar{x}_2)^2 (\bar{x}_3 - \bar{x}_4)^2} (-2(\bar{x}_1 - \bar{x}_3)^2 \log(|\bar{x}_3 - \bar{x}_1|) (\bar{x}_1^2 + \bar{x}_1(-2\bar{x}_2 + \bar{x}_3 - \bar{x}_4) - \bar{x}_2\bar{x}_3 + 3\bar{x}_2\bar{x}_4 + \bar{x}_3^2 - 2\bar{x}_3\bar{x}_4) + \right. \\
& 2(\bar{x}_1 - \bar{x}_4)^2 \log(|\bar{x}_4 - \bar{x}_1|) (\bar{x}_1^2 + \bar{x}_1(-2\bar{x}_2 - \bar{x}_3 + \bar{x}_4) - \bar{x}_4(\bar{x}_2 + 2\bar{x}_3) + 3\bar{x}_2\bar{x}_3 + \bar{x}_4^2) + \\
\Gamma_{22}^{pq} = & \bar{\kappa} \left. 2(\bar{x}_2 - \bar{x}_3)^2 \log(|\bar{x}_3 - \bar{x}_2|) (-\bar{x}_1(2\bar{x}_2 + \bar{x}_3 - 3\bar{x}_4) + \bar{x}_2^2 - \bar{x}_4(\bar{x}_2 + 2\bar{x}_3) + \bar{x}_2\bar{x}_3 + \bar{x}_3^2) - \right. \\
& 2(\bar{x}_2 - \bar{x}_4)^2 \log(|\bar{x}_4 - \bar{x}_2|) (-\bar{x}_1(2\bar{x}_2 - 3\bar{x}_3 + \bar{x}_4) + \bar{x}_2^2 + \bar{x}_2(\bar{x}_4 - \bar{x}_3) + \bar{x}_4(\bar{x}_4 - 2\bar{x}_3)) + \\
& \left. (\bar{x}_2 - \bar{x}_1)(\bar{x}_3 - \bar{x}_4) (2\bar{x}_1^2 - \bar{x}_1(2\bar{x}_2 + \bar{x}_3 + \bar{x}_4) + 2\bar{x}_2^2 - \bar{x}_2(\bar{x}_3 + \bar{x}_4) + 2(\bar{x}_3^2 - \bar{x}_3\bar{x}_4 + \bar{x}_4^2)) \right) \\
& \left[\frac{1}{3(\bar{x}_1 - \bar{x}_2)^2 (\bar{x}_3 - \bar{x}_4)^2} (2(\bar{x}_1 - \bar{x}_2)(\bar{x}_3 - \bar{x}_4) (2\bar{x}_1^2 - 2\bar{x}_2\bar{x}_1 + \bar{x}_3\bar{x}_1 + 2\bar{x}_2^2 + 4\bar{x}_4^2 + \bar{x}_2\bar{x}_3 - \bar{x}_4(3(\bar{x}_1 + \bar{x}_2) + 2\bar{x}_3)) - \right. \\
& (\bar{x}_1 - \bar{x}_4)^2 (2\bar{x}_1^2 + (-4\bar{x}_2 - 3\bar{x}_3 + 3\bar{x}_4)\bar{x}_1 + 4\bar{x}_4^2 + 9\bar{x}_2\bar{x}_3 - 5\bar{x}_2\bar{x}_4 - 6\bar{x}_3\bar{x}_4) (\log(\bar{x}_1 - \bar{x}_4)^2) + \\
\Gamma_{23}^{pq} = & \bar{\kappa} \left. (\bar{x}_1 - \bar{x}_3)^2 (2\bar{x}_1^2 + (-4\bar{x}_2 + \bar{x}_3 - \bar{x}_4)\bar{x}_1 + \bar{x}_2\bar{x}_3 + 3\bar{x}_2\bar{x}_4 - 2\bar{x}_3\bar{x}_4) (\log(\bar{x}_1 - \bar{x}_3)^2) + \right. \\
& (\bar{x}_2 - \bar{x}_4)^2 (2\bar{x}_2^2 - 3\bar{x}_3\bar{x}_2 + 3\bar{x}_4\bar{x}_2 + 4\bar{x}_4^2 - 6\bar{x}_3\bar{x}_4 + \bar{x}_1(-4\bar{x}_2 + 9\bar{x}_3 - 5\bar{x}_4)) (\log(\bar{x}_2 - \bar{x}_4)^2) - \\
& \left. (\bar{x}_2 - \bar{x}_3)^2 (\bar{x}_2(2\bar{x}_2 + \bar{x}_3) - \bar{x}_4(\bar{x}_2 + 2\bar{x}_3) + \bar{x}_1(-4\bar{x}_2 + \bar{x}_3 + 3\bar{x}_4)) (\log(\bar{x}_2 - \bar{x}_3)^2) \right) \\
& \left[\frac{1}{12(\bar{x}_1 - \bar{x}_2)^2 (\bar{x}_3 - \bar{x}_4)^2} (2(\bar{x}_1 - \bar{x}_2)(\bar{x}_3 - \bar{x}_4) (-8\bar{x}_2^2 + 4\bar{x}_1\bar{x}_2 + 11\bar{x}_3\bar{x}_2 - 8\bar{x}_4^2 - 15\bar{x}_1\bar{x}_3 + (11\bar{x}_1 + \bar{x}_2 + 4\bar{x}_3)\bar{x}_4) + \right. \\
& (\bar{x}_2 - \bar{x}_4)^2 (-8\bar{x}_2^2 + 15\bar{x}_3\bar{x}_2 - 11\bar{x}_4\bar{x}_2 - 8\bar{x}_4^2 + 12\bar{x}_3\bar{x}_4 + 3\bar{x}_1(4\bar{x}_2 - 9\bar{x}_3 + 5\bar{x}_4)) (\log(\bar{x}_2 - \bar{x}_4)^2) + \\
\Gamma_{33}^{pq} = & \bar{\kappa} \left. (\bar{x}_2 - \bar{x}_3)^2 (8\bar{x}_2^2 + \bar{x}_3\bar{x}_2 - 5\bar{x}_4\bar{x}_2 - 4\bar{x}_3\bar{x}_4 + 3\bar{x}_1(-4\bar{x}_2 + \bar{x}_3 + 3\bar{x}_4)) (\log(\bar{x}_2 - \bar{x}_3)^2) + \right. \\
& (\bar{x}_1 - \bar{x}_4)^2 (8\bar{x}_4^2 - 5\bar{x}_2\bar{x}_4 - 12\bar{x}_3\bar{x}_4 + 9\bar{x}_2\bar{x}_3 + \bar{x}_1(-4\bar{x}_2 + 3\bar{x}_3 + \bar{x}_4)) (\log(\bar{x}_1 - \bar{x}_4)^2) + \\
& \left. (\bar{x}_1 - \bar{x}_3)^2 (-\bar{x}_2\bar{x}_3 - 4\bar{x}_4\bar{x}_3 + 3\bar{x}_2\bar{x}_4 + \bar{x}_1(-4\bar{x}_2 + 3\bar{x}_3 + \bar{x}_4)) (\log(\bar{x}_1 - \bar{x}_3)^2) \right)
\end{aligned}$$

Type-3:

$$\begin{aligned}
& \frac{1}{160(\bar{x}_1-\bar{x}_2)^3(\bar{x}_3-\bar{x}_4)^3} \left(-(252\bar{x}_1^4-6(111\bar{x}_2-37\bar{x}_3+94\bar{x}_4))\bar{x}_1^3 + (495\bar{x}_2^2+24(65\bar{x}_4-23\bar{x}_3))\bar{x}_2+262\bar{x}_3^2+385\bar{x}_4^2-638\bar{x}_3\bar{x}_4 \right) \bar{x}_1^2 + \\
& 2(165(\bar{x}_3-4\bar{x}_4)\bar{x}_2^2 + (-319\bar{x}_3^2+860\bar{x}_4\bar{x}_3-550\bar{x}_4^2)\bar{x}_2+3\bar{x}_3(\bar{x}_3-\bar{x}_4)(37\bar{x}_3-55\bar{x}_4))\bar{x}_1+55\bar{x}_2^2(7\bar{x}_3^2-20\bar{x}_4\bar{x}_3+22\bar{x}_4^2)+ \\
& 9\bar{x}_3^2(28\bar{x}_3^2-74\bar{x}_4\bar{x}_3+55\bar{x}_4^2)-12\bar{x}_2\bar{x}_3(47\bar{x}_3^2-130\bar{x}_4\bar{x}_3+110\bar{x}_4^2)\log((\bar{x}_1-\bar{x}_3)^2)(\bar{x}_1-\bar{x}_3)^2 + \\
& 3\bar{x}_2(\bar{x}_3-\bar{x}_4)(6\bar{x}_2^4-(5\bar{x}_3+13\bar{x}_4)\bar{x}_2^3+2(69\bar{x}_3^2-115\bar{x}_4\bar{x}_3+82\bar{x}_4^2)\bar{x}_2^2-(292\bar{x}_3^3-526\bar{x}_4\bar{x}_3^2+59\bar{x}_4^2\bar{x}_3+13\bar{x}_4^3)\bar{x}_2+ \\
& 10\bar{x}_1^2(6\bar{x}_2^2-5\bar{x}_3\bar{x}_2-13\bar{x}_4\bar{x}_2+6\bar{x}_3^2+14\bar{x}_4^2-2\bar{x}_3\bar{x}_4)- \\
& 2\bar{x}_1(6\bar{x}_2^3+13\bar{x}_3\bar{x}_2^2-133\bar{x}_3^2\bar{x}_2+94\bar{x}_3^3+4\bar{x}_4^3+2(7\bar{x}_3-94\bar{x}_2)\bar{x}_4^2+(23\bar{x}_2^2+177\bar{x}_3\bar{x}_2-166\bar{x}_3^2)\bar{x}_4)+ \\
& 6(28\bar{x}_3^4-46\bar{x}_4\bar{x}_3^3+9\bar{x}_4^2\bar{x}_3^2-\bar{x}_4^3\bar{x}_3+\bar{x}_4^4)- \\
& 3\bar{x}_1(\bar{x}_3-\bar{x}_4)(168\bar{x}_1^4-4(111\bar{x}_2+26\bar{x}_3+73\bar{x}_4)\bar{x}_1^3+2(165\bar{x}_2^2+149\bar{x}_3\bar{x}_2+409\bar{x}_4\bar{x}_2+11\bar{x}_3^2+69\bar{x}_4^2+37\bar{x}_3\bar{x}_4)\bar{x}_1^2- \\
& (104\bar{x}_3^3-194\bar{x}_4\bar{x}_3^2+31\bar{x}_4^2\bar{x}_3+5\bar{x}_4^3+55\bar{x}_2^2(5\bar{x}_3+13\bar{x}_4)+4\bar{x}_2(-28\bar{x}_3^2+142\bar{x}_4\bar{x}_3+57\bar{x}_4^2))\bar{x}_1+110\bar{x}_2^2(3\bar{x}_3^2-\bar{x}_4\bar{x}_3+7\bar{x}_4^2)- \\
& 8\bar{x}_2(47\bar{x}_3^3-83\bar{x}_4\bar{x}_3^2+7\bar{x}_4^2\bar{x}_3+2\bar{x}_4^3)+6(28\bar{x}_3^4-46\bar{x}_4\bar{x}_3^3+9\bar{x}_4^2\bar{x}_3^2-\bar{x}_4^3\bar{x}_3+\bar{x}_4^4)+ \\
& (\bar{x}_2-\bar{x}_3)^2(9\bar{x}_2^4-18\bar{x}_1\bar{x}_2^3+6\bar{x}_3\bar{x}_2^2+90\bar{x}_1^2\bar{x}_2^2+13\bar{x}_3^2\bar{x}_2^2-66\bar{x}_1\bar{x}_3\bar{x}_2^2-60\bar{x}_3^3\bar{x}_2-74\bar{x}_1\bar{x}_3^2\bar{x}_2+60\bar{x}_1^2\bar{x}_3\bar{x}_2+252\bar{x}_3^4- \\
& 282\bar{x}_1\bar{x}_3^3+70\bar{x}_1^2\bar{x}_3^2+55(2\bar{x}_1+\bar{x}_2-3\bar{x}_3)^2\bar{x}_4^2- \\
& 2(333\bar{x}_3^3-6(65\bar{x}_1+19\bar{x}_2)\bar{x}_3^2+(100\bar{x}_1^2-80\bar{x}_2\bar{x}_1-11\bar{x}_2^2)\bar{x}_3+6\bar{x}_2(20\bar{x}_1^2+5\bar{x}_2\bar{x}_1+2\bar{x}_2^2))\bar{x}_4\log((\bar{x}_2-\bar{x}_3)^2)+ \\
& (\bar{x}_1-\bar{x}_4)^2(252\bar{x}_1^4-6(111\bar{x}_2+47\bar{x}_3+10\bar{x}_4)\bar{x}_1^3+(495\bar{x}_2^2+780\bar{x}_3\bar{x}_2+228\bar{x}_4\bar{x}_2+70\bar{x}_3^2+13\bar{x}_4^2-74\bar{x}_3\bar{x}_4)\bar{x}_1^2+ \\
& 2(-165(2\bar{x}_3+\bar{x}_4)\bar{x}_2^2+(-100\bar{x}_3^2+80\bar{x}_4\bar{x}_3+11\bar{x}_4^2)\bar{x}_2+3(\bar{x}_3-\bar{x}_4)(10\bar{x}_3-\bar{x}_4)\bar{x}_4)\bar{x}_1+55\bar{x}_2^2(2\bar{x}_3+\bar{x}_4)^2+ \\
& 9\bar{x}_4^2(10\bar{x}_3^2-2\bar{x}_4\bar{x}_3+\bar{x}_4^2)-12\bar{x}_2\bar{x}_4(20\bar{x}_3^2+5\bar{x}_4\bar{x}_3+2\bar{x}_4^2)\log((\bar{x}_1-\bar{x}_4)^2)- \\
& (\bar{x}_2-\bar{x}_4)^2(9\bar{x}_2^4-6(2\bar{x}_3+\bar{x}_4)\bar{x}_2^3+2(5\bar{x}_3^2+23\bar{x}_4\bar{x}_3+17\bar{x}_4^2)\bar{x}_2^2-6\bar{x}_4(10\bar{x}_3^2+16\bar{x}_4\bar{x}_3+\bar{x}_4^2)\bar{x}_2+10\bar{x}_1^2(-3\bar{x}_2+2\bar{x}_3+\bar{x}_4)^2+ \\
& 9\bar{x}_4^2(10\bar{x}_3^2-2\bar{x}_4\bar{x}_3+\bar{x}_4^2)-2\bar{x}_1(9\bar{x}_3^3+3(5\bar{x}_3+16\bar{x}_4)\bar{x}_2^2-(20\bar{x}_3^2+110\bar{x}_4\bar{x}_3+23\bar{x}_4^2)\bar{x}_2+3\bar{x}_4(20\bar{x}_3^2+5\bar{x}_4\bar{x}_3+2\bar{x}_4^2)))\log(\bar{x}_2-\bar{x}_4)^2) \\
& \frac{3}{160(\bar{x}_1-\bar{x}_2)^3(\bar{x}_3-\bar{x}_4)^3} (2(252\bar{x}_1^4-2(333\bar{x}_2-64\bar{x}_3+235\bar{x}_4))\bar{x}_1^3+(495\bar{x}_2^2+4(325\bar{x}_4-73\bar{x}_3))\bar{x}_2+109\bar{x}_3^2+210\bar{x}_4^2-310\bar{x}_3\bar{x}_4)\bar{x}_1^2 + \\
& +2(55(\bar{x}_3-10\bar{x}_4)\bar{x}_2^2+(-109\bar{x}_3^2+400\bar{x}_4\bar{x}_3-300\bar{x}_4^2)\bar{x}_2+45\bar{x}_3(\bar{x}_3-\bar{x}_4)(\bar{x}_3-2\bar{x}_4))\bar{x}_1+27\bar{x}_3^2(3\bar{x}_3^2-10\bar{x}_4\bar{x}_3+10\bar{x}_4^2)+ \\
& 55\bar{x}_2^2(\bar{x}_3-4\bar{x}_4\bar{x}_3+12\bar{x}_4^2)-36\bar{x}_2\bar{x}_3(4\bar{x}_3^2-15\bar{x}_4\bar{x}_3+20\bar{x}_4^2)\log((\bar{x}_1-\bar{x}_3)^2)(\bar{x}_1-\bar{x}_3)^2 + \\
& (\bar{x}_1-\bar{x}_2)(\bar{x}_3-\bar{x}_4)(504\bar{x}_1^4-4(207\bar{x}_2+125\bar{x}_3+172\bar{x}_4)\bar{x}_1^3+2(81\bar{x}_2^2+457\bar{x}_3\bar{x}_2+623\bar{x}_4\bar{x}_2+\bar{x}_3^2+59\bar{x}_4^2+291\bar{x}_3\bar{x}_4)\bar{x}_1^2- \\
& (18\bar{x}_2^3+(121\bar{x}_3+149\bar{x}_4)\bar{x}_2^2+2(11\bar{x}_3^2+771\bar{x}_4\bar{x}_3+163\bar{x}_4^2)\bar{x}_2+9(7\bar{x}_3^3-23\bar{x}_4\bar{x}_3^2+2\bar{x}_4^2\bar{x}_3-4\bar{x}_4^3))\bar{x}_1+18\bar{x}_2^4- \\
& (23\bar{x}_3+31\bar{x}_4)\bar{x}_2^3+2(10\bar{x}_3^2+75\bar{x}_4\bar{x}_3+23\bar{x}_4^2)\bar{x}_2^2+9(-23\bar{x}_3^3+67\bar{x}_4\bar{x}_3^2+2\bar{x}_4^2\bar{x}_3+8\bar{x}_4^3)\bar{x}_2+54\bar{x}_3(\bar{x}_3-2\bar{x}_4)(3\bar{x}_3^2-\bar{x}_4\bar{x}_3+\bar{x}_4^2))- \\
& 2(\bar{x}_2-\bar{x}_3)^2(9\bar{x}_2^4-18\bar{x}_1\bar{x}_2^3+2\bar{x}_3\bar{x}_2^2+90\bar{x}_1^2\bar{x}_2^2+10\bar{x}_3^2\bar{x}_2^2-76\bar{x}_1\bar{x}_3\bar{x}_2^2+18\bar{x}_3^3\bar{x}_2-74\bar{x}_1\bar{x}_3^2\bar{x}_2+20\bar{x}_1^2\bar{x}_3\bar{x}_2+81\bar{x}_4^3-72\bar{x}_1\bar{x}_3^3+ \\
& 10\bar{x}_1^2\bar{x}_3^2+30(2\bar{x}_1+\bar{x}_2-3\bar{x}_3)^2\bar{x}_4^2-10(2\bar{x}_3^2-5\bar{x}_3\bar{x}_2^2+27\bar{x}_3^3+4\bar{x}_1^2(5\bar{x}_2+\bar{x}_3)+\bar{x}_1(5\bar{x}_2^2-26\bar{x}_3\bar{x}_2-27\bar{x}_3^2))\bar{x}_4)\log((\bar{x}_2-\bar{x}_3)^2)+ \\
& 2((\bar{x}_2-\bar{x}_4)^2(9\bar{x}_2^4-2(8\bar{x}_3+\bar{x}_4)\bar{x}_2^3+(15\bar{x}_3^2+58\bar{x}_4\bar{x}_3+17\bar{x}_4^2)\bar{x}_2^2+18\bar{x}_4(-5\bar{x}_3^2-6\bar{x}_4\bar{x}_3+2\bar{x}_4^2)\bar{x}_2+27\bar{x}_3\bar{x}_4^2(5\bar{x}_3-2\bar{x}_4)+ \\
& 10\bar{x}_1^2(9\bar{x}_2^2-2(8\bar{x}_3+\bar{x}_4)\bar{x}_2+6\bar{x}_3^2-\bar{x}_4^2+4\bar{x}_3\bar{x}_4)-2\bar{x}_1(9\bar{x}_2^3+(20\bar{x}_3+43\bar{x}_4)\bar{x}_2^2+(-30\bar{x}_3^2-140\bar{x}_4\bar{x}_3+17\bar{x}_4^2)\bar{x}_2-9\bar{x}_4^3+90\bar{x}_3^2\bar{x}_4)) \\
& \log((\bar{x}_2-\bar{x}_4)^2)-(\bar{x}_1-\bar{x}_4)^2(252\bar{x}_1^4+(-666\bar{x}_2-376\bar{x}_3+34\bar{x}_4)\bar{x}_1^3+(495\bar{x}_2^2+16(65\bar{x}_3-2\bar{x}_4)\bar{x}_2+105\bar{x}_3^2+26\bar{x}_4^2-122\bar{x}_3\bar{x}_4)\bar{x}_1^2+ \\
& 2(-55(8\bar{x}_3+\bar{x}_4)\bar{x}_2^2+(-150\bar{x}_3^2+140\bar{x}_4\bar{x}_3+\bar{x}_4^2)\bar{x}_2+9\bar{x}_4(5\bar{x}_3^2-6\bar{x}_4\bar{x}_3+\bar{x}_4^2))\bar{x}_1+ \\
& 27\bar{x}_3\bar{x}_4^2(5\bar{x}_3-2\bar{x}_4)+55\bar{x}_2^2(6\bar{x}_3^2+4\bar{x}_4\bar{x}_3-\bar{x}_4^2)+36\bar{x}_2\bar{x}_4(\bar{x}_4^2-10\bar{x}_3^2))\log((\bar{x}_1-\bar{x}_4)^2))
\end{aligned}$$

$$\begin{aligned}
& \left[\frac{1}{160(\bar{x}_1-\bar{x}_2)^3(\bar{x}_3-\bar{x}_4)^3} \left(-2(252\bar{x}_1^4 + (-666\bar{x}_2 + 34\bar{x}_3 - 376\bar{x}_4)\bar{x}_1^3 + (495\bar{x}_2^2 + 16(65\bar{x}_4 - 2\bar{x}_3)\bar{x}_2 + 26\bar{x}_3^2 + 105\bar{x}_4^2 - 122\bar{x}_3\bar{x}_4)\bar{x}_1^2 + \right. \right. \\
& 2(-55(\bar{x}_3 + 8\bar{x}_4)\bar{x}_2^2 + (\bar{x}_3^2 + 140\bar{x}_4\bar{x}_3 - 150\bar{x}_4^2)\bar{x}_2 + 9\bar{x}_3(\bar{x}_3 - \bar{x}_4)(\bar{x}_3 - 5\bar{x}_4))\bar{x}_1 + \\
& 27\bar{x}_3^2\bar{x}_4(5\bar{x}_4 - 2\bar{x}_3) - 55\bar{x}_2^2(\bar{x}_3^2 - 4\bar{x}_4\bar{x}_3 - 6\bar{x}_4^2) + 36\bar{x}_2(\bar{x}_3^3 - 10\bar{x}_3\bar{x}_4^2)\log((\bar{x}_3 - \bar{x}_1)|(\bar{x}_1 - \bar{x}_3))^2 + \\
& (\bar{x}_2 - \bar{x}_1)(\bar{x}_3 - \bar{x}_4)(504\bar{x}_1^4 - 4(207\bar{x}_2 + 172\bar{x}_3 + 125\bar{x}_4)\bar{x}_1^3 + 2(81\bar{x}_2^2 + 623\bar{x}_3\bar{x}_2 + 457\bar{x}_4\bar{x}_2 + 59\bar{x}_3^2 + \bar{x}_4^2 + 291\bar{x}_3\bar{x}_4)\bar{x}_1^2 - \\
& (18\bar{x}_2^3 + (149\bar{x}_3 + 121\bar{x}_4)\bar{x}_2^2 + 2(163\bar{x}_3^2 + 771\bar{x}_4\bar{x}_3 + 11\bar{x}_4^2)\bar{x}_2 - 9(4\bar{x}_3^3 - 2\bar{x}_4\bar{x}_3^2 + 23\bar{x}_4^2\bar{x}_3 - 7\bar{x}_4^3))\bar{x}_1 + 18\bar{x}_2^4 - \\
& (31\bar{x}_3 + 23\bar{x}_4)\bar{x}_2^3 + 2(23\bar{x}_3^2 + 75\bar{x}_4\bar{x}_3 + 10\bar{x}_4^2)\bar{x}_2^2 + 9(8\bar{x}_3^3 + 2\bar{x}_4\bar{x}_3^2 + 67\bar{x}_4^2\bar{x}_3 - 23\bar{x}_4^3)\bar{x}_2 - 54(2\bar{x}_3 - \bar{x}_4)\bar{x}_4(\bar{x}_3^2 - \bar{x}_4\bar{x}_3 + 3\bar{x}_4^2) \Big) + \\
\Gamma_{13}^{pq} = & \bar{k} \left(2(\bar{x}_2 - \bar{x}_3)^2(9\bar{x}_2^4 - 18\bar{x}_1\bar{x}_2^3 - 2\bar{x}_3\bar{x}_2^3 + 90\bar{x}_1^2\bar{x}_2^2 + 17\bar{x}_3^2\bar{x}_2^2 - 86\bar{x}_1\bar{x}_3\bar{x}_2^2 + 36\bar{x}_3^3\bar{x}_2 - 34\bar{x}_1\bar{x}_3^2\bar{x}_2 - 20\bar{x}_1^2\bar{x}_3\bar{x}_2 + 18\bar{x}_1\bar{x}_3^3 - \right. \\
& 10\bar{x}_2^3\bar{x}_3^2 + 15(2\bar{x}_1 + \bar{x}_2 - 3\bar{x}_3)^2\bar{x}_4^2 - 2(8\bar{x}_3^3 - 29\bar{x}_3\bar{x}_2^2 + 54\bar{x}_4^2\bar{x}_2 + 20\bar{x}_1(\bar{x}_2 - 7\bar{x}_3)\bar{x}_2 + 27\bar{x}_3^3 + 20\bar{x}_1^2(4\bar{x}_2 - \bar{x}_3))\bar{x}_4 \Big) \log((\bar{x}_3 - \bar{x}_2)|) + \\
& 2((\bar{x}_1 - \bar{x}_4)^2(252\bar{x}_1^4 - 2(333\bar{x}_2 + 235\bar{x}_3 - 64\bar{x}_4)\bar{x}_1^3 + (495\bar{x}_2^2 + 4(325\bar{x}_3 - 73\bar{x}_4)\bar{x}_2 + 210\bar{x}_3^2 + 109\bar{x}_4^2 - 310\bar{x}_3\bar{x}_4)\bar{x}_1^2 + \\
& 2(55(\bar{x}_4 - 10\bar{x}_3)\bar{x}_2^2 + (-300\bar{x}_3^2 + 400\bar{x}_4\bar{x}_3 - 109\bar{x}_4^2)\bar{x}_2 + 45\bar{x}_4(2\bar{x}_3^2 - 3\bar{x}_4\bar{x}_3 + \bar{x}_4^2))\bar{x}_1 + \\
& 55\bar{x}_2^2(12\bar{x}_3^2 - 4\bar{x}_4\bar{x}_3 + \bar{x}_4^2) + 27\bar{x}_4^2(10\bar{x}_3^2 - 10\bar{x}_4\bar{x}_3 + 3\bar{x}_4^2) - 36\bar{x}_2\bar{x}_4(20\bar{x}_3^2 - 15\bar{x}_4\bar{x}_3 + 4\bar{x}_4^2)\log((\bar{x}_4 - \bar{x}_1)| - \\
& (\bar{x}_2 - \bar{x}_4)^2(9\bar{x}_2^4 + 2(\bar{x}_4 - 10\bar{x}_3)\bar{x}_2^3 + 10(3\bar{x}_3^2 + 5\bar{x}_4\bar{x}_3 + \bar{x}_4^2)\bar{x}_2^2 + 18\bar{x}_4(\bar{x}_4^2 - 10\bar{x}_3^2)\bar{x}_2 + \\
& 27\bar{x}_4^2(10\bar{x}_3^2 - 10\bar{x}_4\bar{x}_3 + 3\bar{x}_4^2) + 10\bar{x}_1^2(9\bar{x}_2^2 + 2(\bar{x}_4 - 10\bar{x}_3)\bar{x}_2 + 12\bar{x}_3^2 + \bar{x}_4^2 - 4\bar{x}_3\bar{x}_4) - \\
& 2\bar{x}_1(9\bar{x}_2^3 + (25\bar{x}_3 + 38\bar{x}_4)\bar{x}_2^2 + (-60\bar{x}_3^2 - 130\bar{x}_4\bar{x}_3 + 37\bar{x}_4^2)\bar{x}_2 + 9\bar{x}_4(20\bar{x}_3^2 - 15\bar{x}_4\bar{x}_3 + 4\bar{x}_4^2))\log((\bar{x}_4 - \bar{x}_2)|) \Big) \Big) \\
& \left[\frac{1}{160(\bar{x}_1-\bar{x}_2)^3(\bar{x}_3-\bar{x}_4)^3} \left((252\bar{x}_1^4 - 6(111\bar{x}_2 + 10\bar{x}_3 + 47\bar{x}_4)\bar{x}_1^3 + (495\bar{x}_2^2 + 228\bar{x}_3\bar{x}_2 + 780\bar{x}_4\bar{x}_2 + 13\bar{x}_3^2 + 70\bar{x}_4^2 - 74\bar{x}_3\bar{x}_4)\bar{x}_1^2 + \right. \right. \\
& (-330(\bar{x}_3 + 2\bar{x}_4)\bar{x}_2^2 + 2(11\bar{x}_3^2 + 80\bar{x}_4\bar{x}_3 - 100\bar{x}_4^2)\bar{x}_2 + 6\bar{x}_3(\bar{x}_3 - \bar{x}_4)(\bar{x}_3 - 10\bar{x}_4))\bar{x}_1 + 55\bar{x}_2^2(\bar{x}_3 + 2\bar{x}_4)^2 + \\
& 9\bar{x}_3^2(\bar{x}_3^2 - 2\bar{x}_4\bar{x}_3 + 10\bar{x}_4^2) - 12\bar{x}_2\bar{x}_3(2\bar{x}_3^2 + 5\bar{x}_4\bar{x}_3 + 20\bar{x}_4^2)\log((\bar{x}_1 - \bar{x}_3)|(\bar{x}_1 - \bar{x}_3))^2 - \\
& 3\bar{x}_2(\bar{x}_3 - \bar{x}_4)(6\bar{x}_2^4 - 13\bar{x}_3\bar{x}_2^3 + 164\bar{x}_3^2\bar{x}_2^2 - 13\bar{x}_3^3\bar{x}_2 + 6\bar{x}_3^4 + 168\bar{x}_4^4 - 4(73\bar{x}_2 + 69\bar{x}_3)\bar{x}_4^3 + 2(69\bar{x}_2^2 + 263\bar{x}_3\bar{x}_2 + 27\bar{x}_3^2)\bar{x}_4^2 - \\
& (5\bar{x}_2^3 + 230\bar{x}_3\bar{x}_2^2 + 59\bar{x}_3^2\bar{x}_2 + 6\bar{x}_3^3)\bar{x}_4 + 10\bar{x}_1^2(6\bar{x}_2^2 - 13\bar{x}_3\bar{x}_2 - 5\bar{x}_4\bar{x}_2 + 14\bar{x}_3^2 + 6\bar{x}_4^2 - 2\bar{x}_3\bar{x}_4) - \\
& 2\bar{x}_1(6\bar{x}_3^2 + 23\bar{x}_3\bar{x}_2^2 - 188\bar{x}_3^2\bar{x}_2 + 4\bar{x}_3^3 + 94\bar{x}_4^3 - (133\bar{x}_2 + 166\bar{x}_3)\bar{x}_2^2 + (13\bar{x}_2^2 + 177\bar{x}_3\bar{x}_2 + 14\bar{x}_3^2)\bar{x}_4) \Big) + \\
& 3\bar{x}_1(\bar{x}_3 - \bar{x}_4)(168\bar{x}_1^4 - 4(111\bar{x}_2 + 73\bar{x}_3 + 26\bar{x}_4)\bar{x}_1^3 + 2(165\bar{x}_2^2 + 409\bar{x}_3\bar{x}_2 + 149\bar{x}_4\bar{x}_2 + 69\bar{x}_3^2 + 11\bar{x}_4^2 + 37\bar{x}_3\bar{x}_4)\bar{x}_1^2 - \\
& (5\bar{x}_3^3 + 31\bar{x}_4\bar{x}_3^2 - 194\bar{x}_4^2\bar{x}_3 + 104\bar{x}_4^3 + 55\bar{x}_2^2(13\bar{x}_3 + 5\bar{x}_4) + 4\bar{x}_2(57\bar{x}_3^2 + 142\bar{x}_4\bar{x}_3 - 28\bar{x}_4^2))\bar{x}_1 + \\
\Gamma_{14}^{pq} = & \bar{k} \left(2(55(7\bar{x}_3^2 - \bar{x}_4\bar{x}_3 + 3\bar{x}_4^2)\bar{x}_2^2 - 4(2\bar{x}_3^3 + 7\bar{x}_4\bar{x}_3^2 - 83\bar{x}_4^2\bar{x}_3 + 47\bar{x}_4^3)\bar{x}_2 + 3(\bar{x}_3^4 - \bar{x}_4\bar{x}_3^3 + 9\bar{x}_4^2\bar{x}_3^2 - 46\bar{x}_4^3\bar{x}_3 + 28\bar{x}_4^4) \Big) - \right. \\
& (\bar{x}_2 - \bar{x}_3)^2(9\bar{x}_2^4 - 6\bar{x}_3\bar{x}_2^3 + 34\bar{x}_3^2\bar{x}_2^2 - 6\bar{x}_3^3\bar{x}_2 + 9\bar{x}_3^4 + 10(\bar{x}_2 - 3\bar{x}_3)^2\bar{x}_4^2 + 10\bar{x}_1^2(-3\bar{x}_2 + \bar{x}_3 + 2\bar{x}_4)^2 - 2(6\bar{x}_3^2 - 23\bar{x}_3\bar{x}_2 + 48\bar{x}_3^2\bar{x}_2 + 9\bar{x}_3^3)\bar{x}_4 - \\
& 2\bar{x}_1(9\bar{x}_2^3 + 48\bar{x}_3\bar{x}_2^2 - 23\bar{x}_3^2\bar{x}_2 + 6\bar{x}_3^3 - 20(\bar{x}_2 - 3\bar{x}_3)\bar{x}_4^2 + 5(3\bar{x}_2^2 - 22\bar{x}_3\bar{x}_2 + 3\bar{x}_3^2)\bar{x}_4) \Big) \log((\bar{x}_2 - \bar{x}_3)|) - \\
& (\bar{x}_1 - \bar{x}_4)^2(252\bar{x}_1^4 - 6(111\bar{x}_2 + 94\bar{x}_3 - 37\bar{x}_4)\bar{x}_1^3 + (495\bar{x}_2^2 + 24(65\bar{x}_3 - 23\bar{x}_4)\bar{x}_2 + 385\bar{x}_3^2 + 262\bar{x}_4^2 - 638\bar{x}_3\bar{x}_4)\bar{x}_1^2 + \\
& 2(165(\bar{x}_4 - 4\bar{x}_3)\bar{x}_2^2 + (-550\bar{x}_3^2 + 860\bar{x}_4\bar{x}_3 - 319\bar{x}_4^2)\bar{x}_2 + 3(\bar{x}_3 - \bar{x}_4)\bar{x}_4(55\bar{x}_3 - 37\bar{x}_4))\bar{x}_1 + 252\bar{x}_4^4 - \\
& 6(94\bar{x}_2 + 111\bar{x}_3)\bar{x}_4^3 + 1210\bar{x}_2^2\bar{x}_3^2 + 5(77\bar{x}_2^2 + 312\bar{x}_3\bar{x}_2 + 99\bar{x}_3^2)\bar{x}_4^2 - 220\bar{x}_2\bar{x}_3(5\bar{x}_2 + 6\bar{x}_3)\bar{x}_4 \log((\bar{x}_1 - \bar{x}_4)^2) + \\
& (\bar{x}_2 - \bar{x}_4)^2(9\bar{x}_2^4 + 6(\bar{x}_4 - 4\bar{x}_3)\bar{x}_2^3 + (55\bar{x}_3^2 + 22\bar{x}_4\bar{x}_3 + 13\bar{x}_4^2)\bar{x}_2^2 - 6\bar{x}_4(55\bar{x}_3^2 - 38\bar{x}_4\bar{x}_3 + 10\bar{x}_4^2)\bar{x}_2 + \\
& 9\bar{x}_4^2(55\bar{x}_3^2 - 74\bar{x}_4\bar{x}_3 + 28\bar{x}_4^2) + 10\bar{x}_1^2(9\bar{x}_2^2 + 6(\bar{x}_4 - 4\bar{x}_3)\bar{x}_2 + 22\bar{x}_3^2 + 7\bar{x}_4^2 - 20\bar{x}_3\bar{x}_4) - \\
& 2\bar{x}_1(9\bar{x}_2^3 + (30\bar{x}_3 + 33\bar{x}_4)\bar{x}_2^2 + (-110\bar{x}_3^2 - 80\bar{x}_4\bar{x}_3 + 37\bar{x}_4^2)\bar{x}_2 + 3\bar{x}_4(110\bar{x}_3^2 - 130\bar{x}_4\bar{x}_3 + 47\bar{x}_4^2)) \log((\bar{x}_2 - \bar{x}_4)^2) \Big) \Big)
\end{aligned}$$

$$\begin{aligned}
& \frac{1}{160(\bar{x}_1-\bar{x}_2)^3(\bar{x}_3-\bar{x}_4)^3} 27 \left(-2(27\bar{x}_1^4-90\bar{x}_2\bar{x}_1^3+22\bar{x}_3\bar{x}_1^3+90\bar{x}_2^2\bar{x}_1^2+22\bar{x}_3^2\bar{x}_1^2-60\bar{x}_2\bar{x}_3\bar{x}_1^2+22\bar{x}_3^2\bar{x}_1-50\bar{x}_2\bar{x}_3^2\bar{x}_1+20\bar{x}_2^2\bar{x}_3\bar{x}_1+27\bar{x}_3^4- \right. \\
& 40\bar{x}_2\bar{x}_3^3+10\bar{x}_2^2\bar{x}_3^2+10(\bar{x}_1^2+2(\bar{x}_3-2\bar{x}_2)\bar{x}_1+12\bar{x}_2^2+9\bar{x}_3^2-20\bar{x}_2\bar{x}_3)\bar{x}_4^2- \\
& 10(4\bar{x}_1^3+5(\bar{x}_3-3\bar{x}_2)\bar{x}_1^2+2(10\bar{x}_2^2-9\bar{x}_3\bar{x}_2+3\bar{x}_3^2)\bar{x}_1+\bar{x}_3(\bar{x}_2-3\bar{x}_3))(4\bar{x}_2-3\bar{x}_3)\bar{x}_4)\log((\bar{x}_3-\bar{x}_1)|(\bar{x}_1-\bar{x}_3))^2+ \\
& (\bar{x}_2-\bar{x}_1)(\bar{x}_3-\bar{x}_4)(54\bar{x}_1^4-(126\bar{x}_2+37\bar{x}_3+53\bar{x}_4)\bar{x}_1^3+(54\bar{x}_2^2+113\bar{x}_3\bar{x}_2+157\bar{x}_4\bar{x}_2-4\bar{x}_3^2-2\bar{x}_4^2+6\bar{x}_3\bar{x}_4)\bar{x}_1^2- \\
& (36\bar{x}_2^3+2(\bar{x}_3-\bar{x}_4)\bar{x}_2^2-6(\bar{x}_3^2-39\bar{x}_4\bar{x}_3-7\bar{x}_4^2)\bar{x}_2+37\bar{x}_3^3-16\bar{x}_4^3+2\bar{x}_3\bar{x}_4^2-113\bar{x}_3^2\bar{x}_4)\bar{x}_1+4\bar{x}_2^3(4\bar{x}_3+5\bar{x}_4)+ \\
& 18\bar{x}_3(\bar{x}_3-2\bar{x}_4)(3\bar{x}_3^2-\bar{x}_4\bar{x}_3+\bar{x}_4^2)-2\bar{x}_2^2(\bar{x}_3^2+21\bar{x}_4\bar{x}_3+5\bar{x}_4^2)+\bar{x}_2(-53\bar{x}_3^3+157\bar{x}_4\bar{x}_3^2+2\bar{x}_4^2\bar{x}_3+20\bar{x}_4^3))+ \\
& 2(\bar{x}_2-\bar{x}_3)^2(5(9\bar{x}_2^2+2\bar{x}_3\bar{x}_2+\bar{x}_3^2+12\bar{x}_4^2-4(5\bar{x}_2+\bar{x}_3)\bar{x}_4)\bar{x}_1^2+ \\
\Gamma_{22}^{pq} = \bar{x} & 2(-9\bar{x}_2^3-18\bar{x}_3\bar{x}_2^2-17\bar{x}_3^2\bar{x}_2-16\bar{x}_3^3+20(\bar{x}_2-4\bar{x}_3)\bar{x}_4^2+60\bar{x}_3(\bar{x}_2+\bar{x}_3)\bar{x}_4)\bar{x}_1-10(\bar{x}_2^2+2\bar{x}_3\bar{x}_2-9\bar{x}_3^2)\bar{x}_4^2+ \\
& \bar{x}_3(8\bar{x}_2^3+11\bar{x}_3\bar{x}_2^2+14\bar{x}_3^2\bar{x}_2+27\bar{x}_3^3)+10(\bar{x}_2-3\bar{x}_3)(\bar{x}_2^2+2\bar{x}_3\bar{x}_2+3\bar{x}_3^2)\bar{x}_4)\log((\bar{x}_3-\bar{x}_2)|+ \\
& 2((\bar{x}_1-\bar{x}_4)^2(27\bar{x}_1^4-2(45\bar{x}_2+16\bar{x}_3-7\bar{x}_4)\bar{x}_1^3+(90\bar{x}_2^2+30(4\bar{x}_3-\bar{x}_4)\bar{x}_2+5\bar{x}_3^2+11\bar{x}_4^2-34\bar{x}_3\bar{x}_4)\bar{x}_1^2- \\
& 2(10(8\bar{x}_3+\bar{x}_4)\bar{x}_2^2+5(2\bar{x}_3^2-12\bar{x}_4\bar{x}_3+\bar{x}_4^2)\bar{x}_2+\bar{x}_4(-5\bar{x}_3^2+18\bar{x}_4\bar{x}_3-4\bar{x}_4^2))\bar{x}_1+ \\
& 9\bar{x}_3\bar{x}_4^2(5\bar{x}_3-2\bar{x}_4)+10\bar{x}_2^2(6\bar{x}_3^2+4\bar{x}_4\bar{x}_3-\bar{x}_4^2)+10\bar{x}_2\bar{x}_4(\bar{x}_4^2-10\bar{x}_3^2))\log((\bar{x}_4-\bar{x}_1)|- \\
& (\bar{x}_2-\bar{x}_4)^2(2(5\bar{x}_2-9\bar{x}_3)\bar{x}_4^3+(10\bar{x}_2^2-36\bar{x}_3\bar{x}_2+45\bar{x}_3^2)\bar{x}_4^2+2\bar{x}_2(5\bar{x}_2^2-7\bar{x}_3\bar{x}_2-5\bar{x}_3^2)\bar{x}_4+ \\
& \bar{x}_2^2\bar{x}_3(8\bar{x}_2-5\bar{x}_3)+5\bar{x}_1^2(9\bar{x}_2^2-2(8\bar{x}_3+\bar{x}_4)\bar{x}_2+6\bar{x}_3^2-\bar{x}_4^2+4\bar{x}_3\bar{x}_4)- \\
& 2\bar{x}_1(9\bar{x}_2^3+18\bar{x}_4\bar{x}_2^2+(-10\bar{x}_3^2-60\bar{x}_4\bar{x}_3+7\bar{x}_4^2)\bar{x}_2-4\bar{x}_4^3+40\bar{x}_3^2\bar{x}_4))\log((\bar{x}_4-\bar{x}_2)|)) \\
& \frac{1}{160(\bar{x}_1-\bar{x}_2)^3(\bar{x}_3-\bar{x}_4)^3} 27 \left(2(27\bar{x}_1^4-2(45\bar{x}_2-7\bar{x}_3+16\bar{x}_4)\bar{x}_1^3+(90\bar{x}_2^2-30(\bar{x}_3-4\bar{x}_4)\bar{x}_2+11\bar{x}_3^2+5\bar{x}_4^2-34\bar{x}_3\bar{x}_4)\bar{x}_1^2- \right. \\
& 2(10(\bar{x}_3+8\bar{x}_4)\bar{x}_2^2+5(\bar{x}_3^2-12\bar{x}_4\bar{x}_3+2\bar{x}_4^2)\bar{x}_2+\bar{x}_3(-4\bar{x}_3^2+18\bar{x}_4\bar{x}_3-5\bar{x}_4^2))\bar{x}_1+ \\
& 9\bar{x}_3^2\bar{x}_4(5\bar{x}_4-2\bar{x}_3)-10\bar{x}_2^2(\bar{x}_3^2-4\bar{x}_4\bar{x}_3-6\bar{x}_4^2)+10\bar{x}_2(\bar{x}_3^3-10\bar{x}_3\bar{x}_4^2)\log((\bar{x}_3-\bar{x}_1)|(\bar{x}_1-\bar{x}_3))^2+ \\
& (\bar{x}_1-\bar{x}_2)(\bar{x}_3-\bar{x}_4)(54\bar{x}_1^4-(126\bar{x}_2+53\bar{x}_3+37\bar{x}_4)\bar{x}_1^3+(54\bar{x}_2^2+(157\bar{x}_3+113\bar{x}_4)\bar{x}_2-2(\bar{x}_3-2\bar{x}_4)(\bar{x}_3-\bar{x}_4))\bar{x}_1^2+ \\
& (-36\bar{x}_2^3+2\bar{x}_3\bar{x}_2^2-42\bar{x}_3^2\bar{x}_2+16\bar{x}_3^3-37\bar{x}_4^3+(6\bar{x}_2+113\bar{x}_3)\bar{x}_4^2-2(\bar{x}_2+117\bar{x}_3\bar{x}_2+\bar{x}_3^2)\bar{x}_4)\bar{x}_1+4\bar{x}_2^3(5\bar{x}_3+4\bar{x}_4)- \\
& 2(5\bar{x}_3^2+21\bar{x}_4\bar{x}_3+\bar{x}_4^2)\bar{x}_2^2+(20\bar{x}_3^3+2\bar{x}_4\bar{x}_3^2+157\bar{x}_4^2\bar{x}_3-53\bar{x}_4^3)\bar{x}_2-18(2\bar{x}_3-\bar{x}_4)\bar{x}_4(\bar{x}_3^2-\bar{x}_4\bar{x}_3+3\bar{x}_4^2))-2(\bar{x}_2-\bar{x}_3)^2 \\
\Gamma_{23}^{pq} = \bar{x} & (5(9\bar{x}_2^2-2(\bar{x}_3+8\bar{x}_4)\bar{x}_2-\bar{x}_3^2+6\bar{x}_4^2+4\bar{x}_3\bar{x}_4)\bar{x}_1^2-2(9\bar{x}_2^3+18\bar{x}_3\bar{x}_2^2+7\bar{x}_3^2\bar{x}_2-60\bar{x}_3\bar{x}_4\bar{x}_2-4\bar{x}_3^3-10(\bar{x}_2-4\bar{x}_3)\bar{x}_4^2)\bar{x}_1- \\
& 5(\bar{x}_2^2+2\bar{x}_3\bar{x}_2-9\bar{x}_3^2)\bar{x}_4^2+10\bar{x}_2\bar{x}_3(\bar{x}_2^2+\bar{x}_3\bar{x}_2+\bar{x}_3^2)+2(4\bar{x}_2^3-7\bar{x}_3\bar{x}_2^2-18\bar{x}_3^2\bar{x}_2-9\bar{x}_3^3)\bar{x}_4)\log((\bar{x}_3-\bar{x}_2)|+ \\
& 2((\bar{x}_2-\bar{x}_4)^2(27\bar{x}_4^4+2(7\bar{x}_2-45\bar{x}_3)\bar{x}_4^3+(11\bar{x}_2^2-30\bar{x}_3\bar{x}_2+90\bar{x}_3^2)\bar{x}_4^2+2\bar{x}_2(4\bar{x}_2^2-5\bar{x}_3\bar{x}_2-10\bar{x}_3^2)\bar{x}_4+ \\
& 10\bar{x}_2^2(\bar{x}_2-\bar{x}_3)\bar{x}_3+5\bar{x}_1^2(9\bar{x}_2^2-20\bar{x}_3\bar{x}_2+2\bar{x}_4\bar{x}_2+12\bar{x}_3^2+\bar{x}_4^2-4\bar{x}_3\bar{x}_4)- \\
& 2\bar{x}_1(9\bar{x}_2^3+18\bar{x}_4\bar{x}_2^2-20\bar{x}_3^2\bar{x}_2+17\bar{x}_4^2\bar{x}_2-60\bar{x}_3\bar{x}_4\bar{x}_2+16\bar{x}_4^3-60\bar{x}_3\bar{x}_4^2+80\bar{x}_3^2\bar{x}_4))\log((\bar{x}_4-\bar{x}_2)|- \\
& (\bar{x}_1-\bar{x}_4)^2(27\bar{x}_1^4+(-90\bar{x}_2-40\bar{x}_3+22\bar{x}_4)\bar{x}_1^3+2(11\bar{x}_4^2-5(6\bar{x}_2+5\bar{x}_3)\bar{x}_4+5(9\bar{x}_2^2+15\bar{x}_3\bar{x}_2+\bar{x}_3^2))\bar{x}_1^2+ \\
& 2(11\bar{x}_4^3-5(5\bar{x}_2+6\bar{x}_3)\bar{x}_4^2+10(\bar{x}_2^2+9\bar{x}_3\bar{x}_2+\bar{x}_3^2)\bar{x}_4-20\bar{x}_2\bar{x}_3(5\bar{x}_2+\bar{x}_3))\bar{x}_1+27\bar{x}_4^4- \\
& 10(4\bar{x}_2^2+9\bar{x}_3)\bar{x}_4^3+120\bar{x}_2^2\bar{x}_3^2+10(\bar{x}_2^2+15\bar{x}_3\bar{x}_2+9\bar{x}_3^2)\bar{x}_4^2-40\bar{x}_2\bar{x}_3(\bar{x}_2+5\bar{x}_3)\bar{x}_4)\log((\bar{x}_4-\bar{x}_1)|))
\end{aligned}$$

$$\begin{aligned}
& \frac{1}{160(\bar{x}_1-\bar{x}_2)^3(\bar{x}_3-\bar{x}_4)^3} 3(-81\bar{x}_1^4+18(-15\bar{x}_2+\bar{x}_3-4\bar{x}_4)\bar{x}_1^3+2(135\bar{x}_2^2+135\bar{x}_4\bar{x}_2+5\bar{x}_3^2+5\bar{x}_4^2-37\bar{x}_3\bar{x}_4)\bar{x}_1^2+ \\
& 2(-90(\bar{x}_3+2\bar{x}_4)\bar{x}_2^2+5(5\bar{x}_3^2+26\bar{x}_4\bar{x}_3-4\bar{x}_4^2)\bar{x}_2+\bar{x}_3(\bar{x}_3^2-38\bar{x}_4\bar{x}_3+10\bar{x}_4^2))\bar{x}_1+30\bar{x}_2^2(\bar{x}_3+2\bar{x}_4)^2+ \\
& 9\bar{x}_3^2(\bar{x}_3^2-2\bar{x}_4\bar{x}_3+10\bar{x}_4^2)-10\bar{x}_2\bar{x}_3(2\bar{x}_3^2+5\bar{x}_4\bar{x}_3+20\bar{x}_4^2)\log((\bar{x}_1-\bar{x}_3)^2)- \\
& \bar{x}_1(\bar{x}_3-\bar{x}_4)(162\bar{x}_1^4-9(60\bar{x}_2+23\bar{x}_3+7\bar{x}_4)\bar{x}_1^3+2(270\bar{x}_2^2+135(3\bar{x}_3+\bar{x}_4)\bar{x}_2+(\bar{x}_3-\bar{x}_4)(10\bar{x}_3-\bar{x}_4))\bar{x}_1^2- \\
& (23\bar{x}_3^3+121\bar{x}_4\bar{x}_3^2-914\bar{x}_4^2\bar{x}_3+500\bar{x}_4^3-10\bar{x}_2(76\bar{x}_3-85\bar{x}_4)(\bar{x}_3-\bar{x}_4)+90\bar{x}_2^2(13\bar{x}_3+5\bar{x}_4))\bar{x}_1+ \\
& 180\bar{x}_2^2(7\bar{x}_3^2-\bar{x}_4\bar{x}_3+3\bar{x}_4^2)-20\bar{x}_2(2\bar{x}_3^3+7\bar{x}_4\bar{x}_3^2-83\bar{x}_4^2\bar{x}_3+47\bar{x}_4^3)+18(\bar{x}_3^4-\bar{x}_4\bar{x}_3^3+9\bar{x}_4^2\bar{x}_3^2-46\bar{x}_4^3\bar{x}_3+28\bar{x}_4^4)+ \\
& \bar{x}_2(\bar{x}_3-\bar{x}_4)(36(2\bar{x}_3+\bar{x}_4)\bar{x}_2^3+2(23\bar{x}_3^2-163\bar{x}_4\bar{x}_3+59\bar{x}_4^2)\bar{x}_2^2-(31\bar{x}_3^3+149\bar{x}_4\bar{x}_3^2-1246\bar{x}_4^2\bar{x}_3+688\bar{x}_4^3)\bar{x}_2+ \\
& 45\bar{x}_1^2(6\bar{x}_2^2-13\bar{x}_3\bar{x}_2-5\bar{x}_4\bar{x}_2+14\bar{x}_3^2+6\bar{x}_4^2-2\bar{x}_3\bar{x}_4)+18(\bar{x}_3^4-\bar{x}_4\bar{x}_3^3+9\bar{x}_4^2\bar{x}_3^2-46\bar{x}_4^3\bar{x}_3+28\bar{x}_4^4)- \\
\Gamma_{24}^{pq} = -\bar{k} & 2\bar{x}_1(54\bar{x}_2^3+27(\bar{x}_3+\bar{x}_4)\bar{x}_2^2+(-682\bar{x}_3^2+698\bar{x}_4\bar{x}_3-502\bar{x}_4^2)\bar{x}_2+8(2\bar{x}_3^3+7\bar{x}_4\bar{x}_3^2-83\bar{x}_4^2\bar{x}_3+47\bar{x}_4^3))+ \\
& (\bar{x}_2-\bar{x}_3)^2(18(2\bar{x}_3+\bar{x}_4)\bar{x}_2^3+(17\bar{x}_3^2-34\bar{x}_4\bar{x}_3-10\bar{x}_4^2)\bar{x}_2^2-2\bar{x}_3(\bar{x}_3^2+43\bar{x}_4\bar{x}_3+10\bar{x}_4^2)\bar{x}_2+15\bar{x}_1^2(-3\bar{x}_2+\bar{x}_3+2\bar{x}_4)^2+ \\
& 9\bar{x}_3^2(\bar{x}_3^2-2\bar{x}_4\bar{x}_3+10\bar{x}_4^2)+2\bar{x}_1(-27\bar{x}_2^2-54\bar{x}_3\bar{x}_2^2+29\bar{x}_3^2\bar{x}_2-8\bar{x}_3^3+20(\bar{x}_2-4\bar{x}_3)\bar{x}_4^2+20(7\bar{x}_2-\bar{x}_3)\bar{x}_3\bar{x}_4)) \\
& \log((\bar{x}_2-\bar{x}_3)^2)+(\bar{x}_1-\bar{x}_4)^2(81\bar{x}_1^4-18(15\bar{x}_2+8\bar{x}_3-5\bar{x}_4)\bar{x}_1^3+(270\bar{x}_2^2+270(2\bar{x}_3-\bar{x}_4)\bar{x}_2+55\bar{x}_3^2+109\bar{x}_4^2-218\bar{x}_3\bar{x}_4)\bar{x}_1^2+ \\
& 2(90(\bar{x}_4-4\bar{x}_3)\bar{x}_2^2-5(22\bar{x}_3^2-80\bar{x}_4\bar{x}_3+31\bar{x}_4^2)\bar{x}_2+\bar{x}_4(55\bar{x}_3^2-146\bar{x}_4\bar{x}_3+64\bar{x}_4^2))\bar{x}_1+252\bar{x}_4^4- \\
& 2(235\bar{x}_2+333\bar{x}_3)\bar{x}_4^3+660\bar{x}_2^2\bar{x}_3^2+5(42\bar{x}_2^2+260\bar{x}_3\bar{x}_2+99\bar{x}_3^2)\bar{x}_4^2-100\bar{x}_2\bar{x}_3(6\bar{x}_2+11\bar{x}_3)\bar{x}_4\log((\bar{x}_1-\bar{x}_4)^2)- \\
& (\bar{x}_2-\bar{x}_4)^2(18(2\bar{x}_3+\bar{x}_4)\bar{x}_2^3+(-55\bar{x}_3^2+2\bar{x}_4\bar{x}_3+26\bar{x}_4^2)\bar{x}_2^2+2\bar{x}_4(-55\bar{x}_3^2-16\bar{x}_4\bar{x}_3+17\bar{x}_4^2)\bar{x}_2+ \\
& 9\bar{x}_4^2(55\bar{x}_3^2-74\bar{x}_4\bar{x}_3+28\bar{x}_4^2)+15\bar{x}_1^2(9\bar{x}_2^2+6(\bar{x}_4-4\bar{x}_3)\bar{x}_2+22\bar{x}_3^2+7\bar{x}_4^2-20\bar{x}_3\bar{x}_4)- \\
& 2\bar{x}_1(27\bar{x}_2^3+54\bar{x}_4\bar{x}_2^2+(-110\bar{x}_3^2-140\bar{x}_4\bar{x}_3+61\bar{x}_4^2)\bar{x}_2+4\bar{x}_4(110\bar{x}_3^2-130\bar{x}_4\bar{x}_3+47\bar{x}_4^2))\log((\bar{x}_2-\bar{x}_4)^2)) \\
& \frac{1}{160(\bar{x}_1-\bar{x}_2)^3(\bar{x}_3-\bar{x}_4)^3} 27(2(9\bar{x}_2-5\bar{x}_3-4\bar{x}_4)\bar{x}_1^3+(-45\bar{x}_2^2+36\bar{x}_3\bar{x}_2-10\bar{x}_3^2+5\bar{x}_4^2+14\bar{x}_3\bar{x}_4)\bar{x}_1^2+ \\
& 2(5(\bar{x}_3+8\bar{x}_4)\bar{x}_2^2+(7\bar{x}_3^2-60\bar{x}_4\bar{x}_3-10\bar{x}_4^2)\bar{x}_2+\bar{x}_3(-5\bar{x}_3^2+18\bar{x}_4\bar{x}_3+5\bar{x}_4^2))\bar{x}_1+ \\
& 9\bar{x}_3^2\bar{x}_4(2\bar{x}_3-5\bar{x}_4)+5\bar{x}_2^2(\bar{x}_3^2-4\bar{x}_4\bar{x}_3-6\bar{x}_4^2)-8\bar{x}_2(\bar{x}_3^3-10\bar{x}_3\bar{x}_4^2)\log((\bar{x}_1-\bar{x}_3)^2)+ \\
& (\bar{x}_1-\bar{x}_2)(\bar{x}_3-\bar{x}_4)(-54\bar{x}_2^4+(53\bar{x}_3+37\bar{x}_4)\bar{x}_2^3+2(\bar{x}_3-\bar{x}_4)(\bar{x}_3-2\bar{x}_4)\bar{x}_2^2+(-16\bar{x}_3^3+2\bar{x}_4\bar{x}_3^2-113\bar{x}_4^2\bar{x}_3+37\bar{x}_4^3)\bar{x}_2+ \\
& 4\bar{x}_1^3(9\bar{x}_2-5\bar{x}_3-4\bar{x}_4)+18(2\bar{x}_3-\bar{x}_4)\bar{x}_4(\bar{x}_3^2-\bar{x}_4\bar{x}_3+3\bar{x}_4^2)+2\bar{x}_1^2(-27\bar{x}_2^2+(\bar{x}_4-\bar{x}_3)\bar{x}_2+5\bar{x}_3^2+\bar{x}_4^2+21\bar{x}_3\bar{x}_4)+ \\
& \bar{x}_1(126\bar{x}_2^3-(157\bar{x}_3+113\bar{x}_4)\bar{x}_2^2+6(7\bar{x}_3^2+39\bar{x}_4\bar{x}_3-\bar{x}_4^2)\bar{x}_2-20\bar{x}_3^3+53\bar{x}_4^3-157\bar{x}_3\bar{x}_4^2-2\bar{x}_3^2\bar{x}_4))+2(\bar{x}_2-\bar{x}_3)^2 \\
\Gamma_{33}^{pq} = -\bar{k} & 10(9\bar{x}_2^2-2(\bar{x}_3+8\bar{x}_4)\bar{x}_2-\bar{x}_3^2+6\bar{x}_4^2+4\bar{x}_3\bar{x}_4)\bar{x}_1^2+10(-9\bar{x}_2^3-3\bar{x}_3\bar{x}_2^2-\bar{x}_3^2\bar{x}_2+12(\bar{x}_2+\bar{x}_3)\bar{x}_4\bar{x}_2+\bar{x}_3^3-2(\bar{x}_2+5\bar{x}_3)\bar{x}_4^2)\bar{x}_1+ \\
& 5(\bar{x}_2^2+2\bar{x}_3\bar{x}_2+9\bar{x}_3^2)\bar{x}_4^2+\bar{x}_2(27\bar{x}_2^3+14\bar{x}_3\bar{x}_2^2+11\bar{x}_3^2\bar{x}_2+8\bar{x}_3^3)-2(16\bar{x}_2^3+17\bar{x}_3\bar{x}_2^2+18\bar{x}_3^2\bar{x}_2+9\bar{x}_3^3)\bar{x}_4\log((\bar{x}_2-\bar{x}_3)^2)+ \\
& 2((\bar{x}_1-\bar{x}_4)^2(27\bar{x}_4^4-2(16\bar{x}_2+45\bar{x}_3)\bar{x}_4^3+5(\bar{x}_2^2+24\bar{x}_3\bar{x}_2+18\bar{x}_3^2)\bar{x}_4^2-20\bar{x}_2\bar{x}_3(\bar{x}_2+8\bar{x}_3)\bar{x}_4+60\bar{x}_2^2\bar{x}_3^2+ \\
& 2\bar{x}_1^3(-9\bar{x}_2+5\bar{x}_3+4\bar{x}_4)+\bar{x}_1^2(45\bar{x}_2^2-36\bar{x}_4\bar{x}_2-10\bar{x}_3^2+11\bar{x}_4^2-10\bar{x}_3\bar{x}_4)- \\
& 2\bar{x}_1(-7\bar{x}_4^3+(17\bar{x}_2+15\bar{x}_3)\bar{x}_4^2-5(\bar{x}_2^2+12\bar{x}_3\bar{x}_2-2\bar{x}_3^2)\bar{x}_4+10\bar{x}_2\bar{x}_3(5\bar{x}_2-2\bar{x}_3))\log((\bar{x}_1-\bar{x}_4)^2)- \\
& (\bar{x}_2-\bar{x}_4)^2(27\bar{x}_2^4+(22\bar{x}_4-40\bar{x}_3)\bar{x}_2^3+2(5\bar{x}_3^2-25\bar{x}_4\bar{x}_3+11\bar{x}_4^2)\bar{x}_2^2+2\bar{x}_4(10\bar{x}_3^2-30\bar{x}_4\bar{x}_3+11\bar{x}_4^2)\bar{x}_2+ \\
& 10\bar{x}_1^2(9\bar{x}_2^2-20\bar{x}_3\bar{x}_2+2\bar{x}_4\bar{x}_2+12\bar{x}_3^2+\bar{x}_4^2-4\bar{x}_3\bar{x}_4)+9\bar{x}_4^2(10\bar{x}_3^2-10\bar{x}_4\bar{x}_3+3\bar{x}_4^2)- \\
& 10\bar{x}_1(4\bar{x}_4^3+5(\bar{x}_2-3\bar{x}_3)\bar{x}_4^2+2(3\bar{x}_2^2-9\bar{x}_3\bar{x}_2+10\bar{x}_3^2)\bar{x}_4+\bar{x}_2(3\bar{x}_2-\bar{x}_3)(3\bar{x}_2-4\bar{x}_3))\log((\bar{x}_2-\bar{x}_4)^2))
\end{aligned}$$

$$\Gamma_{34}^{pq} = -\bar{\kappa} \left[\frac{1}{160(\bar{\kappa}_1 - \bar{\kappa}_2)^3 (\bar{\kappa}_3 - \bar{\kappa}_4)^3} 3(2(18(-3\bar{\kappa}_2 + 2\bar{\kappa}_3 + \bar{\kappa}_4) \bar{\kappa}_1^3 + (135\bar{\kappa}_2^2 - 108\bar{\kappa}_3\bar{\kappa}_2 + 17\bar{\kappa}_3^2 - 10\bar{\kappa}_4^2 - 34\bar{\kappa}_3\bar{\kappa}_4) \bar{\kappa}_1^2 - 2(45(\bar{\kappa}_3 + 2\bar{\kappa}_4) \bar{\kappa}_2^2 - (29\bar{\kappa}_3^2 + 140\bar{\kappa}_4\bar{\kappa}_3 + 20\bar{\kappa}_4^2) \bar{\kappa}_2 + \bar{\kappa}_3(\bar{\kappa}_3^2 + 43\bar{\kappa}_4\bar{\kappa}_3 + 10\bar{\kappa}_4^2)) \bar{\kappa}_1 + 15\bar{\kappa}_2^2(\bar{\kappa}_3 + 2\bar{\kappa}_4)^2 + 9\bar{\kappa}_3^2(\bar{\kappa}_3^2 - 2\bar{\kappa}_4\bar{\kappa}_3 + 10\bar{\kappa}_4^2) - 8\bar{\kappa}_2\bar{\kappa}_3(2\bar{\kappa}_3^2 + 5\bar{\kappa}_4\bar{\kappa}_3 + 20\bar{\kappa}_4^2)) \log((\bar{\kappa}_1 - \bar{\kappa}_3) | (\bar{\kappa}_1 - \bar{\kappa}_3)^2 + (\bar{\kappa}_2 - \bar{\kappa}_1)(\bar{\kappa}_3 - \bar{\kappa}_4) (-162\bar{\kappa}_2^4 + 9(23\bar{\kappa}_3 + 7\bar{\kappa}_4) \bar{\kappa}_2^3 - 2(\bar{\kappa}_3 - \bar{\kappa}_4)(10\bar{\kappa}_3 - \bar{\kappa}_4) \bar{\kappa}_2^2 + (23\bar{\kappa}_3^3 + 121\bar{\kappa}_4\bar{\kappa}_3^2 - 914\bar{\kappa}_4^2\bar{\kappa}_3 + 500\bar{\kappa}_4^3) \bar{\kappa}_2 + 36\bar{\kappa}_1^3(3\bar{\kappa}_2 - 2\bar{\kappa}_3 - \bar{\kappa}_4) - 2\bar{\kappa}_1^2(81\bar{\kappa}_2^2 + 9(\bar{\kappa}_3 - \bar{\kappa}_4) \bar{\kappa}_2 + 23\bar{\kappa}_3^2 + 59\bar{\kappa}_4^2 - 163\bar{\kappa}_3\bar{\kappa}_4) - 18(\bar{\kappa}_3^4 - \bar{\kappa}_4\bar{\kappa}_3^3 + 9\bar{\kappa}_4^2\bar{\kappa}_3^2 - 46\bar{\kappa}_4^3\bar{\kappa}_3 + 28\bar{\kappa}_4^4) + \bar{\kappa}_1(378\bar{\kappa}_2^3 - 9(67\bar{\kappa}_3 + 23\bar{\kappa}_4) \bar{\kappa}_2^2 - 6(25\bar{\kappa}_3^2 - 257\bar{\kappa}_4\bar{\kappa}_3 + 97\bar{\kappa}_4^2) \bar{\kappa}_2 + 31\bar{\kappa}_3^3 + 688\bar{\kappa}_3^2 - 1246\bar{\kappa}_3\bar{\kappa}_4 + 149\bar{\kappa}_3^2\bar{\kappa}_4)) - 2(\bar{\kappa}_2 - \bar{\kappa}_3)^2(81\bar{\kappa}_2^4 + 18(\bar{\kappa}_3 - 4\bar{\kappa}_4) \bar{\kappa}_2^3 + 2(5\bar{\kappa}_3^2 - 37\bar{\kappa}_4\bar{\kappa}_3 + 5\bar{\kappa}_4^2) \bar{\kappa}_2^2 + 2\bar{\kappa}_3(\bar{\kappa}_3^2 - 38\bar{\kappa}_4\bar{\kappa}_3 + 10\bar{\kappa}_4^2) \bar{\kappa}_2 + 30\bar{\kappa}_1^2(-3\bar{\kappa}_2 + \bar{\kappa}_3 + 2\bar{\kappa}_4)^2 + 9\bar{\kappa}_3^2(\bar{\kappa}_3^2 - 2\bar{\kappa}_4\bar{\kappa}_3 + 10\bar{\kappa}_4^2) - 10\bar{\kappa}_1(27\bar{\kappa}_2^3 - 5\bar{\kappa}_3^2\bar{\kappa}_2 + 2\bar{\kappa}_3^3 + 4(\bar{\kappa}_2 + 5\bar{\kappa}_3) \bar{\kappa}_4^2 + (-27\bar{\kappa}_2^2 - 26\bar{\kappa}_3\bar{\kappa}_2 + 5\bar{\kappa}_3^2) \bar{\kappa}_4) \log((\bar{\kappa}_2 - \bar{\kappa}_3) | + 2((\bar{\kappa}_2 - \bar{\kappa}_4)^2(81\bar{\kappa}_2^4 + 18(5\bar{\kappa}_4 - 8\bar{\kappa}_3) \bar{\kappa}_2^3 + (55\bar{\kappa}_3^2 - 218\bar{\kappa}_4\bar{\kappa}_3 + 109\bar{\kappa}_4^2) \bar{\kappa}_2^2 + 2\bar{\kappa}_4(55\bar{\kappa}_3^2 - 146\bar{\kappa}_4\bar{\kappa}_3 + 64\bar{\kappa}_4^2) \bar{\kappa}_2 + 9\bar{\kappa}_4^2(55\bar{\kappa}_3^2 - 74\bar{\kappa}_4\bar{\kappa}_3 + 28\bar{\kappa}_4^2) + 30\bar{\kappa}_1^2(9\bar{\kappa}_2^2 + 6(\bar{\kappa}_4 - 4\bar{\kappa}_3) \bar{\kappa}_2 + 22\bar{\kappa}_3^2 + 7\bar{\kappa}_4^2 - 20\bar{\kappa}_3\bar{\kappa}_4) - 10\bar{\kappa}_1(27\bar{\kappa}_2^3 + 27(\bar{\kappa}_4 - 2\bar{\kappa}_3) \bar{\kappa}_2^2 + (22\bar{\kappa}_3^2 - 80\bar{\kappa}_4\bar{\kappa}_3 + 31\bar{\kappa}_4^2) \bar{\kappa}_2 + \bar{\kappa}_4(110\bar{\kappa}_3^2 - 130\bar{\kappa}_4\bar{\kappa}_3 + 47\bar{\kappa}_4^2)) \log((\bar{\kappa}_2 - \bar{\kappa}_4) | - (\bar{\kappa}_1 - \bar{\kappa}_4)^2(18(-3\bar{\kappa}_2 + 2\bar{\kappa}_3 + \bar{\kappa}_4) \bar{\kappa}_1^3 + (135\bar{\kappa}_2^2 - 108\bar{\kappa}_4\bar{\kappa}_2 - 55\bar{\kappa}_3^2 + 2\bar{\kappa}_4(\bar{\kappa}_3 + 13\bar{\kappa}_4)) \bar{\kappa}_1^2 + 2(45(\bar{\kappa}_4 - 4\bar{\kappa}_3) \bar{\kappa}_2^2 + (110\bar{\kappa}_3^2 + 140\bar{\kappa}_4\bar{\kappa}_3 - 61\bar{\kappa}_4^2) \bar{\kappa}_2 + \bar{\kappa}_4(-55\bar{\kappa}_3^2 - 16\bar{\kappa}_4\bar{\kappa}_3 + 17\bar{\kappa}_4^2)) \bar{\kappa}_1 + 15\bar{\kappa}_2^2(22\bar{\kappa}_3^2 - 20\bar{\kappa}_4\bar{\kappa}_3 + 7\bar{\kappa}_4^2) + 9\bar{\kappa}_4^2(55\bar{\kappa}_3^2 - 74\bar{\kappa}_4\bar{\kappa}_3 + 28\bar{\kappa}_4^2) - 8\bar{\kappa}_2\bar{\kappa}_4(110\bar{\kappa}_3^2 - 130\bar{\kappa}_4\bar{\kappa}_3 + 47\bar{\kappa}_4^2) \log((\bar{\kappa}_1 - \bar{\kappa}_4) |)) \right]$$

$$\Gamma_{44}^{pq} = -\bar{\kappa} \left[\frac{1}{160(\bar{\kappa}_1 - \bar{\kappa}_2)^3 (\bar{\kappa}_3 - \bar{\kappa}_4)^3} \left(- (9\bar{\kappa}_1^4 - 6(3\bar{\kappa}_2 + \bar{\kappa}_3 + 2\bar{\kappa}_4) \bar{\kappa}_1^3 + 2(45\bar{\kappa}_2^2 - 3(16\bar{\kappa}_3 + 5\bar{\kappa}_4) \bar{\kappa}_2 + 17\bar{\kappa}_3^2 + 5\bar{\kappa}_4^2 + 23\bar{\kappa}_3\bar{\kappa}_4) \bar{\kappa}_1^2 - 2(30(\bar{\kappa}_3 + 2\bar{\kappa}_4) \bar{\kappa}_2^2 - (23\bar{\kappa}_3^2 + 110\bar{\kappa}_4\bar{\kappa}_3 + 20\bar{\kappa}_4^2) \bar{\kappa}_2 + 3\bar{\kappa}_3(\bar{\kappa}_3^2 + 16\bar{\kappa}_4\bar{\kappa}_3 + 10\bar{\kappa}_4^2)) \bar{\kappa}_1 + 10\bar{\kappa}_2^2(\bar{\kappa}_3 + 2\bar{\kappa}_4)^2 + 9\bar{\kappa}_3^2(\bar{\kappa}_3^2 - 2\bar{\kappa}_4\bar{\kappa}_3 + 10\bar{\kappa}_4^2) - 6\bar{\kappa}_2\bar{\kappa}_3(2\bar{\kappa}_3^2 + 5\bar{\kappa}_4\bar{\kappa}_3 + 20\bar{\kappa}_4^2) \log((\bar{\kappa}_1 - \bar{\kappa}_3)^2 | (\bar{\kappa}_1 - \bar{\kappa}_3)^2 + 3\bar{\kappa}_2(\bar{\kappa}_3 - \bar{\kappa}_4)(168\bar{\kappa}_2^4 - 4(73\bar{\kappa}_3 + 26\bar{\kappa}_4) \bar{\kappa}_2^3 + 2(69\bar{\kappa}_3^2 + 37\bar{\kappa}_4\bar{\kappa}_3 + 11\bar{\kappa}_4^2) \bar{\kappa}_2^2 - (5\bar{\kappa}_3^3 + 31\bar{\kappa}_4\bar{\kappa}_3^2 - 194\bar{\kappa}_4^2\bar{\kappa}_3 + 104\bar{\kappa}_4^3) \bar{\kappa}_2 + 55\bar{\kappa}_1^2(6\bar{\kappa}_2^2 - 13\bar{\kappa}_3\bar{\kappa}_2 - 5\bar{\kappa}_4\bar{\kappa}_2 + 14\bar{\kappa}_3^2 + 6\bar{\kappa}_4^2 - 2\bar{\kappa}_3\bar{\kappa}_4) + 6(\bar{\kappa}_3^4 - \bar{\kappa}_4\bar{\kappa}_3^3 + 9\bar{\kappa}_4^2\bar{\kappa}_3^2 - 46\bar{\kappa}_4^3\bar{\kappa}_3 + 28\bar{\kappa}_4^4) - 2\bar{\kappa}_1(222\bar{\kappa}_2^3 - (409\bar{\kappa}_3 + 149\bar{\kappa}_4) \bar{\kappa}_2^2 + 2(57\bar{\kappa}_3^2 + 142\bar{\kappa}_4\bar{\kappa}_3 - 28\bar{\kappa}_4^2) \bar{\kappa}_2 + 4(2\bar{\kappa}_3^3 + 7\bar{\kappa}_4\bar{\kappa}_3^2 - 83\bar{\kappa}_4^2\bar{\kappa}_3 + 47\bar{\kappa}_4^3)) - 3\bar{\kappa}_1(\bar{\kappa}_3 - \bar{\kappa}_4)(6\bar{\kappa}_1^4 - (12\bar{\kappa}_2 + 13\bar{\kappa}_3 + 5\bar{\kappa}_4) \bar{\kappa}_1^3 + 2(30\bar{\kappa}_2^2 - 23\bar{\kappa}_3\bar{\kappa}_2 - 13\bar{\kappa}_4\bar{\kappa}_2 + 82\bar{\kappa}_3^2 + 69\bar{\kappa}_4^2 - 115\bar{\kappa}_3\bar{\kappa}_4) \bar{\kappa}_1^2 - (13\bar{\kappa}_3^3 + 59\bar{\kappa}_4\bar{\kappa}_3^2 - 526\bar{\kappa}_4^2\bar{\kappa}_3 + 292\bar{\kappa}_4^3 + 10\bar{\kappa}_2^2(13\bar{\kappa}_3 + 5\bar{\kappa}_4) + \bar{\kappa}_2(-376\bar{\kappa}_3^2 + 354\bar{\kappa}_4\bar{\kappa}_3 - 266\bar{\kappa}_4^2)) \bar{\kappa}_1 + 2(10(7\bar{\kappa}_3^2 - \bar{\kappa}_4\bar{\kappa}_3 + 3\bar{\kappa}_4^2) \bar{\kappa}_2^2 - 2(2\bar{\kappa}_3^3 + 7\bar{\kappa}_4\bar{\kappa}_3^2 - 83\bar{\kappa}_4^2\bar{\kappa}_3 + 47\bar{\kappa}_4^3) \bar{\kappa}_2 + 3(\bar{\kappa}_3^4 - \bar{\kappa}_4\bar{\kappa}_3^3 + 9\bar{\kappa}_4^2\bar{\kappa}_3^2 - 46\bar{\kappa}_4^3\bar{\kappa}_3 + 28\bar{\kappa}_4^4)) + (\bar{\kappa}_2 - \bar{\kappa}_3)^2(252\bar{\kappa}_2^4 - 6(10\bar{\kappa}_3 + 47\bar{\kappa}_4) \bar{\kappa}_2^3 + (13\bar{\kappa}_3^2 - 74\bar{\kappa}_4\bar{\kappa}_3 + 70\bar{\kappa}_4^2) \bar{\kappa}_2^2 + 6\bar{\kappa}_3(\bar{\kappa}_3 - \bar{\kappa}_4)(\bar{\kappa}_3 - 10\bar{\kappa}_4) \bar{\kappa}_2 + 55\bar{\kappa}_1^2(-3\bar{\kappa}_2 + \bar{\kappa}_3 + 2\bar{\kappa}_4)^2 + 9\bar{\kappa}_3^2(\bar{\kappa}_3^2 - 2\bar{\kappa}_4\bar{\kappa}_3 + 10\bar{\kappa}_4^2) + 2\bar{\kappa}_1(-333\bar{\kappa}_2^3 + 6(19\bar{\kappa}_3 + 65\bar{\kappa}_4) \bar{\kappa}_2^2 + (11\bar{\kappa}_3^2 + 80\bar{\kappa}_4\bar{\kappa}_3 - 100\bar{\kappa}_4^2) \bar{\kappa}_2 - 6\bar{\kappa}_3(2\bar{\kappa}_3^2 + 5\bar{\kappa}_4\bar{\kappa}_3 + 20\bar{\kappa}_4^2)) \log((\bar{\kappa}_2 - \bar{\kappa}_3)^2 | + (\bar{\kappa}_1 - \bar{\kappa}_4)^2(9\bar{\kappa}_1^4 + 6(-3\bar{\kappa}_2 - 4\bar{\kappa}_3 + \bar{\kappa}_4) \bar{\kappa}_1^3 + (90\bar{\kappa}_2^2 - 60\bar{\kappa}_3\bar{\kappa}_2 - 66\bar{\kappa}_4\bar{\kappa}_2 + 55\bar{\kappa}_3^2 + 13\bar{\kappa}_4^2 + 22\bar{\kappa}_3\bar{\kappa}_4) \bar{\kappa}_1^2 + (60(\bar{\kappa}_4 - 4\bar{\kappa}_3) \bar{\kappa}_2^2 + 2(110\bar{\kappa}_3^2 + 80\bar{\kappa}_4\bar{\kappa}_3 - 37\bar{\kappa}_4^2) \bar{\kappa}_2 - 6\bar{\kappa}_4(55\bar{\kappa}_3^2 - 38\bar{\kappa}_4\bar{\kappa}_3 + 10\bar{\kappa}_4^2)) \bar{\kappa}_1 + 252\bar{\kappa}_4^4 - 6(47\bar{\kappa}_2 + 111\bar{\kappa}_3) \bar{\kappa}_4^3 + 220\bar{\kappa}_2^2\bar{\kappa}_3^2 + 5(14\bar{\kappa}_2^2 + 156\bar{\kappa}_3\bar{\kappa}_2 + 99\bar{\kappa}_3^2) \bar{\kappa}_4^2 - 20\bar{\kappa}_2\bar{\kappa}_3(10\bar{\kappa}_2 + 33\bar{\kappa}_3) \bar{\kappa}_4) \log((\bar{\kappa}_1 - \bar{\kappa}_4)^2 | - (\bar{\kappa}_2 - \bar{\kappa}_4)^2(252\bar{\kappa}_2^4 + 6(37\bar{\kappa}_4 - 94\bar{\kappa}_3) \bar{\kappa}_2^3 + (385\bar{\kappa}_3^2 - 638\bar{\kappa}_4\bar{\kappa}_3 + 262\bar{\kappa}_4^2) \bar{\kappa}_2^2 + 6(\bar{\kappa}_3 - \bar{\kappa}_4) \bar{\kappa}_4(55\bar{\kappa}_3 - 37\bar{\kappa}_4) \bar{\kappa}_2 + 9\bar{\kappa}_4^2(55\bar{\kappa}_3^2 - 74\bar{\kappa}_4\bar{\kappa}_3 + 28\bar{\kappa}_4^2) + 55\bar{\kappa}_1^2(9\bar{\kappa}_2^2 + 6(\bar{\kappa}_4 - 4\bar{\kappa}_3) \bar{\kappa}_2 + 22\bar{\kappa}_3^2 + 7\bar{\kappa}_4^2 - 20\bar{\kappa}_3\bar{\kappa}_4) - 2\bar{\kappa}_1(333\bar{\kappa}_2^3 + (276\bar{\kappa}_4 - 780\bar{\kappa}_3) \bar{\kappa}_2^2 + (550\bar{\kappa}_3^2 - 860\bar{\kappa}_4\bar{\kappa}_3 + 319\bar{\kappa}_4^2) \bar{\kappa}_2 + 6\bar{\kappa}_4(110\bar{\kappa}_3^2 - 130\bar{\kappa}_4\bar{\kappa}_3 + 47\bar{\kappa}_4^2)) \log((\bar{\kappa}_2 - \bar{\kappa}_4)^2 |) \right]$$

Type-4:

$$\Gamma_{11}^{pq} = \bar{x} \left[\begin{aligned} & \frac{1}{20(\bar{x}_1 - \bar{x}_2)^3 (\bar{x}_3 - \bar{x}_4)^3} \left((\bar{x}_1 - \bar{x}_3)^4 (4\bar{x}_1^2 + (-6\bar{x}_2 + 7\bar{x}_3 - 9\bar{x}_4)\bar{x}_1 + 4\bar{x}_3^2 - 9\bar{x}_2\bar{x}_3 + 15\bar{x}_2\bar{x}_4 - 6\bar{x}_3\bar{x}_4) (\log(\bar{x}_1 - \bar{x}_3))^2 \right) - \\ & (\bar{x}_1 - \bar{x}_4)^4 (4\bar{x}_1^2 + (-6\bar{x}_2 - 9\bar{x}_3 + 7\bar{x}_4)\bar{x}_1 + 4\bar{x}_4^2 + 15\bar{x}_2\bar{x}_3 - 9\bar{x}_2\bar{x}_4 - 6\bar{x}_3\bar{x}_4) (\log(\bar{x}_1 - \bar{x}_4))^2 \right) + \\ & \bar{x}_1 (\bar{x}_3 - \bar{x}_4) (8\bar{x}_1^4 - 2\bar{x}_1^3 (6\bar{x}_2 + 7(\bar{x}_3 + \bar{x}_4)) + \bar{x}_1^2 (24\bar{x}_2 (\bar{x}_3 + \bar{x}_4) - 23\bar{x}_3^2 + 78\bar{x}_3\bar{x}_4 - 23\bar{x}_4^2) + \\ & \bar{x}_1 (\bar{x}_2 (101\bar{x}_3^2 - 274\bar{x}_3\bar{x}_4 + 101\bar{x}_4^2) - 2(\bar{x}_3 + \bar{x}_4) (7\bar{x}_3^2 - 12\bar{x}_3\bar{x}_4 + 7\bar{x}_4^2)) - 6\bar{x}_2 (\bar{x}_3 + \bar{x}_4) (3\bar{x}_3^2 - 5\bar{x}_3\bar{x}_4 + 3\bar{x}_4^2) + 8\bar{x}_3^4 - \\ & 8\bar{x}_4^4 - 4\bar{x}_3\bar{x}_4^3 - 4\bar{x}_3^2\bar{x}_4^2 + 4\bar{x}_3^3\bar{x}_4) + (\bar{x}_2 - \bar{x}_3)^4 (-4\bar{x}_2^2 - 7\bar{x}_3\bar{x}_2 + 9\bar{x}_4\bar{x}_2 - 4\bar{x}_3^2 + 6\bar{x}_3\bar{x}_4 + 3\bar{x}_1 (2\bar{x}_2 + 3\bar{x}_3 - 5\bar{x}_4)) (\log(\bar{x}_2 - \bar{x}_3))^2 \right) + \\ & (\bar{x}_2 - \bar{x}_4)^4 (4\bar{x}_2^2 - 9\bar{x}_3\bar{x}_2 + 7\bar{x}_4\bar{x}_2 + 4\bar{x}_4^2 - 6\bar{x}_3\bar{x}_4 - 3\bar{x}_1 (2\bar{x}_2 - 5\bar{x}_3 + 3\bar{x}_4)) (\log(\bar{x}_2 - \bar{x}_4))^2 \right) - \\ & \bar{x}_2 (\bar{x}_3 - \bar{x}_4) \left(\bar{x}_1 (-12\bar{x}_2^2 + 24(\bar{x}_3 + \bar{x}_4)\bar{x}_2^2 + (101\bar{x}_3^2 - 274\bar{x}_4\bar{x}_3 + 101\bar{x}_4^2)\bar{x}_2 - 6(\bar{x}_3 + \bar{x}_4) (3\bar{x}_3^2 - 5\bar{x}_4\bar{x}_3 + 3\bar{x}_4^2)) + 8\bar{x}_2^4 - 14\bar{x}_2^3 (\bar{x}_3 + \bar{x}_4) + \right. \\ & \left. 8\bar{x}_3^4 - 4\bar{x}_4\bar{x}_3^3 - 4\bar{x}_4^2\bar{x}_3^2 - 4\bar{x}_4^3\bar{x}_3 + 8\bar{x}_4^4 - 2\bar{x}_2 (\bar{x}_3 + \bar{x}_4) (7\bar{x}_3^2 - 12\bar{x}_4\bar{x}_3 + 7\bar{x}_4^2) + \bar{x}_2^2 (-23\bar{x}_3^2 + 78\bar{x}_4\bar{x}_3 - 23\bar{x}_4^2) \right) \end{aligned} \right]$$

$$\Gamma_{12}^{pq} = \bar{x} \left[\begin{aligned} & \frac{1}{60(\bar{x}_1 - \bar{x}_2)^2 (\bar{x}_3 - \bar{x}_4)^3} (6((\bar{x}_1 - \bar{x}_4)^4 \log(\bar{x}_4 - \bar{x}_1)) (2\bar{x}_1^2 - 3\bar{x}_1 (\bar{x}_2 + \bar{x}_3) + 2\bar{x}_1\bar{x}_4 - 2\bar{x}_4 (\bar{x}_2 + \bar{x}_3) + 5\bar{x}_2\bar{x}_3 + \bar{x}_4^2) - \\ & (\bar{x}_2 - \bar{x}_4)^4 \log(\bar{x}_4 - \bar{x}_2)) (-2\bar{x}_4 (\bar{x}_1 - \bar{x}_2 + \bar{x}_3) - 3\bar{x}_1\bar{x}_2 + 5\bar{x}_1\bar{x}_3 + 2\bar{x}_2^2 - 3\bar{x}_2\bar{x}_3 + \bar{x}_4^2) - 6(\bar{x}_1 - \bar{x}_3)^3 \log(\bar{x}_3 - \bar{x}_1) \right) \\ & 6(\bar{x}_2 - \bar{x}_3)^3 + (2\bar{x}_1^3 - 3\bar{x}_2\bar{x}_1^2 + 3\bar{x}_3\bar{x}_1^2 + 3\bar{x}_3^2\bar{x}_1 - 4\bar{x}_2\bar{x}_3\bar{x}_1 + 2\bar{x}_3^3 - 3\bar{x}_2\bar{x}_3^2 + 5(\bar{x}_1 - 2\bar{x}_2 + \bar{x}_3)\bar{x}_4 - 2\bar{x}_4 (3\bar{x}_1^2 - 5\bar{x}_2\bar{x}_1 + 4\bar{x}_3\bar{x}_1 + 3\bar{x}_3^2 - 5\bar{x}_2\bar{x}_3)) \\ & (2\bar{x}_2^3 - 3\bar{x}_1\bar{x}_2^2 + 3\bar{x}_3\bar{x}_2^2 + 3\bar{x}_3^2\bar{x}_2 - 4\bar{x}_1\bar{x}_3\bar{x}_2 + 2\bar{x}_3^3 - 3\bar{x}_2\bar{x}_3^2 + 5(\bar{x}_1 - 2\bar{x}_2 + \bar{x}_3)\bar{x}_4 + 2(-3\bar{x}_2^2 - 4\bar{x}_3\bar{x}_2 - 3\bar{x}_3^2 + 5\bar{x}_1 (\bar{x}_2 + \bar{x}_3))\bar{x}_4) \log|\bar{x}_3 - \bar{x}_2| + \\ & (\bar{x}_2 - \bar{x}_1) (\bar{x}_3 - \bar{x}_4) (12\bar{x}_1^4 - 6\bar{x}_1^3 (\bar{x}_2 + 2\bar{x}_3 + 5\bar{x}_4) + \bar{x}_1^2 (-6\bar{x}_2^2 + 9\bar{x}_2\bar{x}_3 + 21\bar{x}_2\bar{x}_4 - 5\bar{x}_3^2 + 37\bar{x}_3\bar{x}_4 + 16\bar{x}_4^2) + \\ & \bar{x}_1 (-6\bar{x}_2^3 + 3\bar{x}_2^2 (3\bar{x}_3 + 7\bar{x}_4) + 4\bar{x}_2 (\bar{x}_3^2 - 11\bar{x}_3\bar{x}_4 - 5\bar{x}_4^2) + 3(4\bar{x}_3^3 - 10\bar{x}_3^2\bar{x}_4 + 5\bar{x}_3\bar{x}_4^2 - 3\bar{x}_4^3)) + 12\bar{x}_2^4 - 6\bar{x}_2^3 (2\bar{x}_3 + 5\bar{x}_4) + \\ & (-5\bar{x}_3^2 + 37\bar{x}_4\bar{x}_3 + 16\bar{x}_4^2)\bar{x}_2^2 + 3(4\bar{x}_3^3 - 10\bar{x}_4\bar{x}_3^2 + 5\bar{x}_4^2\bar{x}_3 - 3\bar{x}_4^3)\bar{x}_2 - 6(\bar{x}_3^2 - \bar{x}_4\bar{x}_3 - \bar{x}_4^2) (2\bar{x}_3^2 - 2\bar{x}_4\bar{x}_3 + \bar{x}_4^2) \end{aligned} \right]$$

$$\Gamma_{13}^{pq} = \bar{x} \left[\begin{aligned} & \frac{1}{20(\bar{x}_1 - \bar{x}_2)^3 (\bar{x}_3 - \bar{x}_4)^3} ((\bar{x}_1 - \bar{x}_3)^4 \log((\bar{x}_1 - \bar{x}_3)^2)) (-4\bar{x}_1^2 + \bar{x}_1 (-6\bar{x}_2 + 7\bar{x}_3 - 9\bar{x}_4) - 9\bar{x}_2\bar{x}_3 + 15\bar{x}_2\bar{x}_4 + 4\bar{x}_3^2 - 6\bar{x}_3\bar{x}_4) + \\ & (\bar{x}_1 - \bar{x}_4)^4 \log((\bar{x}_1 - \bar{x}_4)^2) (4\bar{x}_1^2 + \bar{x}_1 (-6\bar{x}_2 - 9\bar{x}_3 + 7\bar{x}_4) + 15\bar{x}_2\bar{x}_3 - 9\bar{x}_2\bar{x}_4 - 6\bar{x}_3\bar{x}_4 + 4\bar{x}_4^2) - \\ & \bar{x}_1 (\bar{x}_3 - \bar{x}_4) (8\bar{x}_1^4 - 2\bar{x}_1^3 (6\bar{x}_2 + 7(\bar{x}_3 + \bar{x}_4)) + \bar{x}_1^2 (24\bar{x}_2 (\bar{x}_3 + \bar{x}_4) - 23\bar{x}_3^2 + 78\bar{x}_3\bar{x}_4 - 23\bar{x}_4^2) + \\ & \bar{x}_1 (\bar{x}_2 (101\bar{x}_3^2 - 274\bar{x}_4\bar{x}_3 + 101\bar{x}_4^2) - 2(\bar{x}_3 + \bar{x}_4) (7\bar{x}_3^2 - 12\bar{x}_4\bar{x}_3 + 7\bar{x}_4^2)) - 6\bar{x}_2 (\bar{x}_3 + \bar{x}_4) (3\bar{x}_3^2 - 5\bar{x}_4\bar{x}_3 + 3\bar{x}_4^2) + 8\bar{x}_3^4 - 4\bar{x}_3^3\bar{x}_4 - \\ & 4\bar{x}_3^2\bar{x}_4^2 - 4\bar{x}_3\bar{x}_4^3 + 8\bar{x}_4^4) + (\bar{x}_2 - \bar{x}_3)^4 \log((\bar{x}_2 - \bar{x}_3)^2) (-3\bar{x}_1 (2\bar{x}_2 + 3\bar{x}_3 - 5\bar{x}_4) + 4\bar{x}_2^2 + 7\bar{x}_2\bar{x}_3 - 9\bar{x}_2\bar{x}_4 + 4\bar{x}_3^2 - 6\bar{x}_3\bar{x}_4) + \\ & (\bar{x}_2 - \bar{x}_4)^4 \log((\bar{x}_2 - \bar{x}_4)^2) (3\bar{x}_1 (2\bar{x}_2 - 5\bar{x}_3 + 3\bar{x}_4) - 4\bar{x}_2^2 + 9\bar{x}_2\bar{x}_3 - 7\bar{x}_2\bar{x}_4 + 6\bar{x}_3\bar{x}_4 - 4\bar{x}_4^2) + \\ & \bar{x}_2 (\bar{x}_3 - \bar{x}_4) \left(\bar{x}_1 (-12\bar{x}_2^2 + 24(\bar{x}_3 + \bar{x}_4)\bar{x}_2^2 + (101\bar{x}_3^2 - 274\bar{x}_4\bar{x}_3 + 101\bar{x}_4^2)\bar{x}_2 - 6(\bar{x}_3 + \bar{x}_4) (3\bar{x}_3^2 - 5\bar{x}_4\bar{x}_3 + 3\bar{x}_4^2)) + 8\bar{x}_2^4 - 14\bar{x}_2^3 (\bar{x}_3 + \bar{x}_4) + \right. \\ & \left. 8\bar{x}_3^4 - 4\bar{x}_4\bar{x}_3^3 - 4\bar{x}_4^2\bar{x}_3^2 - 4\bar{x}_4^3\bar{x}_3 + 8\bar{x}_4^4 - 2\bar{x}_2 (\bar{x}_3 + \bar{x}_4) (7\bar{x}_3^2 - 12\bar{x}_4\bar{x}_3 + 7\bar{x}_4^2) + \bar{x}_2^2 (-23\bar{x}_3^2 + 78\bar{x}_4\bar{x}_3 - 23\bar{x}_4^2) \right) \end{aligned} \right]$$

$$\Gamma_{14}^{pq} = \bar{x} \left[\begin{aligned} & \frac{1}{60(\bar{x}_1 - \bar{x}_2)^2 (\bar{x}_3 - \bar{x}_4)^3} (-6(\bar{x}_1 - \bar{x}_3)^4 \log(\bar{x}_3 - \bar{x}_1)) (2\bar{x}_1^2 + \bar{x}_1 (-3\bar{x}_2 + 2\bar{x}_3 - 3\bar{x}_4) - 2\bar{x}_2\bar{x}_3 + 5\bar{x}_2\bar{x}_4 + \bar{x}_3^2 - 2\bar{x}_3\bar{x}_4) + \\ & 6((\bar{x}_1 - \bar{x}_4)^3 \log(\bar{x}_4 - \bar{x}_1)) (2\bar{x}_1^3 - 3\bar{x}_1^2 (\bar{x}_2 + 2\bar{x}_3 - \bar{x}_4) + \bar{x}_1 (-4\bar{x}_4 (\bar{x}_2 + 2\bar{x}_3) + 5\bar{x}_3 (2\bar{x}_2 + \bar{x}_3) + 3\bar{x}_4^2) - 10\bar{x}_2\bar{x}_3^2 - \\ & 3\bar{x}_4^2 (\bar{x}_2 + 2\bar{x}_3) + 5\bar{x}_3\bar{x}_4 (2\bar{x}_2 + \bar{x}_3) + 2\bar{x}_4^3) + (\bar{x}_2 - \bar{x}_4)^3 \log(\bar{x}_4 - \bar{x}_2)) (\bar{x}_4 (4\bar{x}_1\bar{x}_2 - 10\bar{x}_1\bar{x}_3 - 3\bar{x}_2^2 + 8\bar{x}_2\bar{x}_3 - 5\bar{x}_3^2) + \\ & -2\bar{x}_2^3 + 3\bar{x}_1\bar{x}_2^2 + 6\bar{x}_3\bar{x}_2^2 - 5\bar{x}_3^2\bar{x}_2 - 10\bar{x}_1\bar{x}_3\bar{x}_2 - 2\bar{x}_4^3 + 10\bar{x}_1\bar{x}_3^2 + 3(\bar{x}_1 - \bar{x}_2 + 2\bar{x}_3)\bar{x}_4^2) + \\ & 6(\bar{x}_2 - \bar{x}_3)^4 \log(\bar{x}_3 - \bar{x}_2)) (\bar{x}_1 (-3\bar{x}_2 - 2\bar{x}_3 + 5\bar{x}_4) + 2\bar{x}_2^2 + 2\bar{x}_2\bar{x}_3 - 3\bar{x}_2\bar{x}_4 + \bar{x}_3^2 - 2\bar{x}_3\bar{x}_4) + \\ & (\bar{x}_2 - \bar{x}_1) (\bar{x}_3 - \bar{x}_4) (12\bar{x}_1^4 - 6\bar{x}_1^3 (\bar{x}_2 + 5\bar{x}_3 + 2\bar{x}_4) + \bar{x}_1^2 (-6\bar{x}_2^2 + 21\bar{x}_2\bar{x}_3 + 9\bar{x}_2\bar{x}_4 + 16\bar{x}_3^2 + 37\bar{x}_3\bar{x}_4 - 5\bar{x}_4^2) + \\ & \bar{x}_1 (-6\bar{x}_2^3 + 3\bar{x}_2^2 (7\bar{x}_3 + 3\bar{x}_4) + 4\bar{x}_2 (-5\bar{x}_3^2 - 11\bar{x}_3\bar{x}_4 + \bar{x}_4^2) - 9\bar{x}_3^3 + 15\bar{x}_3^2\bar{x}_4 - 30\bar{x}_3\bar{x}_4^2 + 12\bar{x}_4^3) + 12\bar{x}_2^4 - 6\bar{x}_2^3 (5\bar{x}_3 + 2\bar{x}_4) + \\ & \bar{x}_2^2 (16\bar{x}_3^2 + 37\bar{x}_3\bar{x}_4 - 5\bar{x}_4^2) + 3\bar{x}_2 (-3\bar{x}_3^3 + 5\bar{x}_3^2\bar{x}_4 - 10\bar{x}_3\bar{x}_4^2 + 4\bar{x}_4^3) + 6(\bar{x}_3^2 + \bar{x}_3\bar{x}_4 - \bar{x}_4^2) (\bar{x}_3^2 - 2\bar{x}_3\bar{x}_4 + 2\bar{x}_4^2) \end{aligned} \right]$$

$$\begin{aligned}
& \left[\begin{aligned}
& -\frac{2}{120(\bar{x}_1-\bar{x}_2)(\bar{x}_3-\bar{x}_4)^3} \left(((\bar{x}_2-\bar{x}_4)^4 \log|\bar{x}_4-\bar{x}_2| (2\bar{x}_1(3\bar{x}_2-5\bar{x}_3+2\bar{x}_4)-3\bar{x}_2^2+4\bar{x}_2\bar{x}_3-4\bar{x}_2\bar{x}_4+6\bar{x}_3\bar{x}_4-3\bar{x}_4^2) - (\bar{x}_1-\bar{x}_4)^3 \log|\bar{x}_4-\bar{x}_1| \right. \\
& 6\bar{x}_1^3-6(3\bar{x}_2+\bar{x}_3-\bar{x}_4)\bar{x}_1^2+(5\bar{x}_4^2-2(7\bar{x}_2+4\bar{x}_3)\bar{x}_4+5\bar{x}_2(3\bar{x}_2+4\bar{x}_3))\bar{x}_1+3(\bar{x}_4-2\bar{x}_3)\bar{x}_4^2+5\bar{x}_2^2(\bar{x}_4-4\bar{x}_3)+4\bar{x}_2\bar{x}_4(5\bar{x}_3-2\bar{x}_4) \Big) + \\
& 2(\bar{x}_1-\bar{x}_3)^2 \log|(\bar{x}_3-\bar{x}_1)| (6\bar{x}_1^4+6\bar{x}_1^3(-3\bar{x}_2+\bar{x}_3-2\bar{x}_4)+\bar{x}_1^2(15\bar{x}_2^2+8\bar{x}_2(5\bar{x}_4-2\bar{x}_3)+6\bar{x}_3^2-14\bar{x}_3\bar{x}_4+5\bar{x}_4^2) + \\
& 2\bar{x}_1(5(\bar{x}_3-4\bar{x}_4)\bar{x}_2+(-7\bar{x}_3^2+20\bar{x}_4\bar{x}_3-10\bar{x}_4^2)\bar{x}_2+\bar{x}_3(\bar{x}_3-\bar{x}_4)(3\bar{x}_3-5\bar{x}_4)) + 5\bar{x}_2^2(\bar{x}_3^2-4\bar{x}_4\bar{x}_3+6\bar{x}_4^2) - \\
\Gamma_{22}^{pq} = \bar{x} & 4\bar{x}_2\bar{x}_3(3\bar{x}_3^2-10\bar{x}_3\bar{x}_4+10\bar{x}_4^2)+3\bar{x}_3^2(2\bar{x}_3^2-6\bar{x}_3\bar{x}_4+5\bar{x}_4^2) \Big) + 2(\bar{x}_2-\bar{x}_3)^3 \log|(\bar{x}_3-\bar{x}_2)| \\
& 3\bar{x}_2^3-6\bar{x}_1\bar{x}_2^2+5\bar{x}_3\bar{x}_2^2+6\bar{x}_3^2\bar{x}_2-8\bar{x}_1\bar{x}_3\bar{x}_2+6\bar{x}_3^2-6\bar{x}_1\bar{x}_3^2+5(-4\bar{x}_1+\bar{x}_2+3\bar{x}_3)\bar{x}_4^2+2(-4\bar{x}_2^2-7\bar{x}_3\bar{x}_2-9\bar{x}_3^2+10\bar{x}_1(\bar{x}_2+\bar{x}_3))\bar{x}_4+ \\
& (\bar{x}_1-\bar{x}_2)(\bar{x}_3-\bar{x}_4)(12\bar{x}_1^4-6\bar{x}_1^3(4\bar{x}_2+\bar{x}_3+3\bar{x}_4)+2\bar{x}_1^2(3\bar{x}_2^2+8\bar{x}_2\bar{x}_3+22\bar{x}_2\bar{x}_4-\bar{x}_3^2+3\bar{x}_3\bar{x}_4+\bar{x}_4^2) + \\
& \bar{x}_1(6\bar{x}_2^3-3(3\bar{x}_3+7\bar{x}_4)\bar{x}_2^2+2(3\bar{x}_3^2-13\bar{x}_4\bar{x}_3-5\bar{x}_4^2)\bar{x}_2-6\bar{x}_3^3+5\bar{x}_3^2-9\bar{x}_3\bar{x}_4+16\bar{x}_3^2\bar{x}_4)-6\bar{x}_4^4+\bar{x}_2^3(5\bar{x}_3+13\bar{x}_4) + \\
& 2(\bar{x}_3^2-5\bar{x}_4\bar{x}_3-2\bar{x}_4^2)\bar{x}_2^2+(-18\bar{x}_3^3+44\bar{x}_4\bar{x}_3^2-21\bar{x}_4^2\bar{x}_3+13\bar{x}_4^3)\bar{x}_2+6(\bar{x}_3^2-\bar{x}_4\bar{x}_3-\bar{x}_4^2)(2\bar{x}_3^2-2\bar{x}_4\bar{x}_3+\bar{x}_4^2) \Big) \Big] \\
& \left[\begin{aligned}
& -\frac{1}{60(\bar{x}_1-\bar{x}_2)^2(\bar{x}_3-\bar{x}_4)^3} (3(\bar{x}_1-\bar{x}_3)^3 \log|(\bar{x}_1-\bar{x}_3)| (2\bar{x}_1^3-3\bar{x}_1^2(2\bar{x}_2-\bar{x}_3+\bar{x}_4)+\bar{x}_1(5\bar{x}_2^2-8\bar{x}_2\bar{x}_3+10\bar{x}_2\bar{x}_4+3\bar{x}_3^2-4\bar{x}_3\bar{x}_4) + \\
& 5(\bar{x}_3-2\bar{x}_4)\bar{x}_2^2+2\bar{x}_3(5\bar{x}_4-3\bar{x}_3)\bar{x}_2+\bar{x}_3^2(2\bar{x}_3-3\bar{x}_4) \Big) + \\
& 3((\bar{x}_2-\bar{x}_4)^4 \log|(\bar{x}_2-\bar{x}_4)| (-(\bar{x}_1(-2\bar{x}_2+5\bar{x}_3-3\bar{x}_4)+\bar{x}_2^2-2\bar{x}_2\bar{x}_3+2\bar{x}_2\bar{x}_4-3\bar{x}_3\bar{x}_4+2\bar{x}_4^2) - \\
& (\bar{x}_1-\bar{x}_4)^3 \log|(\bar{x}_1-\bar{x}_4)| (2\bar{x}_1^3-3\bar{x}_1^2(2\bar{x}_2+\bar{x}_3-\bar{x}_4)+\bar{x}_1(-4\bar{x}_4(2\bar{x}_2+\bar{x}_3)+5\bar{x}_2(\bar{x}_2+2\bar{x}_3)+3\bar{x}_4^2) - \\
\Gamma_{23}^{pq} = \bar{x} & 2\bar{x}_1^3-3(2\bar{x}_2+\bar{x}_3)\bar{x}_4^2+5\bar{x}_2(\bar{x}_2+2\bar{x}_3)\bar{x}_4+10\bar{x}_2^2\bar{x}_3) \Big) + \\
& (\bar{x}_1-\bar{x}_2)(\bar{x}_3-\bar{x}_4)(12\bar{x}_1^4-12\bar{x}_1^3(2\bar{x}_2+\bar{x}_3+\bar{x}_4)+\bar{x}_1^2(6\bar{x}_2^2+30\bar{x}_2(\bar{x}_3+\bar{x}_4)+5\bar{x}_3^2-4\bar{x}_3\bar{x}_4+5\bar{x}_4^2) + \\
& \bar{x}_1(6\bar{x}_2^3-15(\bar{x}_3+\bar{x}_4)\bar{x}_2^2+(-37\bar{x}_3^2+44\bar{x}_4\bar{x}_3-37\bar{x}_4^2)\bar{x}_2+3(\bar{x}_3+\bar{x}_4)(4\bar{x}_3^2-7\bar{x}_4\bar{x}_3+4\bar{x}_4^2) - \\
& 6\bar{x}_2^4+9\bar{x}_2^3(\bar{x}_3+\bar{x}_4)-4\bar{x}_2^2(4\bar{x}_3^2-5\bar{x}_4\bar{x}_3+4\bar{x}_4^2) + \\
& 3\bar{x}_2(\bar{x}_3+\bar{x}_4)(10\bar{x}_3^2-17\bar{x}_4\bar{x}_3+10\bar{x}_4^2) + 6(-2\bar{x}_3^4+\bar{x}_4\bar{x}_3^3+\bar{x}_4^2\bar{x}_3^2+\bar{x}_4^3\bar{x}_3-2\bar{x}_4^4) \Big) + \\
& 3(\bar{x}_2-\bar{x}_3)^4 \log|(\bar{x}_2-\bar{x}_3)| (|\bar{x}_1(-2\bar{x}_2-3\bar{x}_3+5\bar{x}_4)+\bar{x}_2^2+2\bar{x}_2(\bar{x}_3-\bar{x}_4)+\bar{x}_3(2\bar{x}_3-3\bar{x}_4)|) \Big) \Big] \\
& \left[\begin{aligned}
& -\frac{1}{120(\bar{x}_1-\bar{x}_2)(\bar{x}_3-\bar{x}_4)^3} (2(\bar{x}_1-\bar{x}_3)^3 \log|\bar{x}_3-\bar{x}_1| (6\bar{x}_1^3-6\bar{x}_1^2(3\bar{x}_2-\bar{x}_3+\bar{x}_4)+\bar{x}_1(15\bar{x}_2^2-14\bar{x}_2\bar{x}_3+20\bar{x}_2\bar{x}_4+5\bar{x}_3^2-8\bar{x}_3\bar{x}_4) + \\
& 5(\bar{x}_3-4\bar{x}_4)\bar{x}_2^2+4\bar{x}_3(5\bar{x}_4-2\bar{x}_3)\bar{x}_2+3\bar{x}_3^2(\bar{x}_3-2\bar{x}_4) \Big) + \\
& 2((\bar{x}_2-\bar{x}_4)^3 \log|(\bar{x}_4-\bar{x}_2)| (\bar{x}_4(8\bar{x}_1\bar{x}_2-20\bar{x}_1\bar{x}_3-5\bar{x}_2^2+14\bar{x}_2\bar{x}_3-15\bar{x}_3^2)+6\bar{x}_1\bar{x}_2^2+ \\
& -3\bar{x}_3^2+8\bar{x}_3\bar{x}_2^2-5\bar{x}_3^2\bar{x}_2-20\bar{x}_1\bar{x}_3\bar{x}_2-6\bar{x}_4^3+20\bar{x}_1\bar{x}_3^2+6(\bar{x}_1-\bar{x}_2+3\bar{x}_3)\bar{x}_4^2) - \\
\Gamma_{24}^{pq} = \bar{x} & (\bar{x}_1-\bar{x}_4)^2 \log|(\bar{x}_4-\bar{x}_1)| (6\bar{x}_1^4+6\bar{x}_1^3(-3\bar{x}_2-2\bar{x}_3+\bar{x}_4)+\bar{x}_1^2(5(3\bar{x}_2^2+8\bar{x}_2\bar{x}_3+\bar{x}_3^2)-2\bar{x}_4(8\bar{x}_2+7\bar{x}_3)+6\bar{x}_4^2) + \\
& 2\bar{x}_1(3\bar{x}_3^2-(7\bar{x}_2+8\bar{x}_3)\bar{x}_4+5(\bar{x}_2^2+4\bar{x}_3\bar{x}_2+\bar{x}_3^2)\bar{x}_4-10\bar{x}_2\bar{x}_3(2\bar{x}_2+\bar{x}_3)) + \\
& 6\bar{x}_4^4-6(2\bar{x}_2+3\bar{x}_3)\bar{x}_4^3+5(\bar{x}_2^2+8\bar{x}_3\bar{x}_2+3\bar{x}_3^2)\bar{x}_4^2-20\bar{x}_2\bar{x}_3(\bar{x}_2+2\bar{x}_3)\bar{x}_4+30\bar{x}_2^2\bar{x}_3^2) \Big) + \\
& 2(\bar{x}_2-\bar{x}_3)^4 \log|(\bar{x}_3-\bar{x}_2)| (-2\bar{x}_1(3\bar{x}_2+2\bar{x}_3-5\bar{x}_4)+3\bar{x}_2^2+4\bar{x}_2(\bar{x}_3-\bar{x}_4)+3\bar{x}_3(\bar{x}_3-2\bar{x}_4) \Big) + \\
& (\bar{x}_1-\bar{x}_2)(\bar{x}_3-\bar{x}_4)(12\bar{x}_1^4-6\bar{x}_1^3(4\bar{x}_2+3\bar{x}_3+\bar{x}_4)+2\bar{x}_1^2(3\bar{x}_2^2+22\bar{x}_2\bar{x}_3+8\bar{x}_2\bar{x}_4+\bar{x}_3^2+3\bar{x}_3\bar{x}_4-\bar{x}_4^2) + \\
& \bar{x}_1(6\bar{x}_2^3-3(7\bar{x}_3+3\bar{x}_4)\bar{x}_2^2-2(5\bar{x}_3^2+13\bar{x}_4\bar{x}_3-3\bar{x}_4^2)\bar{x}_2+5\bar{x}_3^3-6\bar{x}_3^2+16\bar{x}_3\bar{x}_4-9\bar{x}_3^2\bar{x}_4) - \\
& 6\bar{x}_2^4+\bar{x}_2^3(13\bar{x}_3+5\bar{x}_4)+2\bar{x}_2^2(-2\bar{x}_3^2-5\bar{x}_4\bar{x}_3+\bar{x}_4^2) + \\
& \bar{x}_2(13\bar{x}_3^3-21\bar{x}_4\bar{x}_3^2+44\bar{x}_4^2\bar{x}_3-18\bar{x}_4^3)-6(\bar{x}_2^2+\bar{x}_4\bar{x}_3-\bar{x}_4^2)(\bar{x}_3^2-2\bar{x}_4\bar{x}_3+2\bar{x}_4^2) \Big) \Big]
\end{aligned}
\right.
\end{aligned}$$

$$\begin{aligned}
\Gamma_{33}^{pq} = & \bar{\kappa} \left[\frac{1}{20(\bar{\kappa}_1 - \bar{\kappa}_2)^3 (\bar{\kappa}_3 - \bar{\kappa}_4)^3} \left((\bar{\kappa}_1 - \bar{\kappa}_3)^4 (4\bar{\kappa}_1^2 + (-6\bar{\kappa}_2 + 7\bar{\kappa}_3 - 9\bar{\kappa}_4) \bar{\kappa}_1 + 4\bar{\kappa}_3^2 - 9\bar{\kappa}_2 \bar{\kappa}_3 + 15\bar{\kappa}_2 \bar{\kappa}_4 - 6\bar{\kappa}_3 \bar{\kappa}_4) (\log(\bar{\kappa}_1 - \bar{\kappa}_3))^2 \right) - \right. \\
& (\bar{\kappa}_1 - \bar{\kappa}_4)^4 (4\bar{\kappa}_1^2 + (-6\bar{\kappa}_2 - 9\bar{\kappa}_3 + 7\bar{\kappa}_4) \bar{\kappa}_1 + 4\bar{\kappa}_4^2 + 15\bar{\kappa}_2 \bar{\kappa}_3 - 9\bar{\kappa}_2 \bar{\kappa}_4 - 6\bar{\kappa}_3 \bar{\kappa}_4) (\log(\bar{\kappa}_1 - \bar{\kappa}_4))^2 + \\
& \bar{\kappa}_1 (\bar{\kappa}_3 - \bar{\kappa}_4) (8\bar{\kappa}_1^4 - 2\bar{\kappa}_1^3 (6\bar{\kappa}_2 + 7(\bar{\kappa}_3 + \bar{\kappa}_4)) + \bar{\kappa}_1^2 (24\bar{\kappa}_2 (\bar{\kappa}_3 + \bar{\kappa}_4) - 23\bar{\kappa}_3^2 + 78\bar{\kappa}_3 \bar{\kappa}_4 - 23\bar{\kappa}_4^2) + \\
& \bar{\kappa}_1 (\bar{\kappa}_2 (101\bar{\kappa}_3^2 - 274\bar{\kappa}_4 \bar{\kappa}_3 + 101\bar{\kappa}_4^2) - 2(\bar{\kappa}_3 + \bar{\kappa}_4) (7\bar{\kappa}_3^2 - 12\bar{\kappa}_4 \bar{\kappa}_3 + 7\bar{\kappa}_4^2)) - \\
& 8\bar{\kappa}_3^4 - 4\bar{\kappa}_4 \bar{\kappa}_3^3 - 4\bar{\kappa}_4^2 \bar{\kappa}_3^2 - 4\bar{\kappa}_4^3 \bar{\kappa}_3 + 8\bar{\kappa}_4^4 + 6\bar{\kappa}_2 (\bar{\kappa}_3 + \bar{\kappa}_4) (3\bar{\kappa}_3^2 - 5\bar{\kappa}_4 \bar{\kappa}_3 + 3\bar{\kappa}_4^2) + \\
& (\bar{\kappa}_2 - \bar{\kappa}_3)^4 \log((\bar{\kappa}_2 - \bar{\kappa}_3)^2) (3\bar{\kappa}_1 (2\bar{\kappa}_2 + 3\bar{\kappa}_3 - 5\bar{\kappa}_4) - 4\bar{\kappa}_2^2 - 7\bar{\kappa}_2 \bar{\kappa}_3 + 9\bar{\kappa}_2 \bar{\kappa}_4 - 4\bar{\kappa}_3^2 + 6\bar{\kappa}_3 \bar{\kappa}_4) + \\
& (\bar{\kappa}_2 - \bar{\kappa}_4)^4 \log((\bar{\kappa}_2 - \bar{\kappa}_4)^2) (-3\bar{\kappa}_1 (2\bar{\kappa}_2 - 5\bar{\kappa}_3 + 3\bar{\kappa}_4) + 4\bar{\kappa}_2^2 - 9\bar{\kappa}_2 \bar{\kappa}_3 + 7\bar{\kappa}_2 \bar{\kappa}_4 - 6\bar{\kappa}_3 \bar{\kappa}_4 + 4\bar{\kappa}_4^2) - \\
& \bar{\kappa}_2 (\bar{\kappa}_3 - \bar{\kappa}_4) (\bar{\kappa}_1 (-12\bar{\kappa}_2^3 + 24\bar{\kappa}_2^2 (\bar{\kappa}_3 + \bar{\kappa}_4) + \bar{\kappa}_2 (101\bar{\kappa}_3^2 - 274\bar{\kappa}_3 \bar{\kappa}_4 + 101\bar{\kappa}_4^2) - 6(\bar{\kappa}_3 + \bar{\kappa}_4) (3\bar{\kappa}_3^2 - 5\bar{\kappa}_4 \bar{\kappa}_3 + 3\bar{\kappa}_4^2)) + \\
& 8\bar{\kappa}_2^4 - 14\bar{\kappa}_2^3 (\bar{\kappa}_3 + \bar{\kappa}_4) + \bar{\kappa}_2^2 (-23\bar{\kappa}_3^2 + 78\bar{\kappa}_4 \bar{\kappa}_3 - 23\bar{\kappa}_4^2) - \\
& \left. 8\bar{\kappa}_3^4 - 4\bar{\kappa}_4 \bar{\kappa}_3^3 - 4\bar{\kappa}_4^2 \bar{\kappa}_3^2 - 4\bar{\kappa}_4^3 \bar{\kappa}_3 + 8\bar{\kappa}_4^4 + 2\bar{\kappa}_2 (\bar{\kappa}_3 + \bar{\kappa}_4) (7\bar{\kappa}_3^2 - 12\bar{\kappa}_4 \bar{\kappa}_3 + 7\bar{\kappa}_4^2) \right) \\
\Gamma_{34}^{pq} = & \bar{\kappa} \left[\frac{1}{60(\bar{\kappa}_1 - \bar{\kappa}_2)^3 (\bar{\kappa}_3 - \bar{\kappa}_4)^3} (6(\bar{\kappa}_1 - \bar{\kappa}_3)^4 \log(\bar{\kappa}_3 - \bar{\kappa}_1)) (2\bar{\kappa}_1^2 + \bar{\kappa}_1 (-3\bar{\kappa}_2 + 2\bar{\kappa}_3 - 3\bar{\kappa}_4) - 2\bar{\kappa}_2 \bar{\kappa}_3 + 5\bar{\kappa}_2 \bar{\kappa}_4 + \bar{\kappa}_3^2 - 2\bar{\kappa}_3 \bar{\kappa}_4) + \right. \\
& 6((\bar{\kappa}_2 - \bar{\kappa}_4)^3 \log(\bar{\kappa}_4 - \bar{\kappa}_2)) (-\bar{\kappa}_1 (3\bar{\kappa}_2^2 - 10\bar{\kappa}_2 \bar{\kappa}_3 + 4\bar{\kappa}_2 \bar{\kappa}_4 + 10\bar{\kappa}_3^2 - 10\bar{\kappa}_3 \bar{\kappa}_4 + 3\bar{\kappa}_4^2) + \bar{\kappa}_2 (2\bar{\kappa}_2^2 - 6\bar{\kappa}_2 \bar{\kappa}_3 + 5\bar{\kappa}_3^2) + \\
& 3\bar{\kappa}_4^2 (\bar{\kappa}_2 - 2\bar{\kappa}_3) + \bar{\kappa}_4 (\bar{\kappa}_2 - \bar{\kappa}_3) (3\bar{\kappa}_2 - 5\bar{\kappa}_3) + 2\bar{\kappa}_4^3) - (\bar{\kappa}_1 - \bar{\kappa}_4)^3 \log(\bar{\kappa}_4 - \bar{\kappa}_1) (2\bar{\kappa}_1^2 - 3\bar{\kappa}_1^2 (\bar{\kappa}_2 + 2\bar{\kappa}_3 - \bar{\kappa}_4) + \\
& 2\bar{\kappa}_4^3 - 3(\bar{\kappa}_2 + 2\bar{\kappa}_3) \bar{\kappa}_4^2 + 5\bar{\kappa}_3 (2\bar{\kappa}_2 + \bar{\kappa}_3) \bar{\kappa}_4 - 10\bar{\kappa}_2 \bar{\kappa}_3^2 + \bar{\kappa}_1 (3\bar{\kappa}_2^2 - 4(\bar{\kappa}_2 + 2\bar{\kappa}_3) \bar{\kappa}_4 + 5\bar{\kappa}_3 (2\bar{\kappa}_2 + \bar{\kappa}_3))) - \\
& 6(\bar{\kappa}_2 - \bar{\kappa}_3)^4 \log(\bar{\kappa}_3 - \bar{\kappa}_2) (\bar{\kappa}_1 (-3\bar{\kappa}_2 - 2\bar{\kappa}_3 + 5\bar{\kappa}_4) + 2\bar{\kappa}_2^2 + 2\bar{\kappa}_2 \bar{\kappa}_3 - 3\bar{\kappa}_3 \bar{\kappa}_4 + \bar{\kappa}_3^2 - 2\bar{\kappa}_3 \bar{\kappa}_4) + \\
& \bar{\kappa}_1 (-6\bar{\kappa}_2^3 + 3\bar{\kappa}_2^2 (7\bar{\kappa}_3 + 3\bar{\kappa}_4) + 4\bar{\kappa}_2 (-5\bar{\kappa}_3^2 - 11\bar{\kappa}_3 \bar{\kappa}_4 + \bar{\kappa}_4^2) - 9\bar{\kappa}_3^3 + 15\bar{\kappa}_3^2 \bar{\kappa}_4 - 30\bar{\kappa}_3 \bar{\kappa}_4^2 + 12\bar{\kappa}_4^3) + \\
& 12\bar{\kappa}_2^4 - 6\bar{\kappa}_2^3 (5\bar{\kappa}_3 + 2\bar{\kappa}_4) + \bar{\kappa}_2^2 (16\bar{\kappa}_3^2 + 37\bar{\kappa}_4 \bar{\kappa}_3 - 5\bar{\kappa}_4^2) + \\
& \left. 6(\bar{\kappa}_3^2 + \bar{\kappa}_4 \bar{\kappa}_3 - \bar{\kappa}_4^2) (\bar{\kappa}_3^2 - 2\bar{\kappa}_4 \bar{\kappa}_3 + 2\bar{\kappa}_4^2) + 3\bar{\kappa}_2 (-3\bar{\kappa}_3^3 + 5\bar{\kappa}_4 \bar{\kappa}_3^2 - 10\bar{\kappa}_2 \bar{\kappa}_3 + 4\bar{\kappa}_4^3) \right) \\
\Gamma_{44}^{pq} = & \bar{\kappa} \left[\frac{1}{120(\bar{\kappa}_1 - \bar{\kappa}_2) (\bar{\kappa}_3 - \bar{\kappa}_4)^3} (2(\bar{\kappa}_2 - \bar{\kappa}_3)^3 \log(\bar{\kappa}_3 - \bar{\kappa}_2)) (5\bar{\kappa}_1^2 (3\bar{\kappa}_2 + \bar{\kappa}_3 - 4\bar{\kappa}_4) - 2\bar{\kappa}_1 (9\bar{\kappa}_2^2 + 7\bar{\kappa}_2 \bar{\kappa}_3 + 4\bar{\kappa}_3^2) + 20\bar{\kappa}_1 \bar{\kappa}_4 (\bar{\kappa}_2 + \bar{\kappa}_3) + 6\bar{\kappa}_2^3 + \right. \\
& 6(\bar{\kappa}_3 - \bar{\kappa}_4) \bar{\kappa}_2^2 + \bar{\kappa}_3 (5\bar{\kappa}_3 - 8\bar{\kappa}_4) \bar{\kappa}_2 + 3\bar{\kappa}_3^2 (\bar{\kappa}_3 - 2\bar{\kappa}_4)) + \\
& 2(\bar{\kappa}_1 - \bar{\kappa}_3)^4 \log(\bar{\kappa}_3 - \bar{\kappa}_1) (3\bar{\kappa}_1^2 + \bar{\kappa}_1 (-6\bar{\kappa}_2 + 4\bar{\kappa}_3 - 4\bar{\kappa}_4) + \bar{\kappa}_2 (10\bar{\kappa}_4 - 4\bar{\kappa}_3) + 3\bar{\kappa}_3 (\bar{\kappa}_3 - 2\bar{\kappa}_4)) + \\
& 2(\log(\bar{\kappa}_4 - \bar{\kappa}_2)) (-5\bar{\kappa}_1^2 (\bar{\kappa}_2 - \bar{\kappa}_4)^2 (3\bar{\kappa}_2^2 + 2\bar{\kappa}_2 (\bar{\kappa}_4 - 4\bar{\kappa}_3) + 6\bar{\kappa}_3^2 - 4\bar{\kappa}_3 \bar{\kappa}_4 + \bar{\kappa}_4^2) + 2\bar{\kappa}_1 (\bar{\kappa}_2 - \bar{\kappa}_4)^2 \\
& 6\bar{\kappa}_3^3 + (7\bar{\kappa}_2 - 20\bar{\kappa}_3) \bar{\kappa}_2^2 + 4(2\bar{\kappa}_2^2 - 5\bar{\kappa}_3 \bar{\kappa}_2 + 5\bar{\kappa}_3^2) \bar{\kappa}_4 + \bar{\kappa}_2 (9\bar{\kappa}_2^2 - 20\bar{\kappa}_3 \bar{\kappa}_2 + 10\bar{\kappa}_3^2) - 6\bar{\kappa}_2^5 + \\
& 6(2\bar{\kappa}_3 + \bar{\kappa}_4) \bar{\kappa}_2^5 - 5\bar{\kappa}_3 (\bar{\kappa}_3 + 2\bar{\kappa}_4) \bar{\kappa}_2^4 + 2\bar{\kappa}_4^3 (10\bar{\kappa}_3^2 - 10\bar{\kappa}_4 \bar{\kappa}_3 + 3\bar{\kappa}_4^2) \bar{\kappa}_2 - 3\bar{\kappa}_4^4 (5\bar{\kappa}_3^2 - 6\bar{\kappa}_4 \bar{\kappa}_3 + 2\bar{\kappa}_4^2)) - \\
& (\bar{\kappa}_1 - \bar{\kappa}_4)^3 \log(\bar{\kappa}_4 - \bar{\kappa}_1) (3\bar{\kappa}_1^3 + \bar{\kappa}_1^2 (-6\bar{\kappa}_2 - 8\bar{\kappa}_3 + 5\bar{\kappa}_4) + \bar{\kappa}_1 (-2\bar{\kappa}_4 (4\bar{\kappa}_2 + 7\bar{\kappa}_3) + 5\bar{\kappa}_3 (4\bar{\kappa}_2 + \bar{\kappa}_3) + 6\bar{\kappa}_4^2) - \\
& 6\bar{\kappa}_4^3 - 6(\bar{\kappa}_2 + 3\bar{\kappa}_3) \bar{\kappa}_4^2 + 5\bar{\kappa}_3 (4\bar{\kappa}_2 + 3\bar{\kappa}_3) \bar{\kappa}_4 + 20\bar{\kappa}_2 \bar{\kappa}_3^2)) + \\
& (\bar{\kappa}_1 - \bar{\kappa}_2) (\bar{\kappa}_3 - \bar{\kappa}_4) (6\bar{\kappa}_1^4 - \bar{\kappa}_1^3 (6\bar{\kappa}_2 + 13\bar{\kappa}_3 + 5\bar{\kappa}_4) + \bar{\kappa}_1^2 (-6\bar{\kappa}_2^2 + 21\bar{\kappa}_2 \bar{\kappa}_3 + 9\bar{\kappa}_2 \bar{\kappa}_4 + 4\bar{\kappa}_3^2 + 10\bar{\kappa}_3 \bar{\kappa}_4 - 2\bar{\kappa}_4^2) + \\
& \bar{\kappa}_1 (24\bar{\kappa}_3^3 - 4(11\bar{\kappa}_3 + 4\bar{\kappa}_4) \bar{\kappa}_2^2 + 2(5\bar{\kappa}_3^2 + 13\bar{\kappa}_4 \bar{\kappa}_3 - 3\bar{\kappa}_4^2) \bar{\kappa}_2 - 13\bar{\kappa}_3^3 + 18\bar{\kappa}_3^2 \bar{\kappa}_4 - 44\bar{\kappa}_3 \bar{\kappa}_4^2 + 21\bar{\kappa}_3^2 \bar{\kappa}_4) - \\
& 12\bar{\kappa}_2^4 + 6\bar{\kappa}_2^3 (3\bar{\kappa}_3 + \bar{\kappa}_4) - 2\bar{\kappa}_2^2 (\bar{\kappa}_3^2 + 3\bar{\kappa}_4 \bar{\kappa}_3 - \bar{\kappa}_4^2) + \\
& \left. 6(\bar{\kappa}_3^2 + \bar{\kappa}_4 \bar{\kappa}_3 - \bar{\kappa}_4^2) (\bar{\kappa}_3^2 - 2\bar{\kappa}_4 \bar{\kappa}_3 + 2\bar{\kappa}_4^2) + \bar{\kappa}_2 (-5\bar{\kappa}_3^3 + 9\bar{\kappa}_4 \bar{\kappa}_3^2 - 16\bar{\kappa}_4^2 \bar{\kappa}_3 + 6\bar{\kappa}_4^3) \right)
\end{aligned}$$

A.5 Explicit Expression for P_j^e for Linear Normal Traction

Type-4:

$$\mathbf{P}^e = \bar{t}_o \left\{ \frac{1}{10} (\bar{\kappa}_1 - \bar{\kappa}_2) (7\bar{\kappa}_1 + 3\bar{\kappa}_2) - \frac{1}{30} (\bar{\kappa}_1 - \bar{\kappa}_2)^2 (3\bar{\kappa}_1 + 2\bar{\kappa}_2) - \frac{1}{10} (\bar{\kappa}_1 - \bar{\kappa}_2) (3\bar{\kappa}_1 + 7\bar{\kappa}_2) - \frac{1}{30} (\bar{\kappa}_1 - \bar{\kappa}_2)^2 (2\bar{\kappa}_1 + 3\bar{\kappa}_2) \right\}^T, -1 < \bar{\kappa}_1, \bar{\kappa}_2 < 0$$

$$\mathbf{P}^e = \bar{t}_o \left\{ -\frac{1}{10} (\bar{\kappa}_1 - \bar{\kappa}_2) (7\bar{\kappa}_1 + 3\bar{\kappa}_2) - \frac{1}{30} (\bar{\kappa}_1 - \bar{\kappa}_2)^2 (3\bar{\kappa}_1 + 2\bar{\kappa}_2) - \frac{1}{10} (\bar{\kappa}_1 - \bar{\kappa}_2) (3\bar{\kappa}_1 + 7\bar{\kappa}_2) - \frac{1}{30} (\bar{\kappa}_1 - \bar{\kappa}_2)^2 (2\bar{\kappa}_1 + 3\bar{\kappa}_2) \right\}^T, (0 < \bar{\kappa}_1, \bar{\kappa}_2 < 1)$$

A.6 Explicit Expression for P_j^e for Quadratic Normal Traction

Type-4:

$$\mathbf{P}^e = \bar{t}_o \begin{pmatrix} \frac{1}{15}(\bar{x}_1 - \bar{x}_2)(8\bar{x}_1^2 + 5\bar{x}_2\bar{x}_1 + 2\bar{x}_2^2 - 15) \\ -\frac{1}{30}(\bar{x}_1 - \bar{x}_2)^2(2\bar{x}_1^2 + 2\bar{x}_2\bar{x}_1 + \bar{x}_2^2 - 5) \\ \frac{1}{15}(\bar{x}_1 - \bar{x}_2)(2\bar{x}_1^2 + 5\bar{x}_2\bar{x}_1 + 8\bar{x}_2^2 - 15) \\ \frac{1}{30}(\bar{x}_1 - \bar{x}_2)^2(\bar{x}_1^2 + 2\bar{x}_2\bar{x}_1 + 2\bar{x}_2^2 - 5) \end{pmatrix}$$



VITA

The author, Nguyen Ngoc Son, was born in Daklak province, Vietnam, on November 23, 1989. He graduated his Bachelor of Engineering degree in Civil Engineering from Hochiminh City University of Technology in 2012. He then worked as a Structural Engineer, Hydraulic Engineering Consultants Corp.II - Hochiminh City, Vietnam for one year. Due to his interested in structure, he achieved the scholarship by Chulalongkorn University Scholarship Program for ASEAN Countries and Ratchadaphiseksomphot Endowment Fund of Chulalongkorn University (CU-56-908) for master degree in Civil Engineering at Chulalongkorn University in 2013 under the supervision of Associate Professor Dr. Jaroon Rungamornrat and Professor Dr. Teerapong Senjuntichai.

